Alma Mater Studiorum – Università di Bologna

DOTTORATO DI RICERCA IN
MECCANICA DEI MATERIALI
E PROCESSI TECNOLOGICI

XXI Ciclo

SOME ISSUES CONCERNING THE DYNAMIC RESPONSE AND DAMAGE OF COMPOSITE LAMINATES SUBJECTED TO LOW VELOCITY IMPACT

Candidato: DANIELE GHELLI

Coordinatore:
prof. ing. TULLIO TROMBETTI

Relatore:
ing. GIANGIACOMO MINAK

Settore scientifico-disciplinare di afferenza:

ING-IND/14
PROGETTAZIONE MECCANICA
E COSTRUZIONE DI MACCHINE

Esame finale anno 2009

Contents

Preface

Laminated composite materials have several advantages over metals: first of all a lower stiffness-to-weight and strength-to-weight ratio, as well as the possibility for the designer to vary their structural properties within wide ranges and tailor them to meet the requirements of specific applications. These advantages led to an extensive use of composite materials for structural components in a number of industrial products, ranging from primary load-bearing members of airplanes to civil constructions and sporting goods.

Laminated composites, however, are usually brittle materials. As a consequence, they do not exhibit phenomena of energy absorption and dissipation through plastic strain which in many cases enable metals to maintain their structural integrity after undergoing high stresses, such as those arising from impulsive loads. For this reason energy absorption in composites usually takes place through material damage. In addition, the internal structure of laminates, which commonly consist of several plies stacked together to form a single body, facilitates the creation of embedded flaws, named delaminations, between adjacent plies because of the poor strength of their interface. This kind of damage can be undetectable by visual inspection, but at the same time can lower the resistance of a laminate significantly.

Given that impacts of a variety of objects, from tools to stones or hail in the case of aircrafts, cannot be avoided during the life of a component, the susceptibility of composites to impact damage has justified an extensive research effort during the last four decades, aimed at understanding both the failure mechanisms and the influence of damage on the mechanical properties of the material. A great interest still exists in this topic, because while there is a substantial agreement on certain issues other problems cannot be considered completely solved.

Research studies resulted in the publication of several hundreds of articles: at present the vastness of the subject and the complexity of the questions that have arisen prevent a comprehensive investigation of the topic of impact on composite materials. In view of this, it was chosen to treat in detail only a few particular aspects, whose common features are on the one hand the importance, both theoretical and practical, on the other hand the relatively limited attention received so far. All of these aspects refer to low velocity impact.

Chapter 2 deals with the comparison between the effects of low velocity impact and of quasi-static indentation. This issue has considerable practical interest because carrying out a quasi-static experimental test is much easier than performing a dynamic test: therefore if the

mechanical response of a laminate, especially as regards damage, to indentation was found to be analogous to the response to impact, the examination of impact behaviour would be greatly simplified. A few research papers are available which do not seem to provide a definitive answer, also because in most of them the assessment of the analogy between impact and indentation is not the main object. A direct comparison, by means of both experimental testing and numerical analysis, is presented here, which aims at establishing to what extent that analogy can be considered valid.

Chapter 3 discusses the effect of different dimensions and boundary conditions of the specimens on the experimentally recorded low velocity impact behaviour and damage. This problem arises when experimental results obtained in different test configurations are to be compared, as well as when one attempts to use results from laboratory tests in the design of real structures. Interesting relationships of the extent of damage with two significant impact parameters, that are the absorbed energy and the peak contact force, are commented on and shown to be independent of the geometry and boundary conditions with reasonable approximation. The possibility of predicting, by means of a simplified numerical analysis, whether delaminations are induced or not during a specific impact event is also discussed.

In chapter 4 the results of impact and compression after impact tests, carried out according to two different standards, are presented. It is known that the strength reduction caused by low velocity impact is usually the largest when the damaged laminate is loaded in compression. Therefore the study of the compression behaviour of composites after impact has received considerable attention. In most of the numerous articles concerned with this topic, however, the test apparatus is designed in such a way as to avoid global buckling of the specimen, in order to obtained strength values which can be attributed to the material itself, regardless of the specimen geometry. The present study focuses on test conditions where instability is not prevented. With the aid of a numerical analysis of the postbuckling regime, some aspects of the interaction between global buckling of the laminate, local buckling of the delaminated region and impact damage are highlighted.

Chapter 5 focuses on another issue that has received limited attention: the influence of pre-existing membrane loading on the impact response and damage of laminates. The significance of this problem is obvious since hardly ever is a structure completely unloaded when is subjected to an impact during service or maintenance; only a laboratory apparatus can ensure that a specimen undergoes an impact being free of in-plane stresses. The available literature provides quite limited information, mainly on tests carried out in a small number of special cases, and appears far from giving conclusive answers on how a preload can affect the material failures. A more comprehensive investigation is presented here, based on a number of numerical simulations, which is thought to be useful in providing general guidelines, especially on how the influence of preload changes depending on the test conditions. The results provide a better explanation of experimental findings reported in the literature.

It appears from the brief summary above that in each of the presented studies the numerical modelling plays a fundamental role. Although the present knowledge about the impact behaviour of composite materials is not sufficiently established for a research activity to be done without experimental testing, a sound theoretical basis also appears necessary to interpret the test results correctly. This provided the motivation for developing a finite element program which has been employed for both static and dynamic calculations, since the applicability of analytical or semi-analytical models to impact problems is limited to a few special cases. The main features of the program are described in the first chapter.

CHAPTER 1

Main features of the finite element program used for numerical analysis

In the study of laminated plates or shells, analytical solutions are available only for a limited number of special problems, even in the case of a linear static analysis which is by far the simplest one. When impact problems are dealt with, closed-form solutions can be obtained only for extremely simple models where, in addition, suitable assumptions are introduced which lead to linearized equations to be solved. In impact phenomena, however, several nonlinear effects are present: first of all contact between impactor and target, as well as large displacements and nonlinear constitutive equations in many cases. Accounting for such effects, even in a single-degree-of-freedom model, requires some form of numerical solution procedure to be employed [1].

This provided the motivation for an extensive use of numerical computation in all of the specific topics which are treated in chapters 2-5. Simplified models with a very small number of degrees of freedom can be helpful for gaining a general understanding of impact phenomena, and establishing some overall guidelines regarding the influence of the main impact parameters. However for a more detailed study, especially when a reliable evaluation of the stress field in an impacted laminate is needed, a different approach appeared necessary. To this end the finite element method was chosen.

The development of an in-house program was preferred to the use of a commercial code for several reasons. First of all, a general-purpose package has many features which one never employs when rather specific analyses, such as impact on composites in the present case, are to be carried out. On the other hand, for a specific task several peculiar capabilities are often required, for example regarding control of the finite element formulation or the solution method, or suitable post-processing techniques, which are often difficult to find or to implement or not available at all in commercial programs. Most importantly, the first concern for the aims of the present thesis was a complete control on the capabilities and limits of the numerical model and the results, rather than the use of very sophisticated models which would be so difficult to verify and validate that one would end up by treating them as black boxes.

A description of the features of the program can be found in what follows. Its reliability was checked by a large number of tests, some of which are reported in [2].

The program was first conceived to perform a numerical analysis of the transient response of a laminated plate or shell. Explicit time integration is carried out by means of the central difference method; geometrical nonlinearity is implemented according to the total lagrangian (TL) formulation [3]. The reasons that justify these choices are explained in the following.

The starting point of the numerical model is the principle of virtual displacements, which can be expressed in the general form valid for a three-dimensional problem [3]:

$$\begin{aligned} \delta W_{ve} &= \int_{V^0} \rho^0 \left[b_i^0(t) - \ddot{u}_i(t) \right] \delta u_i \, dV^0 + \int_{\partial V^0} p_i^0(t) \delta u_i \, dS^0 = \\ &= \int_{V^0} s_{AB}(t) \delta E_{AB} \, dV^0 = \delta W_{vi} \end{aligned} \tag{1}$$

where s_{AB} is the second Piola-Kirchhoff stress tensor, E_{AB} is the Lagrangian finite strain tensor [4], b_i^0 are the body forces per unit mass, p_i^0 are the surface loads per unit area, u_i are displacement components along the three cartesian axes x_i. The summation convention has been used in (1) for subscripts A, B and i. The superscript 0 means that the material volume V^0 and its boundary ∂V^0, as well as external forces, stresses and strains, refer to the initial configuration of the body which is taken as the reference configuration, according to the TL approach [3]. Stress and force values at time t appear in (1) because the central difference method requires solving the equilibrium equation at time t to find the solution at time $t + h$, h being the time integration step [3]. This leads to great simplifications in the treatment of nonlinear phenomena, because the system of equations to be solved at each time step is linear; thus no incremental decomposition of stresses and strains is needed, and iterative solution within each time step is not necessary [3]. On the other hand, the time step must be lower than a critical value to ensure stability of the algorithm [3].

Since the TL and updated lagrangian (UL) formulations are equivalent in the description of nonlinear phenomena, the choice between them is driven by computational efficiency considerations, particularly regarding calculation of strain-displacement matrices [3]. In explicit dynamic analysis the same kind of matrices must be used for both formulations; the UL requires them to be recalculated at each time step, while in the TL they refer to the initial configuration, so they remain the same during the whole time interval to be analysed. For this reason the TL formulation has been adopted here.

The general equation (1) can be rewritten in the suitable form for plate analysis by introducing the kinematic assumptions of a plate theory. For the Reissner-Mindlin plate model, used in the present formulation, they are [1]:

$$\begin{aligned} u(x,y,z) &= u_0(x,y) + z\,\vartheta_y(x,y) \\ v(x,y,z) &= v_0(x,y) - z\,\vartheta_x(x,y) \\ w(x,y,z) &= w_0(x,y) \end{aligned} \tag{2}$$

where the z direction is perpendicular to the middle plane; u, v, w are displacements of any point in the x, y, z direction respectively, while u_0, v_0, w_0 are the displacements of the middle plane; ϑ_x and ϑ_y are the section rotations about the x and y axes respectively. To obtain a two-dimensional problem, further simplification is necessary concerning geometrical nonlinearity. Here it is assumed that the only significant nonlinear terms in finite strain tensor $\mathbf{E}$ are those due to w_0 displacement appearing in the in-plane strains; this hypothesis corresponds to the Von Kármán's model for plates subjected to large deflections [5]. Therefore, using subscripts x, y and z instead of 1, 2 and 3:

$$\begin{aligned}
E_x &= \frac{\partial u_0}{\partial x} + \frac{1}{2}\left(\frac{\partial w_0}{\partial x}\right)^2 + z\frac{\partial \vartheta_y}{\partial x} \\
E_y &= \frac{\partial v_0}{\partial y} + \frac{1}{2}\left(\frac{\partial w_0}{\partial y}\right)^2 - z\frac{\partial \vartheta_x}{\partial y} \\
E_{xy} &= \frac{1}{2}\left(\frac{\partial u_0}{\partial y} + \frac{\partial v_0}{\partial x}\right) + \frac{1}{2}\frac{\partial w_0}{\partial x}\frac{\partial w_0}{\partial y} + \frac{z}{2}\left(\frac{\partial \vartheta_y}{\partial y} - \frac{\partial \vartheta_x}{\partial x}\right) \\
E_{xz} &= \frac{1}{2}\left(\frac{\partial w_0}{\partial x} + \vartheta_y\right) \\
E_{yz} &= \frac{1}{2}\left(\frac{\partial w_0}{\partial y} - \vartheta_x\right)
\end{aligned} \tag{3}$$

The assumptions in (2) and (3) limit the applicability of the present model to cases where the strains are small, even if displacements and rotations can be relatively large. With all these assumptions the internal virtual work in (1) becomes, after some manipulation:

$$\delta W_{vi} = \int_{A^0} \left[\left(\delta \mathbf{E}^{(\mathbf{m})\mathbf{l}}\right)^T \mathbf{N} + \delta \mathbf{c}^T \mathbf{M} + \left(\delta \mathbf{E}^{(\mathbf{s})}\right)^T \mathbf{Q} \right] dA^0 + \int_{A^0} \delta \partial \mathbf{w}_\mathbf{0}^T \widetilde{\mathbf{N}}\, \partial \mathbf{w}_\mathbf{0}\, dA^0 \tag{4}$$

$\mathbf{c}$, $\mathbf{E}^{(\mathbf{s})}$, $\partial \mathbf{w}_\mathbf{0}$ and $\mathbf{E}^{(\mathbf{m})\mathbf{l}}$ being the vectors of curvatures, out-of-plane shear strains, derivatives of w_0 and linear part of middle plane strains respectively:

$$\mathbf{c} = \begin{bmatrix} \dfrac{\partial \vartheta_y}{\partial x} \\ -\dfrac{\partial \vartheta_x}{\partial y} \\ \dfrac{\partial \vartheta_y}{\partial y} - \dfrac{\partial \vartheta_x}{\partial x} \end{bmatrix} \quad ; \quad \mathbf{E}^{(\mathbf{s})} = \begin{bmatrix} 2E_{xz} \\ 2E_{yz} \end{bmatrix}$$

$$\mathbf{E}^{(\mathbf{m})\mathbf{l}} = \begin{bmatrix} \dfrac{\partial u_0}{\partial x} \\ \dfrac{\partial v_0}{\partial y} \\ \dfrac{\partial u_0}{\partial y} + \dfrac{\partial v_0}{\partial x} \end{bmatrix} \quad ; \quad \partial \mathbf{w_0} = \begin{bmatrix} \dfrac{\partial w_0}{\partial x} \\ \dfrac{\partial w_0}{\partial y} \end{bmatrix}$$

N, **M** and **Q** are the vectors of membrane forces, moments and shear forces per unit length; $\widetilde{\mathbf{N}}$ is a matrix containing the membrane forces:

$$\mathbf{N} = \begin{bmatrix} N_x \\ N_y \\ N_{xy} \end{bmatrix} \quad ; \quad \mathbf{M} = \begin{bmatrix} M_x \\ M_y \\ M_{xy} \end{bmatrix} \quad ; \quad \mathbf{Q} = \begin{bmatrix} Q_x \\ Q_y \end{bmatrix} \quad ; \quad \widetilde{\mathbf{N}} = \begin{bmatrix} N_x & N_{xy} \\ N_{xy} & N_y \end{bmatrix}$$

The integrals in (4) are performed over the middle surface A^0 of the plate, because to obtain (4) from (1) integration along z is carried out.

In the most general case of asymmetric laminate, the internal force and moment resultants per unit length are related to the strains by the constitutive equations [1]:

$$\begin{aligned} \mathbf{N} &= \mathbf{A}\,\mathbf{E}^{(\mathbf{m})} + \mathbf{B}\,\mathbf{c} \\ \mathbf{M} &= \mathbf{B}\,\mathbf{E}^{(\mathbf{m})} + \mathbf{D}\,\mathbf{c} \\ \mathbf{Q} &= \mathbf{D}^{(\mathbf{s})}\,\mathbf{E}^{(\mathbf{s})} \end{aligned} \tag{5}$$

where the constitutive matrices of the laminate are:

$$\mathbf{A} = \sum_{k=1}^{n} \mathbf{D}_k^{(\mathbf{m})} \left(z_k - z_{k-1} \right) \quad ; \quad \mathbf{B} = \sum_{k=1}^{n} \mathbf{D}_k^{(\mathbf{m})} \frac{z_k^2 - z_{k-1}^2}{2}$$

$$\mathbf{D} = \sum_{k=1}^{n} \mathbf{D}_k^{(\mathbf{m})} \frac{z_k^3 - z_{k-1}^3}{3} \quad ; \quad \mathbf{D}^{(\mathbf{s})} = \frac{1}{\chi} \sum_{k=1}^{n} \mathbf{D}_k^{(\mathbf{s})} \left(z_k - z_{k-1} \right)$$

$\mathbf{D}_k^{(\mathbf{m})}$ and $\mathbf{D}_k^{(\mathbf{s})}$ are the in-plane and shear constitutive matrices of the k^{th} ply respectively; z_k and z_{k-1} are the z coordinates (with respect to the middle plane) of the upper and lower surface of the k^{th} ply; n is the total number of plies; χ is the shear correction factor. In (5) $\mathbf{E}^{(\mathbf{m})}$ contains also the nonlinear terms of middle plane strains. In general an orthotropic material behaviour is considered, so that isotropic behaviour can also be modelled as a special case.

The kinematic assumptions (2) lead also to the following expression of the external work:

$$\delta W_{ve} = \int_{A^0} \delta \mathbf{V}^T \mathbf{f}_\mathbf{s}^\mathbf{0}\, dA^0 + \int_{\partial A^0} \delta \mathbf{V}^T \mathbf{f}_\mathbf{l}^\mathbf{0}\, dl^0 - \int_{A^0} \delta \mathbf{V}^T \mathbf{I}^\mathbf{0}\, \ddot{\mathbf{V}}\, dA^0 \tag{6}$$

$\mathbf{f_s^0}$ and $\mathbf{f_l^0}$ being the surface and boundary load vectors, $\mathbf{I}^0$ being the inertia matrix and $\mathbf{V}$ being the degrees of freedom vector:

$$\mathbf{V}^T = \begin{bmatrix} u_0 & v_0 & w_0 & \vartheta_x & \vartheta_y \end{bmatrix}$$

Equating (4) and (6) and introducing the nodal interpolation of degrees of freedom:

$$\mathbf{V} = \mathbf{H}\,\boldsymbol{\Delta}$$
$$\mathbf{E^{(m)l}} = \mathbf{B^{(m)l}}\boldsymbol{\Delta} \quad ; \quad \mathbf{c} = \mathbf{B^{(f)}}\boldsymbol{\Delta} \quad ; \quad \mathbf{E^{(s)}} = \mathbf{B^{(s)}}\boldsymbol{\Delta} \quad ; \quad \partial\mathbf{w_0} = \mathbf{B^{(m)nl}}\boldsymbol{\Delta}$$

the principle of virtual displacements (1) can be rewritten in the form:

$$\delta\boldsymbol{\Delta}^T \int_{A^0} \mathbf{H}^T \mathbf{f_s^0}\, dA^0 + \delta\boldsymbol{\Delta}^T \int_{\partial A^0} \mathbf{H}^T \mathbf{f_l^0}\, dl^0 - \delta\boldsymbol{\Delta}^T \int_{A^0} \mathbf{H}^T \mathbf{I^0}\, \mathbf{H}\, dA^0\, \ddot{\boldsymbol{\Delta}} =$$
$$= \delta\boldsymbol{\Delta}^T \int_{A^0} \left[\left(\mathbf{B^{(m)l}}\right)^T \mathbf{N} + \left(\mathbf{B^{(f)}}\right)^T \mathbf{M} + \left(\mathbf{B^{(s)}}\right)^T \mathbf{Q} \right] dA^0 + \delta\boldsymbol{\Delta}^T \int_{A^0} \left(\mathbf{B^{(m)nl}}\right)^T \widetilde{\mathbf{N}}\, \mathbf{B^{(m)nl}}\, dA^0\, \boldsymbol{\Delta}$$

where $\boldsymbol{\Delta}$ is the vector of nodal degrees of freedom, containing as many subvectors analogous to $\mathbf{V}$ as the nodes of the finite element model are. Finally, applying the principle of virtual displacements, the dynamic equilibrium equation for the discretized plate is obtained:

$$\mathbf{R_s^0} + \mathbf{R_l^0} - \mathbf{M}\,\ddot{\boldsymbol{\Delta}} = \mathbf{F^l} + \mathbf{K^{nl}}\boldsymbol{\Delta} \qquad (7)$$

Here $\mathbf{R_s^0}$ and $\mathbf{R_l^0}$ are the surface and boundary external load vectors, $\mathbf{M}$ is the mass matrix, $\mathbf{F^l}$ is the linear part of the internal forces vector and $\mathbf{K^{nl}}$ is the nonlinear (geometrical) stiffness matrix. $\mathbf{R_s^0}$, $\mathbf{R_l^0}$, $\mathbf{F^l}$, $\boldsymbol{\Delta}$ and $\ddot{\boldsymbol{\Delta}}$ refer to time *t*.

Instead of calculating the $\mathbf{B^{(s)}}$ matrix according to the standard procedure of isoparametric elements, a particular formulation proposed by Hughes has been adopted, in which the out-of-plane shear strains are interpolated separately rather than deduced from nodal displacements and rotations. This element ensures low shear locking without the need for reduced or selective integration, thus without rank reduction [6]. Three- and four-node elements are available [7].

The in-plane stiffness has been added to flexural behaviour of Hughes' element, following the usual isoparametric formulation; then a flat shell element has been implemented with a simple coordinates change by means of rotation matrices, thus allowing to locate the finite element in a three-dimensional frame. Obviously the third rotation ϑ_z must be added in this case.

By expressing velocities and accelerations in terms of the nodal degrees of freedom, according to the central difference method [3]:

$$\dot{\boldsymbol{\Delta}}(t)=\frac{\boldsymbol{\Delta}(t+h)-\boldsymbol{\Delta}(t-h)}{2h}$$
$$\ddot{\boldsymbol{\Delta}}(t)=\frac{\boldsymbol{\Delta}(t+h)-2\boldsymbol{\Delta}(t)+\boldsymbol{\Delta}(t-h)}{h^2} \tag{8}$$

a system of linear algebraic equations can be derived from (7):

$$\frac{\mathbf{M}}{h^2}\boldsymbol{\Delta}(t+h) \;=\; \mathbf{R}^{\mathbf{0}}(t)-\mathbf{F}(t)+\frac{2\mathbf{M}}{h^2}\boldsymbol{\Delta}(t)-\frac{\mathbf{M}}{h^2}\boldsymbol{\Delta}(t-h) \tag{9}$$

where $\mathbf{R}^{\mathbf{0}}=\mathbf{R}_{\mathbf{s}}^{\mathbf{0}}+\mathbf{R}_{\mathbf{l}}^{\mathbf{0}}$ is the external load vector and $\mathbf{F}=\mathbf{F}^{\mathbf{l}}+\mathbf{K}^{\mathbf{nl}}\boldsymbol{\Delta}$ is the internal load vector. The equations, to be solved for the unknowns $\boldsymbol{\Delta}(t + h)$, are uncoupled if the mass matrix is diagonal; thus a lumped matrix has been chosen. To ensure that the mass matrix remains diagonal in every coordinate system, the same mass has been attributed to all the nodal displacements, and all the three nodal rotations have been assigned the same rotary inertia.

In order to extend the capabilities of the program and make it possible to perform also static analyses, a dynamic relaxation [8] algorithm has been subsequently implemented. With this technique, and taking advantage of the explicit integration scheme, static computations in presence of strongly nonlinear phenomena, such as elastic instability, can be carried out in a robust and efficient way. As known, the dynamic relaxation technique consists in introducing an artificial viscous damping action, thus equation (7) becomes:

$$\mathbf{R}_{\mathbf{s}}^{\mathbf{0}}+\mathbf{R}_{\mathbf{l}}^{\mathbf{0}}-\mathbf{C}\dot{\boldsymbol{\Delta}}-\mathbf{M}\ddot{\boldsymbol{\Delta}} \;=\; \mathbf{F}^{\mathbf{l}}+\mathbf{K}^{\mathbf{nl}}\boldsymbol{\Delta} \tag{10}$$

If constant external loads are applied, the transient solution of the system (10) converges to its steady state part, which satisfies the equilibrium equations:

$$\mathbf{R}_{\mathbf{s}}^{\mathbf{0}}+\mathbf{R}_{\mathbf{l}}^{\mathbf{0}} \;=\; \mathbf{F}^{\mathbf{l}}+\mathbf{K}^{\mathbf{nl}}\boldsymbol{\Delta}$$

Since in this case the aim of the explicit analysis is to reach a static solution, which depends only on the stiffness properties of the structure contained in the internal load vector **F** on the right hand side, while the transient part of the solution is not of interest, the mass matrix **M** need not reproduce the real inertial properties of the structure. In the present study, during the dynamic relaxation calculations the elements of **M** were given fictitious values, obtained with a procedure based upon Gershgorin's circle theorem which improves the computational efficiency of the algorithm [8].

When the damping actions are present, by substituting expressions (8) in the equation of motion (10) a new system of linear algebraic equations is derived, which replaces (9):

$$\left(\frac{\mathbf{M}}{h^2}+\frac{\mathbf{C}}{2h}\right)\boldsymbol{\Delta}(t+h) \;=\; \mathbf{R}(t)-\mathbf{F}(t)+\frac{2\mathbf{M}}{h^2}\boldsymbol{\Delta}(t)+\left(\frac{\mathbf{C}}{2h}-\frac{\mathbf{M}}{h^2}\right)\boldsymbol{\Delta}(t-h) \tag{11}$$

To preserve the simplicity of uncoupled equations in the system (11), the damping matrix **C** was set proportional to **M**, so that both matrices were diagonal; the ratio between the elements of **C** and the elements of **M** was adjusted in order to approximate the condition of critical damping for the first (fictitious) vibration mode, because in this way the number of iterations required for convergence is the lowest [8].

A simplified contact model has been implemented to allow a dynamic analysis of impact of external bodies on the plate or shell. The impactor is considered a rigid body in translational motion (thus treated as a heavy material point), and the force taking place between impactor and laminate is concentrated on one node. The indentation is determined as the difference between the displacement of the impactor and that of the node on which contact is intended to occur; the contact force P is related to the indentation α by the Hertz's generalized contact law [1]:

$$P \;=\; C\,\alpha^{n} \tag{12}$$

At present, contact and large deflections are the only nonlinear phenomena accounted for in the numerical model. In particular, no post-failure degradation criterion of the material properties has been implemented, so that the elastic constants do not change during the simulations even if failure is predicted. This simplifying assumption makes it possible to obtain reliable results as long as the actual material damage is limited. Given the absence of a damage model, for the sake of simplicity the same contact law (12) is employed for both loading and unloading phase of contact.

Although the central difference method usually requires small time steps because the algorithm is conditionally stable [3], this scheme has been preferred because it lets the program open to a number of future improvements, including the implementation of damage models of the material. Indeed the explicit integration makes it possible to derive a linear system of algebraic equations (see (9) and (11)) whatever the nonlinear effect one may introduce. Otherwise an iterative solution process would be needed within each time step, which would make the computation extremely expensive. In addition, the choice of a lumped mass matrix, which can always be maintained regardless of the other features of the model, results in a system of decoupled equations, thus the necessity of implementing suitable solution algorithms is avoided.

References for chapter 1

1. Abrate S. *Impact on composite structures*. Cambridge: Cambridge University Press, 1998.

2. Ghelli D. *Dynamic numerical analysis of composite plates and shells with geometrical nonlinearity*. In: Proceedings of the ANASS 2007 Special Workshop, Sorić J, Gruttmann F, Wagner W, editors, p. 161-168. Zagreb (HR): Croatian Society of Mechanics, 2007.
3. Bathe KJ. *Finite element procedures in engineering analysis*. Englewood Cliffs, New Jersey: Prentice-Hall, 1982.
4. Mase GT, Mase GE. *Continuum mechanics for engineers*, 2nd ed. Boca Raton, Florida: CRC Press, 1999.
5. Timoshenko SP, Woinowsky-Krieger S. *Theory of plates and shells*, 2nd ed. Singapore: McGraw-Hill, 1959.
6. Hughes TJR, Tezduyar TE. *Finite elements based upon Mindlin plate theory with particular reference to the four-node bilinear isoparametric element*. J Appl Mech-T ASME 1981;48(3):587-596.
7. Hughes TJR. *The finite element method - linear static and dynamic finite element analysis*. Englewood Cliffs, New Jersey: Prentice-Hall, 1987.
8. Underwood P. *Dynamic relaxation*. In: Computational methods for transient analysis, Belytschko T, Hughes TJR, editors, p. 245-265. Amsterdam: North-Holland, 1983.

CHAPTER 2

Discussion on the analogy between low velocity impact and quasi-static indentation*

2.1. Introduction

Carbon Fibre Reinforced Polymers (CFRP) are widely used in applications requiring high specific strength and stiffness. Well known problems arise, however, when the resistance of this kind of material to foreign object impact is considered. The essentially brittle mechanical behaviour of CFRPs makes them vulnerable even to low velocity and low energy impact [1-4].

Impacts are usually classified according to initial velocity, because collisions at different velocities can lead to different dynamic responses and damage in the target. Dropping a tool is considered an example of what is called a "low velocity" impact, while, for instance, small stones striking an airplane during takeoff are said to cause a "high velocity" impact [4]. A more rigorous definition of these velocity fields is, however, required prior to investigation of different phenomena taking place in either field.

At least two definitions of "low velocity" impact can be found in the literature [5]. The one proposed by Robinson and Davies [6] and adopted by Abrate [4] is based on the propagation of elastic waves through the thickness of the impacted laminate. When the ratio between initial velocity and phase velocity is smaller than the strain which causes failure in the thickness direction, the role played by this kind of wave is considered negligible and impact velocity is said to be "low". This defines a low velocity collision as one in which possible damage is caused by overall deformation of the laminate, thought of as a two-dimensional solid, rather than by local compression of the material at the impact point, which should be treated as a three-dimensional phenomenon.

Another definition is proposed by Sjöblom et al. [7]: "by low velocity we mean an impact velocity low enough to justify a static analysis of the response of the structure". Hence a collision should be said to take place at low velocity if the contact duration is much greater than the time required for flexural elastic waves to reach the boundary and be reflected back, as pointed out in [8-10]. Strain rate effects on material behaviour must also be negligible [7]; this

* A revised version of this study has been accepted for publication as Ghelli D, Minak G. *Comparison between low velocity impact and quasi-static indentation tests on CFRP composite laminates*. In: Composite laminates: properties, performance and applications, Columbus F, editor. Nova Science Publishers, Hauppauge, NY.

condition is met by many classes of polymer matrix composites, but some exceptions, e. g. polyester-glass, are known [4, 10].

The two definitions are quite different. According to the first one, the transition velocity between the "low" and "high" fields depends on laminate material properties only (typical values are 10 ÷ 20 m/s [6]); according to the second one, it also depends on the dimensions and boundary conditions of the laminate and on the impactor mass, ranging from tens of m/s to cm/s [7].

Comparisons between low and high velocity impacts, in the sense of the first definition, show dissimilar dynamic response and damage [4, 6, 11] which call for high velocity impact to be considered as a separate problem [7]. On the other hand, experimental evidence exists that damage caused by low velocity impact and quasi-static indentation is similar, if not equivalent [7, 9, 11-16]. An undoubted analogy would be interesting for research purposes, since both numerical modelling and experimental testing are much simpler for a static problem than for a dynamic one [10, 14].

For this reason several available studies concern the mechanical behaviour of composite laminates subjected to quasi-static indentation, for instance [8, 16-19]. The most common justification for this choice is based upon the same arguments used by Sjöblom et al. [7] to introduce their definition of low-velocity impact: when certain conditions are met, dynamic effects are thought to be negligible. Therefore, from the above considerations about which velocity can be named "low", one may conclude that both the reported definitions should be satisfied to attempt a comparison between quasi-static indentation and impact.

Some researchers carry out such a comparison in order to establish to what extent the resulting damage is similar. In [7] force-displacement diagrams are presented that show quite good agreement between quasi-static and dynamic tests; the damage in the laminate section also appears very similar. In [10] an energy balance approach is employed to relate impact energy and contact force and is verified experimentally. This model is based on the hypothesis that all the kinetic energy of the impactor is converted in work done on the specimen (measurable as the area enclosed by the load-displacement curve). The relationship based upon data obtained in indentation tests can also be applied to low velocity impact with good accuracy, except for the case of polyester-glass composites which exhibit rate-dependent constitutive behaviour. In [11] the difference in the delamination area for indented and impacted specimens is within the scatter of experimental data; permanent indentation, however, seems larger in quasi-static tests (the total work done during the loading phase of indentation/impact being the same). Elber [12] concludes that a static analysis can be used to characterize the impact resistance of a material; he remarks, however, that slightly more fibre damage and less extensive delamination is observed in the impacted specimens than in the indented ones. In [13] the relationship between delamination area and maximum contact force is examined; the results for indentation and impact are again identical, and also a force threshold value necessary to propagate delamination

is the same in both cases. Another comparison can be found in [14], where the authors state that static tests can be used in place of impact tests to characterize the low velocity impact response of a material, as regards contact force values and extent of delamination. Nevertheless, a diagram is reported where the experimental relationship between impact energy and maximum contact force is not the same for the two cases. In [15] empirical relationships are established between imparted energy and dent depth induced on laminates, with similar results for impact and quasi-static indentation. [9] and [16] also present similar force-displacement curves. On the other hand, numerical simulations of the dynamic behaviour of composite laminates subjected to impact show that the main features of the transient response (contact duration, maximum contact force, maximum plate deflection, maximum stresses) change when the impactor mass and velocity are modified, initial energy remaining constant [20]. This appears to be in contrast with the results reported in [6], indicating that energy is the only significant parameter of a low velocity impact.

The above observations suggest that, even if several research results seem to support the equivalence between quasi-static indentation and low velocity impact, some evidence exists that this equivalence is not always valid, and in any case it is not fully understood. Therefore further experimental testing appears necessary to provide insight into this important topic, partly because only a few recent papers specifically deal with this subject.

The present study describes the outcome of a comparison between the effects of impact and indentation on CFRP quasi-isotropic laminated plates. Both types of experimental test were performed in the same conditions; the impact velocity ranged from 3 to 5 m/s, while the energy varied from 6 to 18 J approximately. Two specimen dimensions and two boundary conditions were considered. The analysis of the experimental results was completed with a finite element numerical simulation. The specimens were inspected after testing, to assess the types and extent of damage, mainly by visual observation, but also by optical microscope and Scanning Electron Microscope (SEM).

The comparison between quasi-static and dynamic tests showed that the induced damage is qualitatively similar as regards the types of failure observed. Experimental and numerical results made it possible to recognize three characteristic contact force thresholds related to the main steps in the progression of damage which are equal in the two types of tests. The energy absorbed during impact and indentation was found to be the same. On the other hand a larger delaminated area was recorded in the quasi-static case, while evidence existed that in impact tests a more severe damage was produced, probably in the form of more significant localized fibre fracture near the impact point.

2.2. Experimental procedure

The specimens tested in this study were 16 ply quasi-isotropic plane laminates with stacking sequence $[0_2/90_2/45/-45/45/-45]_S$, made of T300 carbon fibre-epoxy resin matrix prepregs. Rectangular plates measuring 247 by 250 mm were obtained by curing in an autoclave. The specimen thickness was 2.7 ± 0.05 mm; the average density of the material was 1490 ± 10 kg/m^3; the values of the in-plane elastic moduli and strengths supplied by the manufacturer are reported in table 1.

2.2.1. *Low velocity impact tests*

Low velocity impact tests were performed by means of a drop-weight machine (see figure 1). The impactor mass was 1.22 ± 0.01 kg; three different drop heights of 0.5, 1 and 1.5 m, corresponding to impact velocities of 3, 4 and 5 m/s approximately, and nominal impact energies of 6, 12 and 18 J, were chosen. As will be shown later, these energy levels did not cause penetration of the specimens.

Table 1 – Mechanical properties of the single ply of the laminates tested.

Elastic constants	
E_1	100 GPa
E_2	11 GPa
G_{12}	4.2 GPa
ν_{12}	0.28
In-plane strengths	
X_t	1270 MPa
X_c	1130 MPa
Y_t	30 MPa
Y_c	141 MPa
S	63 MPa

The laminates were placed in a clamping fixture which consisted of two steel rings fastened to a cylindrical base, so that the geometry of a circular plate was reproduced; impact occurred exactly at its centre. Two pairs of rings of 200 and 76 mm internal diameter, respectively, were used to test the impact response of specimens of different sizes (see figures 1c and 1d); the second diameter was chosen according to [21].

When a 200 mm diameter circular plate was simulated, the original 247 by 250 mm laminates were placed on the suitable clamping fixture; after impact, four smaller square specimens of 100 mm per side were obtained by cutting the original laminates (excluding two perpendicular 50 mm wide strips, centred on the median axes, containing the damaged zone) and were employed with the smaller rings for impact tests on 76 mm diameter plates. As explained in section 2.4, the delaminated area created by impact had an elongated shape; its largest extent was approximately 100 by 25 mm. The width of the central strips was much larger than the maximum delamination width, thus ensuring that the smaller specimens did not have any pre-existing damage before testing.

Two different boundary conditions were studied: full clamp and simple support. The first condition was accomplished by clamping the laminates between the two steel rings by four bolts; the second one was reproduced by simply placing the laminates on one ring (which was, obviously, fixed to the base) without using the second ring. It should be noted that the first arrangement was intended to prevent any motion of the plate boundary, both in-plane and out-

of-plane, while the central circular region was completely free to move; in the second condition the in-plane motion of any point of the plate was free, upward and downward motion was allowed in the region bounded by the inner ring diameter, while only upward displacement was possible outside this region. Two (in the case of larger laminates) or three (in the case of smaller laminates) tests were performed for each combination of specimen diameter, constraint condition and drop height.

Impact occurred exactly at the centre between the laminate and the hemispherical head (12.7 mm diameter) of a piezoelectric load cell attached to the impactor, which measured the contact force history (see figure 1b). The impactor fall and rebound velocity was calculated from the signal of a laser device placed 41 mm above the laminate upper surface. Both load cell and laser signals were acquired at 100 kHz sampling frequency, without any filtering in the measurement chain. An electromagnetic braking system stopped the impactor after rebound, preventing repeated strikes on the target. Further details on the impact facility can be found in [22].

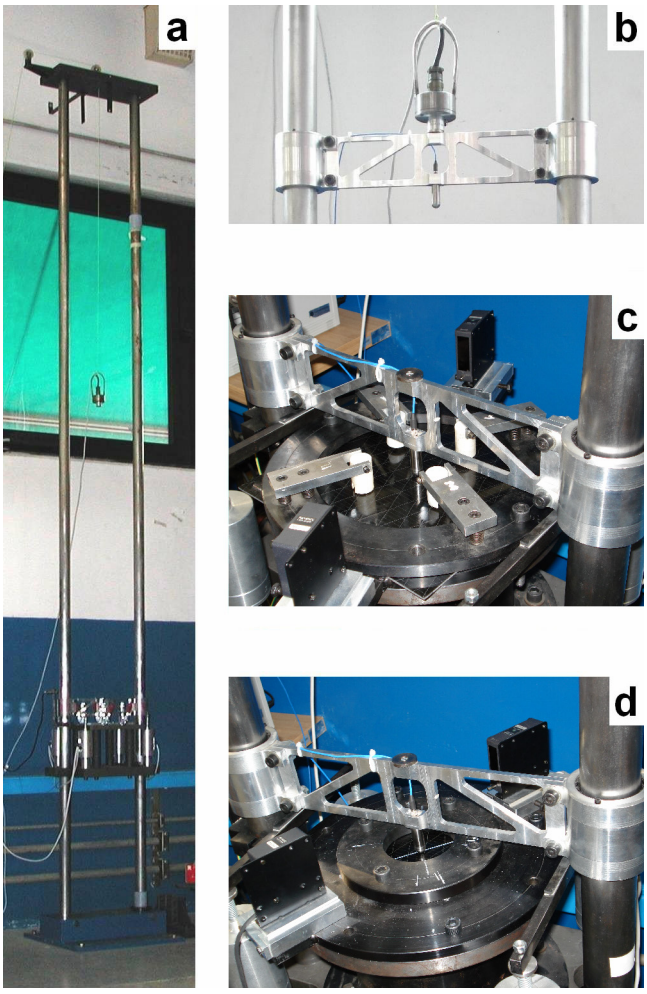

Figure 1 – Drop-weight impact tester. a) Overall view. b) Impactor; the piezoelectric load cell with hemispherical head is visible in the lowest part of the image, in central position. c) Clamping fixture with impactor, laser sensors and 200 mm diameter rings. d) Clamping fixture with impactor, laser sensors and 76 mm diameter rings.

The contact force signal was used to obtain the impactor displacement as a function of time by the second Newton law, as indicated in ASTM D7136M - 05 [23]: double numerical integration was performed with the initial conditions given by the laser sensor.

2.2.2. *Quasi-static indentation tests*

An Instron 8033 servo-hydraulic machine was used for quasi-static indentation tests, where the contact force was applied gradually rather than by means of a collision. The laminates were held by the same fixture used on the drop-weight rig, creating identical boundary conditions; to also ensure the same contact behaviour, the head of the impactor load cell was chosen as the indentor. The experiments were performed in displacement control, moving the indentor according to a sinusoidal displacement law at an average velocity of 0.1 mm/s.

The test plan of the quasi-static experiments was analogous to what is explained above for the dynamic ones: namely, all of the four combinations of specimen diameter and boundary conditions were covered with a similar number of tests. For each configuration, several values were chosen for the maximum displacement to be imparted to the indentor; these values were approximately within the range of maximum impactor displacements calculated for the impact tests.

2.2.3. *Specimen inspection*

After testing, all the specimens were first examined by visual inspection to assess the damage visible by the naked eye. In some laminates the central zone (near the impact or indentation point) was cut and incorporated in polyester resin; the obtained coupon was then cut along the 0° and 90° directions of the laminate and polished to observe its normal section by an optical microscope. To examine the external damage, some specimens were analysed, without cutting them, by a Scanning Electron Microscope.

2.3. Numerical modelling

The transient dynamic analysis of impact events was carried out by the finite element program described in chapter 1. The same code was used also for the numerical analysis of the quasi-static indentation tests, by means of the dynamic relaxation algorithm.

In the simulation of impact tests, the contact between laminate and impactor was modelled in a simplified way by applying the contact force as an external load only on the node where contact occurred, and introducing a nonlinear relationship between the contact force P and the indentation α, following the commonly accepted generalized Hertzian law [4]:

$$P = k\,\alpha^{3/2} \tag{1}$$

where the constant k was determined according to the formula proposed by Yang and Sun [24]:

$$k = \frac{4}{3}\frac{\sqrt{R}}{\dfrac{1-\nu^2}{E}+\dfrac{1}{E_2}}$$

In this expression E and ν are the Young's modulus and Poisson's coefficient of the impactor, R is the radius of curvature of its head, while E_2 is the transverse modulus of the composite material. With E = 210 GPa, ν = 0.3, R = 6.35 mm and E_2 = 11 GPa, the resulting value of k is $1.116 \cdot 10^9$ N/m$^{3/2}$.

Since in the quasi-static indentation the applied load was controlled by the test machine, in the relevant simulation the contact force was simply imposed as a concentrated load. To obtain the overall displacement of the indentor for a given force, the indentation determined according to the contact law was added to the calculated deflection of the specimen.

Before numerical analysis, a convergence test was performed to decide what mesh refinement was necessary to achieve reliable results. All of the discretizations used consisted of four-node elements, and covered the entire laminate surface, to account for bending-twisting coupling due to ±45° layers.

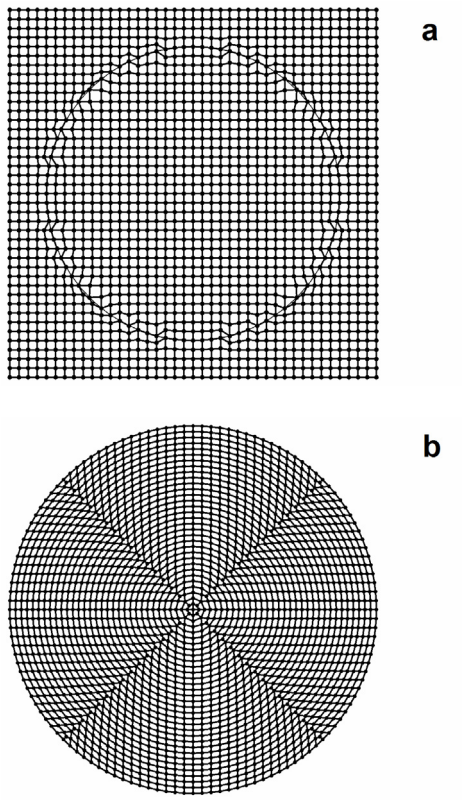

Figure 2 – Discretizations of the specimens employed for the numerical analysis. a) Discretization of the whole square laminate for the simply supported specimens. b) Discretization of the circular free zone of the clamped specimens.

In the case of simply supported specimens, the whole square laminate was discretized by a mesh of 1600 elements (figure 2a), obtaining satisfactory results. The mesh was uniform apart from some elements in the vicinity of the inner circumference of the supporting ring, which were slightly distorted in order to place their nodes exactly on that circumference. This made it possible to apply the simple support condition to them. In the case of clamped specimens, only their free region bounded by the inner circumference of the fixture was modelled. The discretizations were drawn in such a way that the elements had a regular shape and similar dimensions, in order to keep the time integration step as large as possible. The convergence test indicated that in order to achieve sufficient accuracy, especially as regards strains and stresses (as well as the contact force history in dynamic tests), a finer discretization, consisting of 2112 elements (figure 2b), was required.

Due to the lack of experimental values, the out-of-plane shear moduli G_{13} and G_{23} were assumed to be equal to G_{12} in all calculations, although this is not true also for transversally isotropic materials. A discussion on this approximation can be found in chapter 3, section 3.3. It is shown that the influence of the value of G_{23} is usually negligible with respect to the other simplifying assumptions, in particular the absence of a damage model.

2.4. Results of the experimental tests

As regards qualitative failure patterns of the material, no appreciable difference could be seen between impact and indentation tests. All laminates, both impacted and indented, showed back-face splitting starting from the impact point; a delaminated area, whose shape resembled

that of an ellipse or a rhombus, elongated in the direction of the fibres of the lowermost ply, was also clearly visible to the naked eye. After the higher energy events, several parallel surface splittings were noted; when the back-face splitting was held open by failures in internal layers, fibre fracture was also visible, especially in the 90° plies just above the external 0° plies. The indented (or impacted) side of the laminates loaded with the lowest energy levels showed only permanent indentation without failures; when a higher energy was imparted, the dent became much larger due to clearly visible matrix and fibre failure. However, no test approached the penetration of the laminate. Another failure mode was fibre microbuckling, observed on the front laminate surface in some cases (see the SEM picture in figure 3).

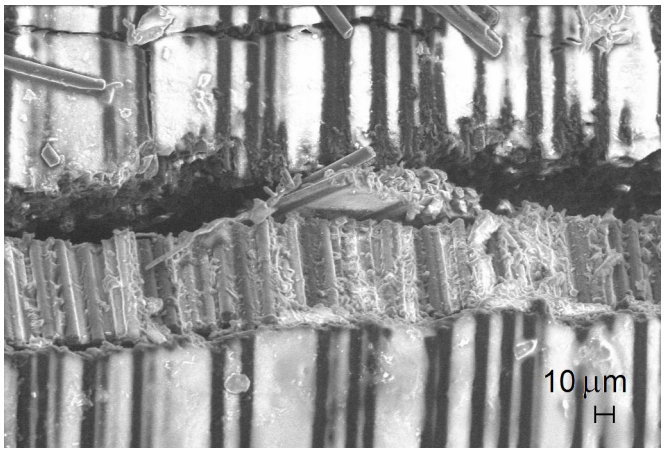

Figure 3 – SEM photograph of a fibre microbuckling band observed on the indented surface of a specimen.

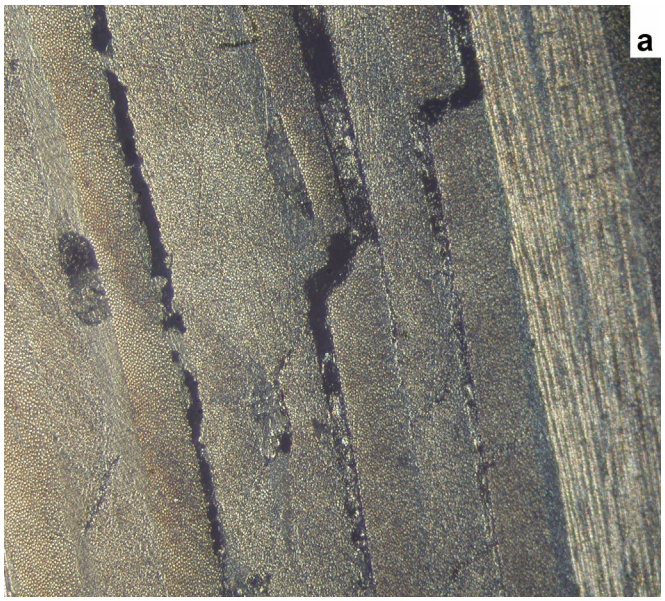

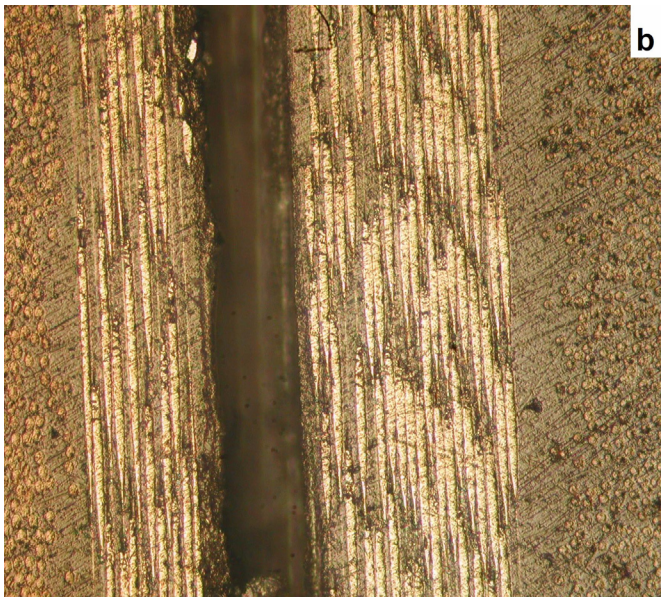

Observation of some sectioned specimens by an optical microscope showed matrix cracking, delamination and fibre fracture (two examples are reported in figure 4). The largest delamination was between the two external 0° plies on the back surface and the adjacent 90° plies; measurement of the diagonals of this delamination under the microscope confirmed the validity of the estimates made by visual inspection of the external surface of the specimen. Therefore a good approximation of the projected delaminated area was obtained as the area

Figure 4 – Sectioned laminates observed with an optical microscope. a) Delamination between 90° and 45° layers (top right); delamination and matrix cracking in the central group of plies with +/-45° fibre orientation. b) Delamination between two adjacent plies with the same fibre orientation (90°).

of a rhombus whose diagonals were measured visually in the principal directions of the lowermost ply. The following quantitative results refer to these estimates. In general, in the laminates which underwent higher energy events, delaminations in all interfaces between plies were observed. Internal alternated ±45° layers also showed extended delamination.

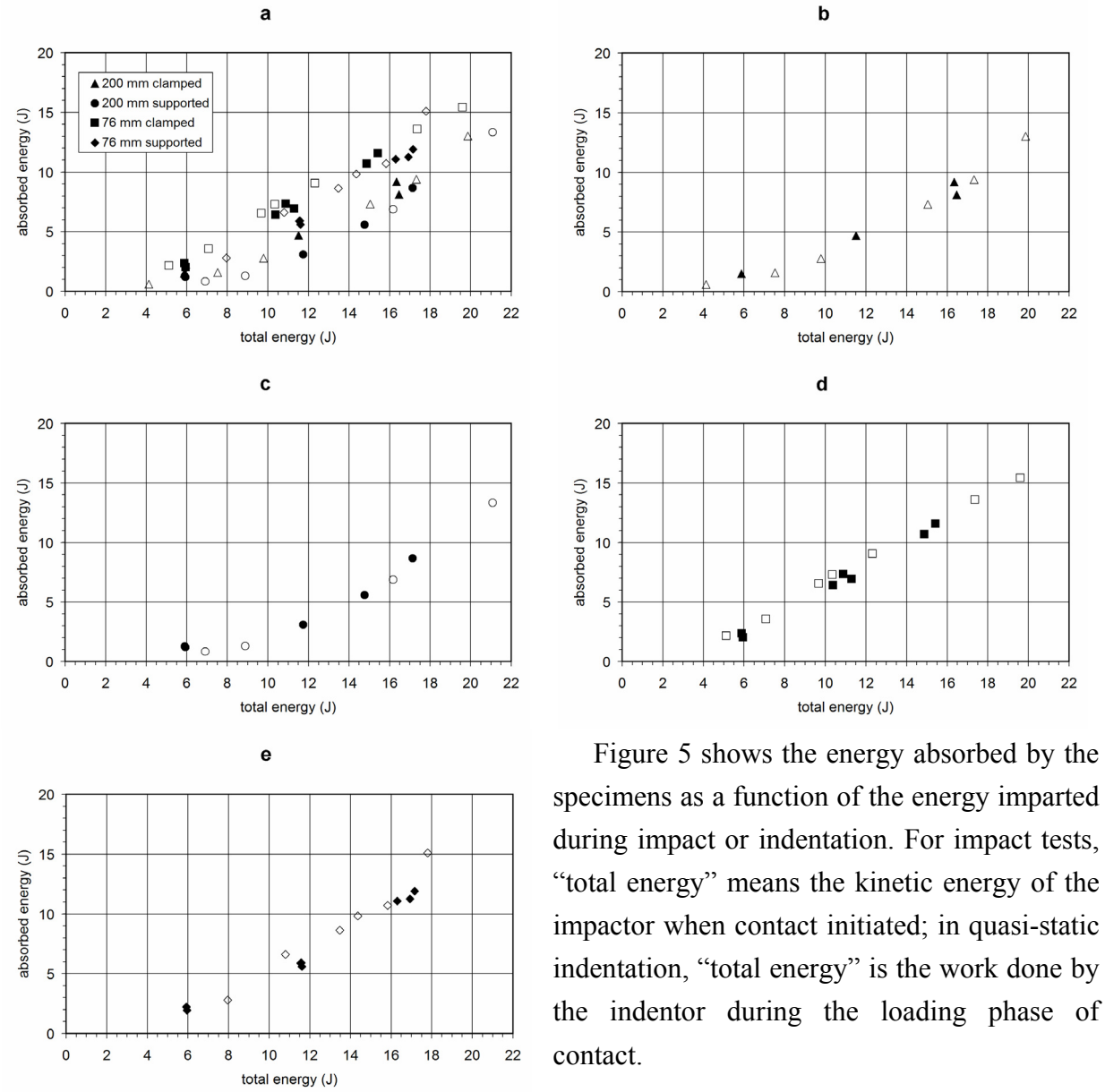

Figure 5 – Absorbed energy during impact or indentation as a function of total energy. Filled symbols refer to impact tests, empty symbols refer to indentation tests. a) Overall diagram of the four test configurations. b) Clamped 200 mm specimens. c) Simply supported 200 mm specimens. d) Clamped 76 mm specimens. e) Simply supported 76 mm specimens.

Figure 5 shows the energy absorbed by the specimens as a function of the energy imparted during impact or indentation. For impact tests, "total energy" means the kinetic energy of the impactor when contact initiated; in quasi-static indentation, "total energy" is the work done by the indentor during the loading phase of contact.

As figure 5a illustrates, the points relevant to different test conditions fall on different lines. The stiffer configurations absorbed a larger fraction of the total energy because they can store a lesser amount of elastic energy before damage initiation (see chapter 3, section 3.5). This explains why the energy absorption was larger in the smaller laminates, and also in the clamped specimens with respect to the supported ones. However, in each of the groups of

coupons tested in the same configuration the energy absorption showed no appreciable difference between quasi-static and dynamic tests, as can be seen in figures 5b-e.

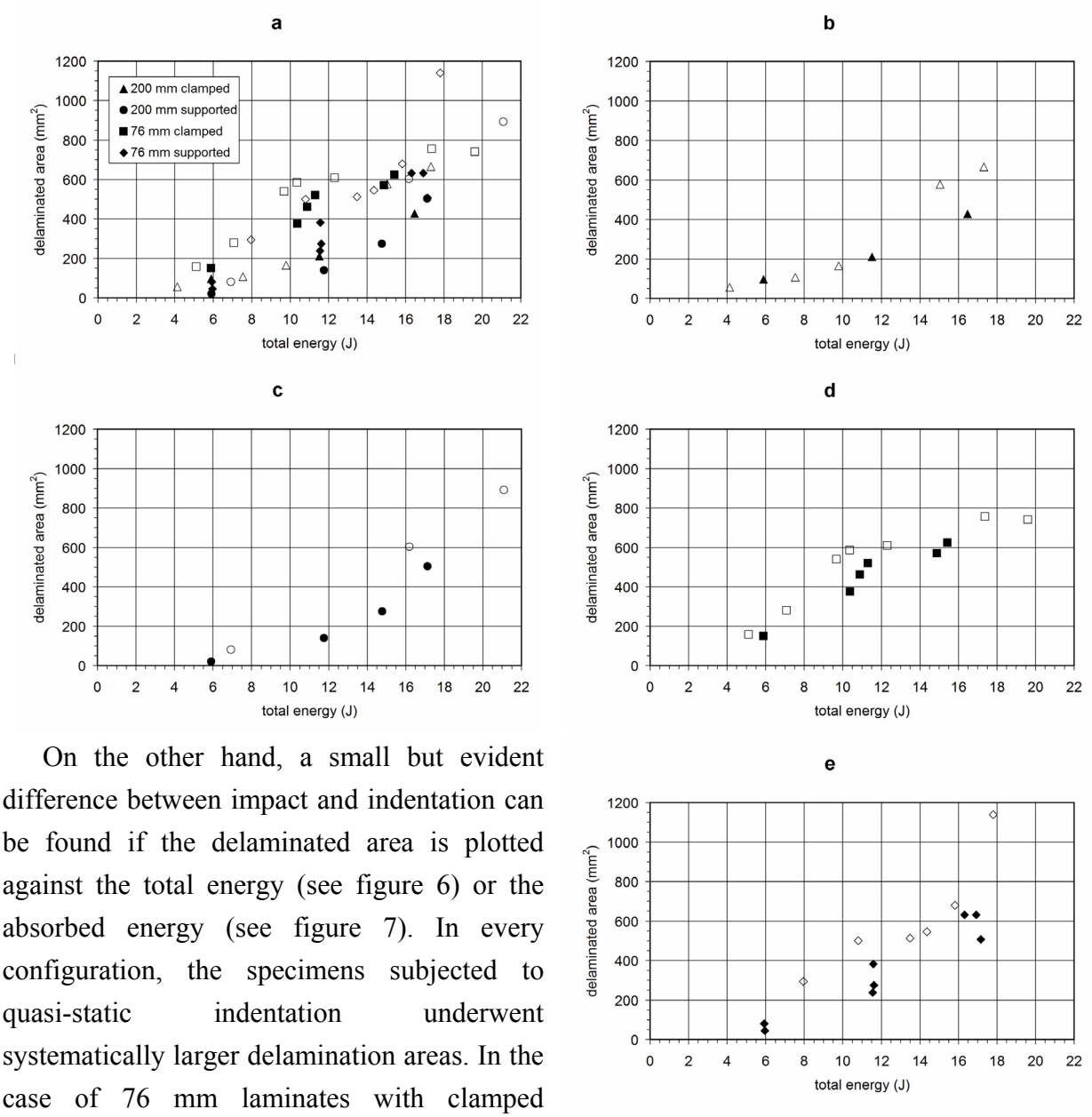

Figure 6 – Delaminated area as a function of total energy. Filled symbols refer to impact tests, empty symbols refer to indentation tests. a) Overall diagram of the four test configurations. b) Clamped 200 mm specimens. c) Simply supported 200 mm specimens. d) Clamped 76 mm specimens. e) Simply supported 76 mm specimens.

On the other hand, a small but evident difference between impact and indentation can be found if the delaminated area is plotted against the total energy (see figure 6) or the absorbed energy (see figure 7). In every configuration, the specimens subjected to quasi-static indentation underwent systematically larger delamination areas. In the case of 76 mm laminates with clamped boundary, the data obtained in impact and indentation seem to approach each other at the highest energy level. It should be noted, however, that in these cases the length of the major diagonal of the delaminated zone reached approximately 75 mm after 10 ÷ 12 J events. Thus it is likely that at higher energies further propagation of delamination was prevented by the clamping rings.

The diagram of delaminated area versus absorbed energy is of particular interest because for low velocity impacts a unique relationship can be found between these two quantities, regardless of the specimen diameter and boundary condition [6] (see chapter 3). Figure 7a confirms the

validity of this finding for the present impact tests, and indicates that a similar correlation holds for quasi-static indentation; however, in the latter case the delaminated area was greater in every test configuration (see figures 7b-e), or in other words a larger amount of energy was necessary in the dynamic tests to create the same damage area observed after the quasi-static ones.

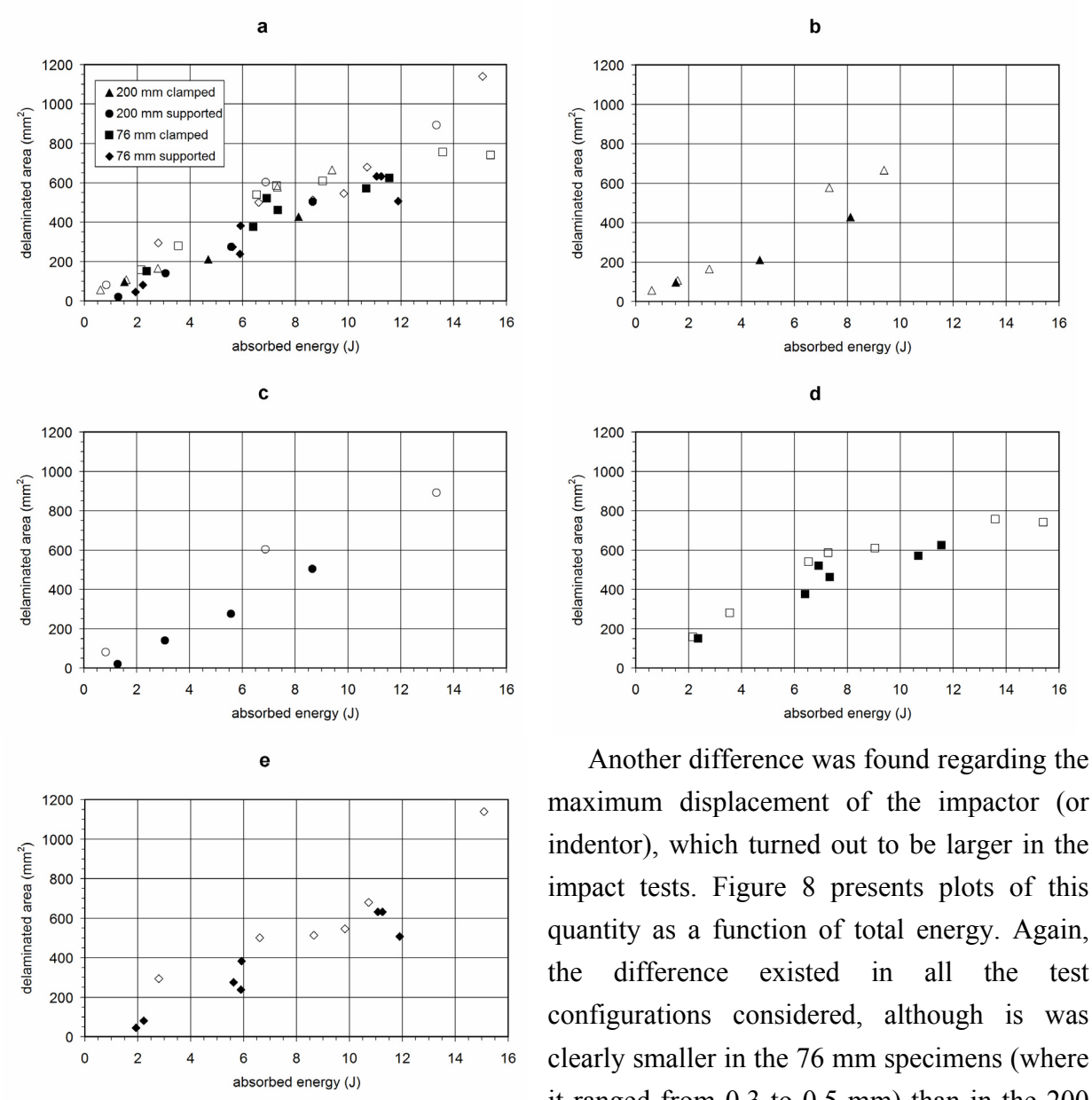

Figure 7 – Delaminated area as a function of the energy absorbed during impact or indentation. Filled symbols refer to impact tests, empty symbols refer to indentation tests. a) Overall diagram of the four test configurations. b) Clamped 200 mm specimens. c) Simply supported 200 mm specimens. d) Clamped 76 mm specimens. e) Simply supported 76 mm specimens.

Another difference was found regarding the maximum displacement of the impactor (or indentor), which turned out to be larger in the impact tests. Figure 8 presents plots of this quantity as a function of total energy. Again, the difference existed in all the test configurations considered, although is was clearly smaller in the 76 mm specimens (where it ranged from 0.3 to 0.5 mm) than in the 200 mm (where it was close to 1 mm).

It is also interesting to examine the relationship between the delaminated area and the maximum contact force. Similarly to what happens with absorbed energy, in low velocity impact tests this relationship does not depend

on the specimen dimensions and boundary conditions [25] (see chapter 3). Figure 9 illustrates that this proved true also in the present research and, most importantly, no difference could be detected between impact and indentation.

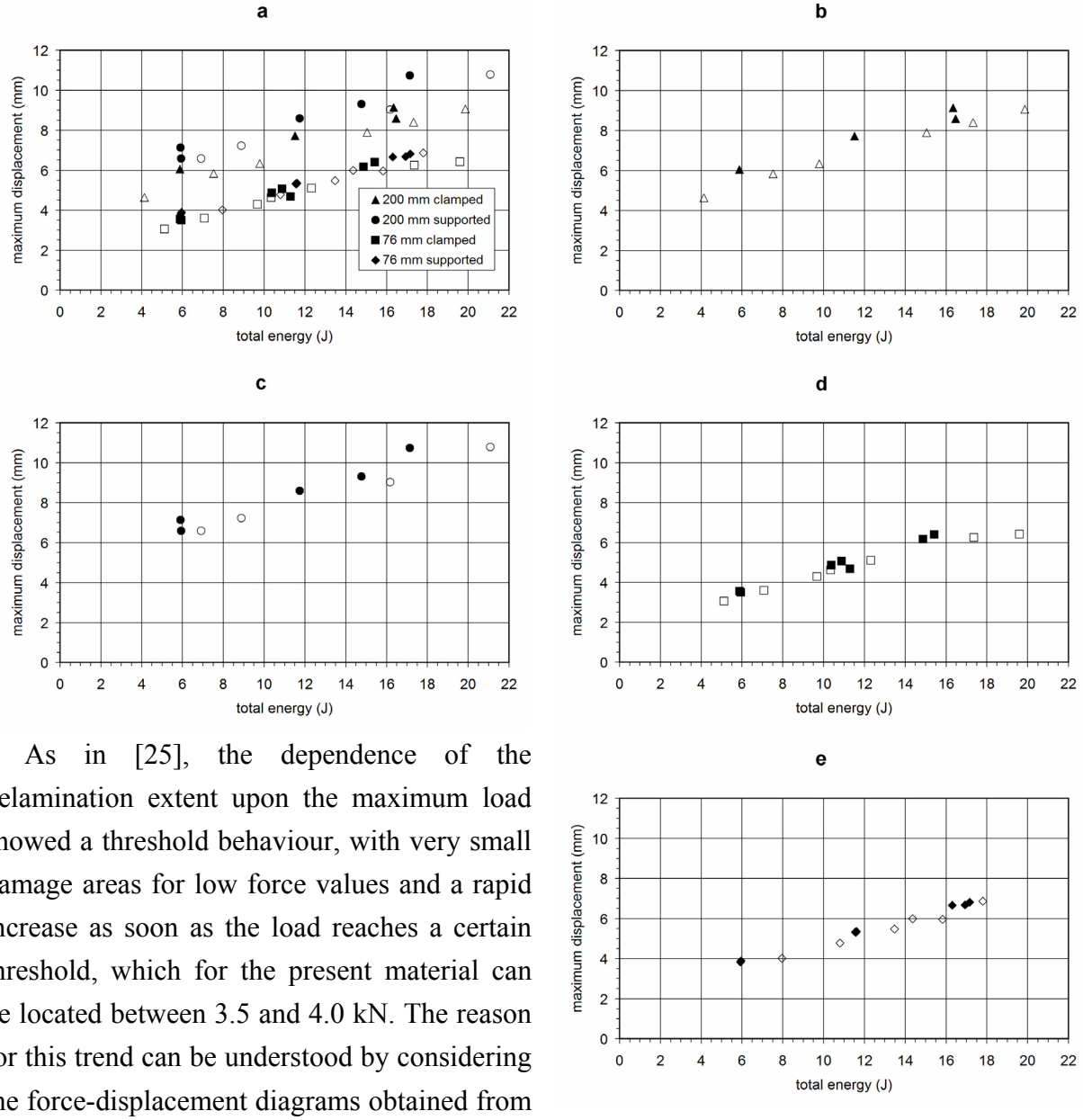

Figure 8 – Maximum displacement of the impactor or indentor during impact or indentation, as a function of total energy. Filled symbols refer to impact tests, empty symbols refer to indentation tests. a) Overall diagram of the four test configurations. b) Clamped 200 mm specimens. c) Simply supported 200 mm specimens. d) Clamped 76 mm specimens. e) Simply supported 76 mm specimens.

As in [25], the dependence of the delamination extent upon the maximum load showed a threshold behaviour, with very small damage areas for low force values and a rapid increase as soon as the load reaches a certain threshold, which for the present material can be located between 3.5 and 4.0 kN. The reason for this trend can be understood by considering the force-displacement diagrams obtained from the indentation tests (figure 10). As soon as the indentor displacement was large enough for the threshold load to be attained, the contact force could not increase any more, because further increase of the displacement led to a rapid propagation of the delamination. The progression of damage was clearly signalled by significant noise during the tests, accompanied by the evident load drops visible in figure 10. The existence of another contact force threshold, probably smaller than 2 kN, can also be hypothesized based on the data reported in figure 9.

This should be the limit load at which the first delamination (observed in all the specimens) was created, as stated also in [13, 25]. As long as the contact force was lower than 3.5 kN, the area of this initial delamination remained within 200 mm^2, as can be seen in the diagram; beyond that load value, the delamination quickly began to propagate.

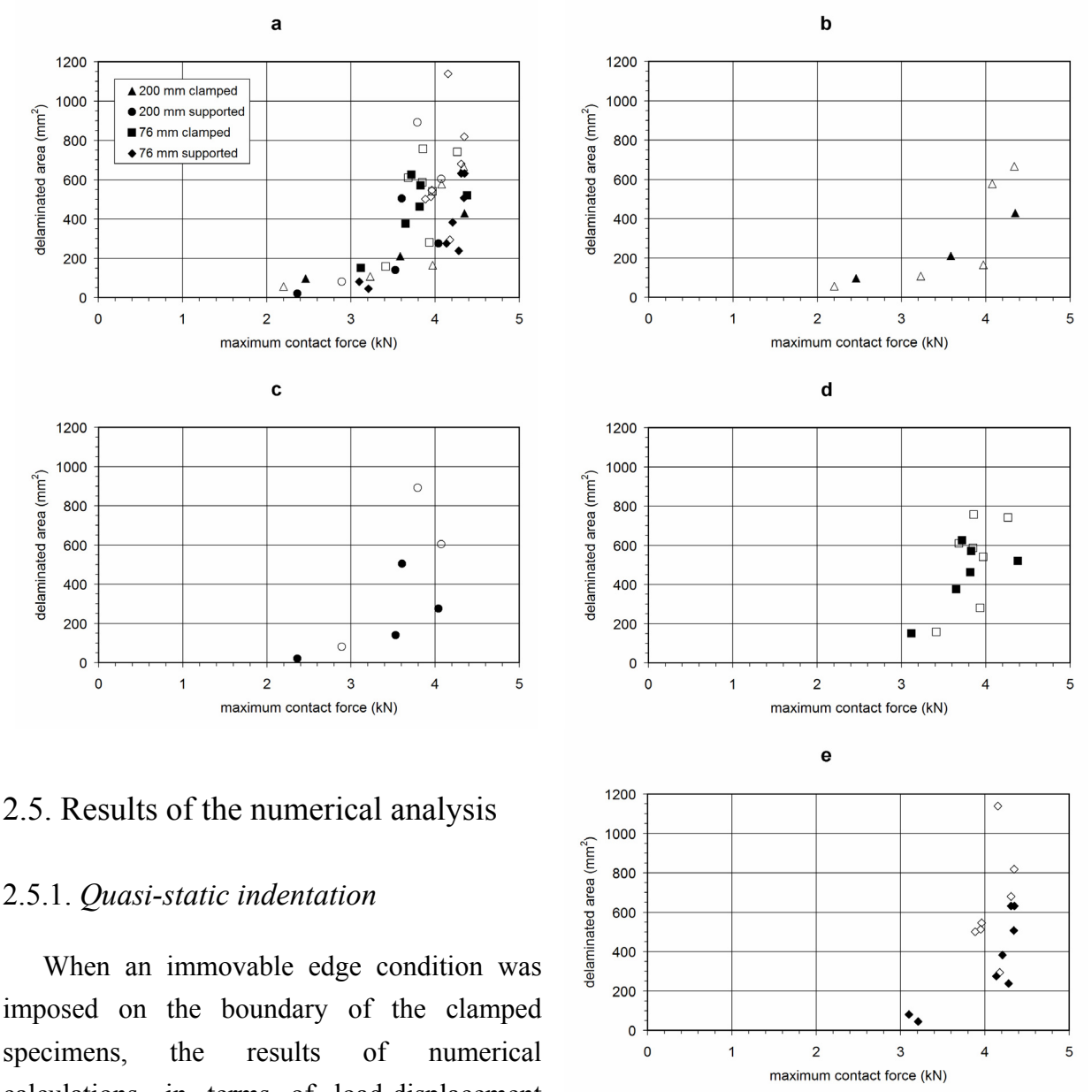

Figure 9 – Delaminated area as a function of maximum contact force. Filled symbols refer to impact tests, empty symbols refer to indentation tests. a) Overall diagram of the four test configurations. b) Clamped 200 mm specimens. c) Simply supported 200 mm specimens. d) Clamped 76 mm specimens. e) Simply supported 76 mm specimens.

2.5. Results of the numerical analysis

2.5.1. *Quasi-static indentation*

When an immovable edge condition was imposed on the boundary of the clamped specimens, the results of numerical calculations, in terms of load-displacement curves, did not agree with the experimental observations, even for very low contact forces at which one can reasonably suppose that the material damage was absent or negligible. This error was attributed to the imperfect constraint on the internal diameter of the clamping rings, where a small chamfer was machined in order to avoid crushing of the laminate due to the tightening load, as well as to facilitate handling of the

rings. Of course such a constraint did not completely prevent the rotation of the specimen along its boundary.

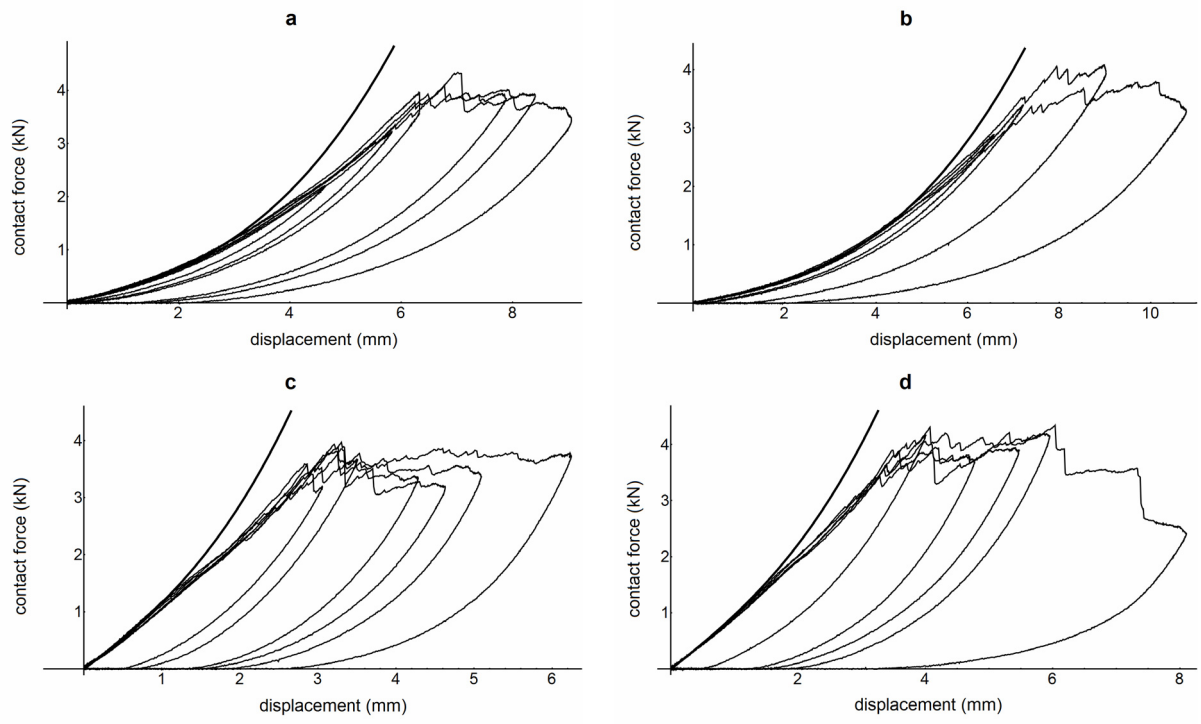

Figure 10 – Contact force-displacement curves recorded during quasi-static indentation tests (thin lines) and comparison with the numerically predicted behaviour for the loading phase (thick line). a) Clamped 200 mm specimens. b) Simply supported 200 mm specimens. c) Clamped 76 mm specimens. d) Simply supported 76 mm specimens.

To correctly reproduce the mechanical behaviour of the laminates, an elastic boundary condition was therefore applied to the rotation about the tangential direction along the circumference. The stiffness of this constraint was found by trial and error, comparing the numerical results to interpolations of the experimental load-displacement curves made according to the following formula [17]:

$$P = A_1\left[w-\left(\frac{P}{k}\right)^{\frac{2}{3}}\right]+A_2\left[w-\left(\frac{P}{k}\right)^{\frac{2}{3}}\right]^3 \qquad (2)$$

where the constants A_1 and A_2 were determined by least-square fitting, while the contact stiffness k of expression (1) was assigned the value of $1.116 \cdot 10^9$ N/m$^{3/2}$, as explained in section 2.3. w represents the overall displacement of the indentor, the quantity $(P/k)^{2/3}$ is the indentation α as in (1), thus the difference $w-(P/k)^{2/3}$ is the deflection of the laminated plate without including the local indentation. The formula (2) was chosen because it includes a linear flexural stiffness (A_1) and a nonlinear membrane stiffness (A_2), thus it can represent the behaviour of a plate undergoing large deflections.

The interpolations of the experimental data were based on the load range between 0.2 and 0.5 kN; the points acquired at lower loads were excluded to discard possible errors in the force measurement, while at loads higher than 0.5 kN the results may have been influenced by material damage. The constraint stiffness per unit length was found to be 3.5 kNm/m for the 200 mm laminates and 2.0 kNm/m for the 76 mm laminates. With these values a very good agreement between experimental and numerical load-displacement curves was achieved until the material failed, as shown in figure 10.

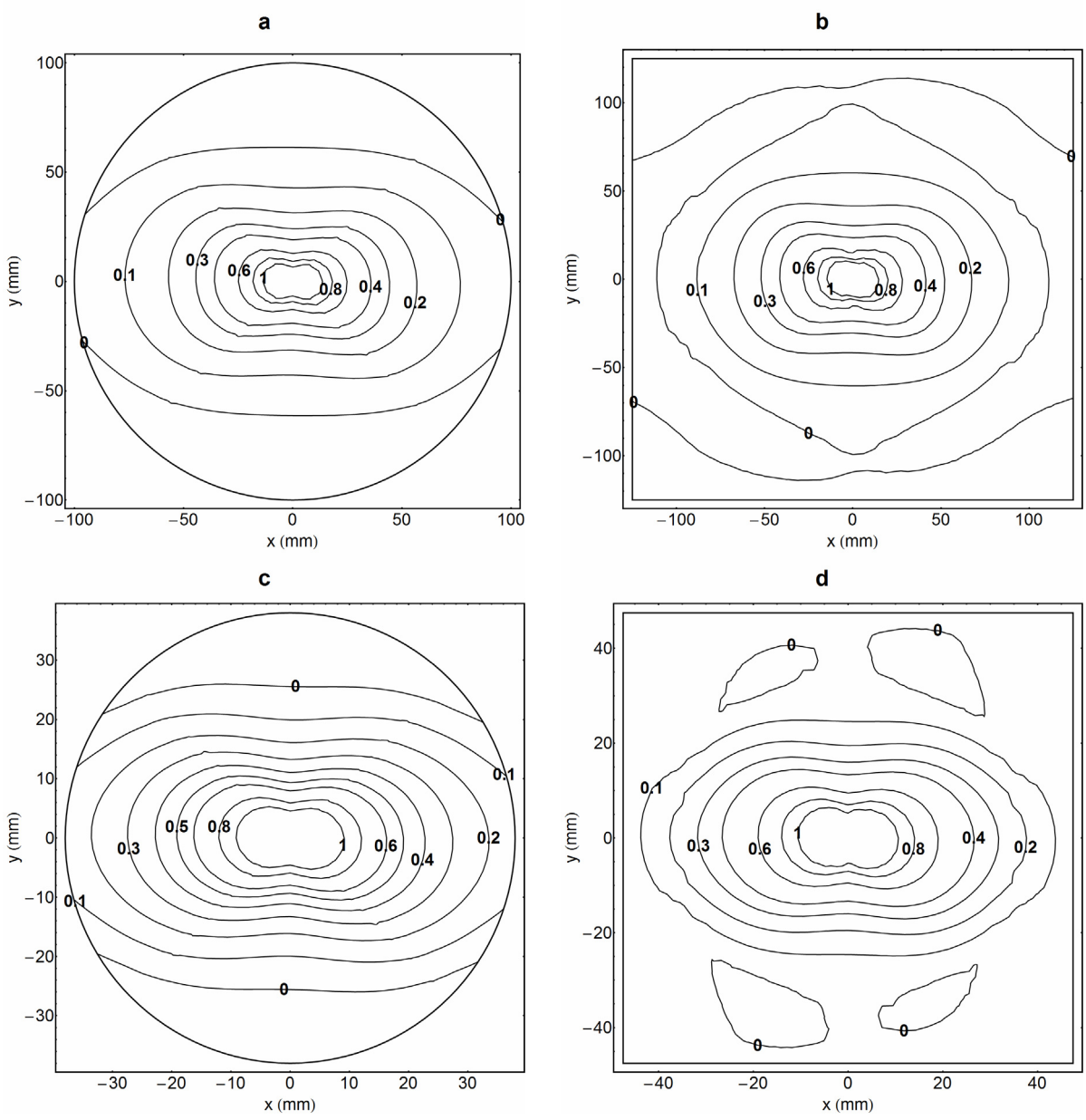

Figure 11 – Tsai-Wu failure index calculated for the lowermost ply of laminates subjected to quasi-static indentation with a numerically predicted contact force of 1 kN. a) Clamped 200 mm specimen. b) Simply supported 200 mm specimen. c) Clamped 76 mm specimen. d) Simply supported 76 mm specimen.

Above a threshold load which was slightly different depending on the size and boundary conditions, but in any case not larger than 1.5 kN, a significant deviation of the experimental

curves from the theoretical one was observed (see figure 10). This is most likely related to the first important material damage, probably the onset of the first delamination, deduced from the diagram in figure 9 as explained above.

However, the analysis of stresses in the laminates predicted the first failure at even smaller loads. The plots in figure 11 present the value of the failure index according to the Tsai-Wu criterion [26] calculated for the lowermost ply (opposite to the indented surface of the specimen), which was subjected to the highest stresses, and for a contact force of 1 kN. The index was larger than 1 (which in the present case corresponded to matrix failure in tension) in a wide region surrounding the indentation point. Therefore it can be concluded that the first damage, probably the initiation of the first back-face splitting of the laminate, did not produce any visible effect on the global mechanical behaviour of the specimens, as is pointed out also in [17]. It is possible that only the first delamination induced a stiffness loss large enough to become visible in the load-displacement curves.

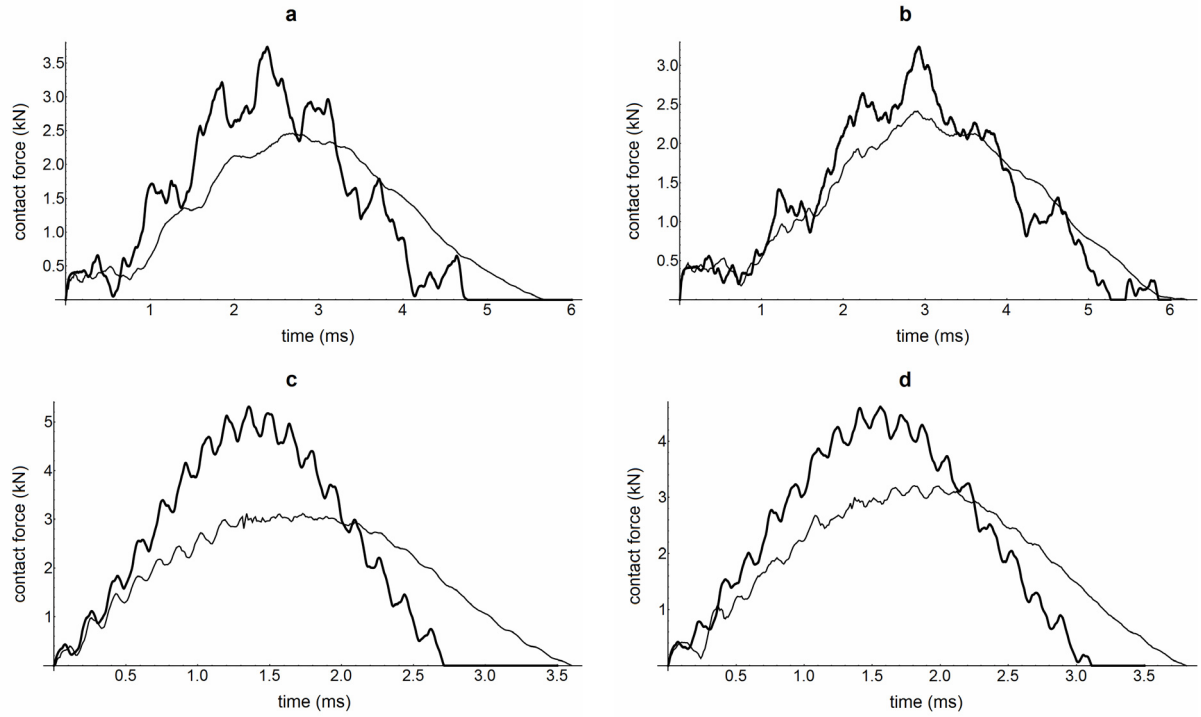

Figure 12 – Experimental (thin line) and numerical (thick line) contact force history for four representative impact events (0.5 m drop height). a) Clamped 200 mm specimen. b) Simply supported 200 mm specimen. c) Clamped 76 mm specimen. d) Simply supported 76 mm specimen.

2.5.2. *Low velocity impact*

As for the quasi-static indentation experiments, an analogous comparison between numerical and experimental results can be carried out for the low velocity impact tests. Such a comparison is reported in figure 12, where the contact force is plotted as a function of time for one representative test of each configuration, and in figure 13, where three impact events at different

drop heights are collected. In the numerical model, an elastic constraint was applied to the boundary of the clamped plates, with the same stiffness already used for the quasi-static tests.

These diagrams show a reasonably good agreement at force levels within 1.0 ÷ 1.5 kN. Beyond this limit, which was difficult to evaluate exactly due to the oscillations, the numerical calculation generally overestimated the contact load, similarly to what happened in the analysis of the indentation tests. Again, the disagreement can be attributed to the progressive propagation of damage in the laminates. It can be noted from the curves in figure 13 that the difference between numerical and experimental results became larger and larger for increasing impact energy and consequent damage in the specimen.

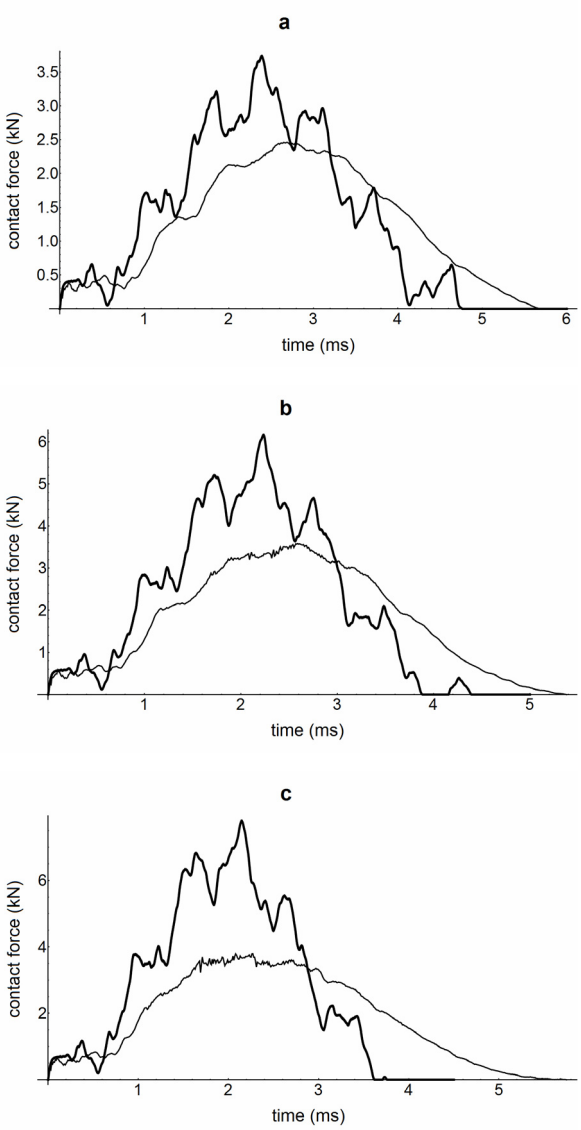

Figure 13 – Experimental (thin line) and numerical (thick line) contact force history for three representative impact events with different drop heights on clamped 200 mm laminates. a) 0.5 m drop height (impact velocity 3.10 m/s). b) 1.0 m drop height (impact velocity 4.34 m/s). c) 1.5 m drop height (impact velocity 5.18 m/s).

Figure 14 presents some representative plots of the Tsai-Wu failure index calculated for the lowermost ply, which was subjected to the highest stresses in every case. All the images refer to instants at which the contact force was exactly 1 kN, and can thus be directly compared to the pictures in figure 11. The difference between quasi-static and dynamic tests was found to be negligible, except for the case of the clamped 200 mm laminate of figures 14a-b. These two images refer to the same impact event whose contact force history is plotted in figure 13c, and represent the stress state in two distinct instants at the beginning of contact, at both of which the predicted load was equal to 1 kN. A slight difference can be seen between them and also with respect to figure 11a which refers to the same contact force applied quasi-statically. This can help in establishing to what extent the impact velocity can be considered low in the present test configuration, according to the second definition previously cited [7].

That definition is based on the propagation of elastic waves from the impacted point towards the boundary. Thus the larger the in-plane dimensions of the specimen, the longer the time required for the waves to reach the boundary. As a consequence, contact duration remaining

equal, the response of the larger specimen will be more evidently affected by wave propagation. The greater amplitude of the secondary oscillations in the contact force history of the 200 mm with respect to the 76 mm specimens demonstrates this fact. For this reason it can be expected that the upper limit of the low impact velocity range will be smaller for the 200 mm specimens, and that the behaviour of the larger laminate impacted from the greatest drop height will be the most significantly influenced by wave propagation. This is confirmed by the stress plots in figure 14. The faint difference between the quasi-static state in figure 11a and the dynamic counterparts in figures 14a-b may indicate that for the 200 mm laminate of the present study an impact velocity of 5 m/s can actually be considered low, but is not far from the limit of the low range.

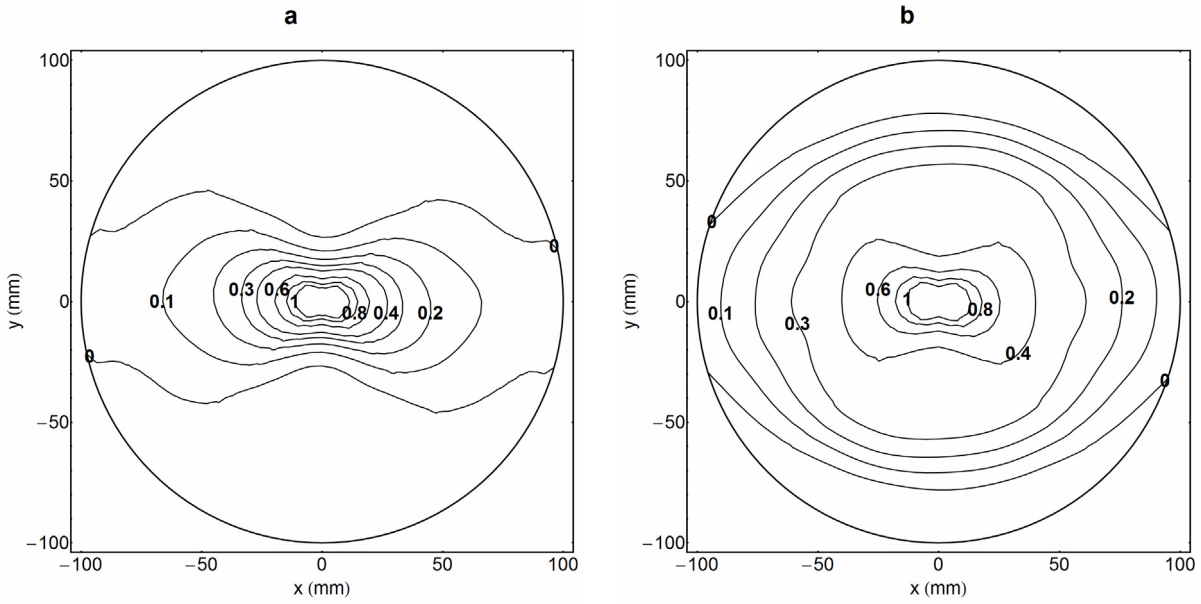

Figure 14 – Tsai-Wu failure index calculated for the lowermost ply of laminates subjected to low velocity impact, at an instant at which the numerically predicted contact force was 1 kN. a) Clamped 200 mm laminate, 1.5 m drop height, 5.18 m/s, 340 μs after the beginning of contact. b) The same as in a), but 643 μs after the beginning of contact.

2.6. Comparison between impact and indentation

As pointed out above, the test conditions considered in the present study met both the second definition of low velocity impact [7] and the first one [6], since the impact velocity was much lower than the typical threshold of 10 ÷ 20 m/s. Therefore it is meaningful to compare the experimental results obtained in impact with the ones of quasi-static indentation.

From the results of the experimental tests and of the numerical simulation, it was possible to deduce the existence of three contact force thresholds which played an important role in the progression of material damage.

The first one is the load at which the very first damage took place, probably in the form of a matrix fracture on the back face of the specimen under the impact or indentation point. The existence of this characteristic force level could be hypothesized only by means of the numerical

stress analysis, because this first failure did not produce any visible effect on the global mechanical behaviour of the laminate in terms of load-displacement curve.

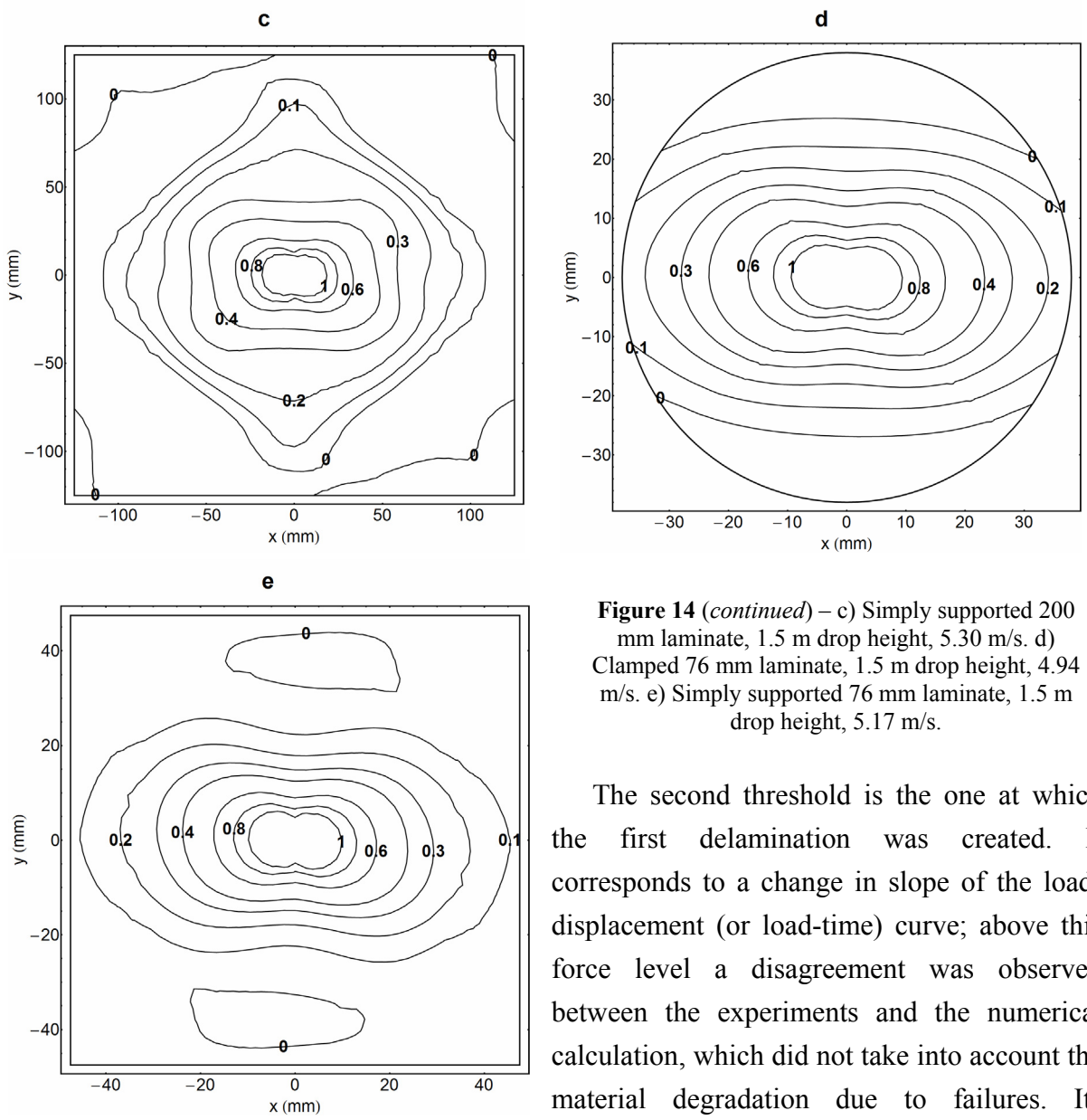

Figure 14 (*continued*) – c) Simply supported 200 mm laminate, 1.5 m drop height, 5.30 m/s. d) Clamped 76 mm laminate, 1.5 m drop height, 4.94 m/s. e) Simply supported 76 mm laminate, 1.5 m drop height, 5.17 m/s.

The second threshold is the one at which the first delamination was created. It corresponds to a change in slope of the load-displacement (or load-time) curve; above this force level a disagreement was observed between the experiments and the numerical calculation, which did not take into account the material degradation due to failures. Its existence could also be inferred from the relationship between delaminated area and maximum contact force (figure 9): although a delamination was found after all the tests, it is obvious that if the imparted energy was small enough no delamination would be induced [13, 25].

The third characteristic force is the one beyond which the delamination area began to increase very rapidly, as shown in figure 9. It can be recognized only by analysing the experimental data, because the results obtained by the numerical model, which did not account for damage, were not reliable at this load level.

The present research demonstrates that, at least in the impact velocity and energy range considered, these contact force thresholds are equal for low velocity impact and quasi-static indentation, within the attainable experimental accuracy. This agrees with the conclusions of [13]. In addition, no significant difference was found between the two specimen dimensions and

the two boundary conditions tested. Thus it can be concluded that, as long as the contact force is chosen as the independent variable, the main steps of material damage development are very similar for quasi-static and dynamic application of the force. It should be emphasized, however, that once the highest threshold has been overtaken the extent of delamination cannot be practically predicted from the maximum load. It appears from figure 9 that a peak force larger than 3.5 kN may result in a damage area of 200 or 1000 mm^2. Therefore it cannot be excluded that differences between impact and indentation tests exist at this load level.

Actually such differences were highlighted by using energy in place of contact force as the independent variable, as illustrated by figures 6-7. While a similar energy absorption was observed in quasi-static and dynamic tests where the same total energy was imparted, the delaminated area was larger in the first case. This may be explained in two ways. It is possible that a larger amount of energy was required to create the same delamination extent during impact than was the case during indentation; however with the specimen detection methods used in the present study one can not verify nor refute this hypothesis. Another possibility is that in impact tests a larger part of the available energy was spent in dissipating mechanisms other than delamination propagation.

In principle, one of these mechanisms could be the partial dissipation (through vibration phenomena) of the kinetic energy transferred from the impactor to the target, which can act during an impact but not in quasi-static indentation. However, in the present study, due to the limited impact velocity and to the relatively large impactor mass, the amount of kinetic energy acquired by the specimens was very small. The numerical calculations indicated that during the transient response of the laminates their kinetic energy was never greater than 5% of the initial energy of the impactor, and in many cases it was less than 2%. Even if this amount had been entirely dissipated during the contact duration (in which the energy absorption was computed), it would not account for the much larger difference shown in figure 7 (in terms of energy required to produce the same damage area). Actually the specimen vibration induced by impact continued for some time after contact ceased, thus the energy dissipation in the contact interval was even less significant.

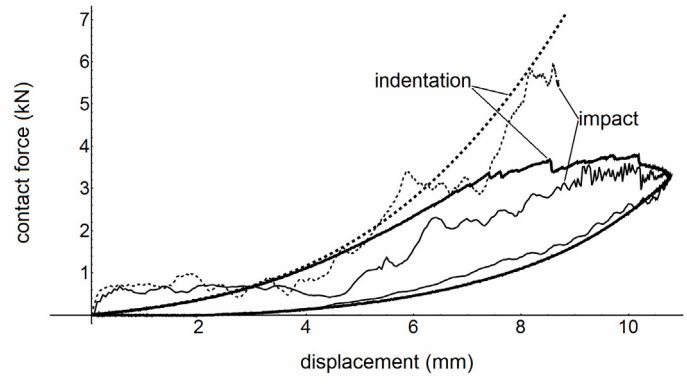

Figure 15 – Example of comparison between impact (1.5 m drop height) and indentation on two representative tests with similar values of maximum displacement (10.75 mm). The solid lines refer to experimental data, the dotted lines are the relevant numerical predictions for the loading phase of contact. The maximum contact force was 3.60 kN (impact) versus 3.79 kN (indentation); the total energy was 17.1 J and 21.1 J, respectively.

Consequently, the possible phenomena responsible for a more efficient energy absorption must be looked for among the damage

mechanisms. Since matrix failure did not affect the load-displacement behaviour, it is unlikely that it was related to a significant energy absorption. On the other hand, fibre fracture, which occurred at the highest energy levels, may account for the difference between impact and indentation. In other words, it seems reasonable that a larger amount of energy was spent to cause fibre damage in the dynamic tests, thus the delamination was less extended with the same energy dissipation. It has to be noted that the same hypothesis is proposed also in [12, 20].

One piece of experimental evidence that could support this hypothesis is the greater impactor displacement recorded in impact tests (figure 8). With the aid of the numerical simulations, it can be concluded that this can not be attributed to the transient response of the laminates, for example to the oscillations the specimen may undergo after a collision. In fact, as shown in figure 15, the predicted force-displacement relationship is quite similar in static and dynamic conditions, and the same must hold also for the total energy (which is the area under the curves in the graph). Thus the numerical model without material degradation cannot explain the systematically larger displacements in figure 8. As a consequence, this result must be related to some form of damage, probably a more severe fibre fracture in a small zone surrounding the impact point, although this was not evident from the appearance of the specimens.

It can also be noted from the plots in figure 15 that the experimental dynamic curves tend to be lower than the experimental quasi-static ones, unlike the results presented in [7, 9] where almost superimposable plots are shown; actually this explains why during an impact test it is necessary to reach a larger displacement than in a corresponding indentation test to do the same work on the specimen. Again, this difference can suggest that some dissimilar phenomena act in the specimens as regards damage development, but due to the oscillations it is not possible to assess a precise load value at which the dynamic force-displacement plot departs definitely from the quasi-static one.

2.7. Conclusions

In order to compare the effects of low velocity impact and quasi-static indentation on CFRP laminated plates, experimental tests of both loading conditions were carried out. The elastic behaviour and material damage were studied by visual inspection, optical and scanning electron microscopy and examination of load-displacement relationship and energy absorption due to failures. Both impact and indentation tests were simulated by a two-dimensional finite element model including geometrical nonlinearity. In all the impact experiments, the impactor velocity was low according to two different criteria commonly adopted in the literature, so that appropriate conditions existed for a comparison with quasi-static indentation tests. On the basis of the results obtained, the following conclusions can be drawn:

1) Both after impact and after quasi-static indentation of laminates, the same failure types, namely matrix cracking, delamination, fibre fracture (both in tension and in compression) were

observed on specimens. The material damage can therefore be considered qualitatively similar in static and dynamic conditions.

2) The existence of three characteristic contact force thresholds, which were related to significant steps in the damage development, was verified. In agreement with previous studies by other authors, these thresholds, together with the relationship between maximum contact force and delaminated area, were found to be equal for quasi-static and dynamic tests.

3) An equal energy absorption led to a slightly larger delaminated area in indentation tests with respect to impact tests. This indicated that in the second case a larger amount of energy was spent in other damage mechanisms, probably a more severe fibre fracture in the vicinity of the impact point, as hypothesized also by other authors. Larger values of the maximum displacement in the impact events, related to a lower stiffness with respect to analogous indentation tests, may support this explanation.

References for chapter 2

1. Cantwell WJ, Morton J. *The impact resistance of composite materials - a review*. Composites 1991;22(5):347-362.
2. Abrate S. *Impact on laminated composite materials*. Appl Mech Rev 1991;44(4):155-190.
3. Abrate S. *Impact on laminated composites: recent advances*. Appl Mech Rev 1994;47(11):517-544.
4. Abrate S. *Impact on composite structures*. Cambridge: Cambridge University Press, 1998.
5. Richardson MOW, Wisheart MJ. *Review of low-velocity impact properties of composite materials*. Compos Part A-Appl S 1996;27(12):1123-1131.
6. Robinson P, Davies GAO. *Impactor mass and specimen geometry effects in low velocity impact of laminated composites*. Int J Impact Eng 1992;12(2):189-207.
7. Sjöblom PO, Hartness JT, Cordell TM. *On low-velocity impact testing of composite materials*. J Compos Mater 1988;22(1):30-52.
8. Sridhar C, Rao KP. *Estimation of low-velocity impact damage in laminated composite circular plates using nonlinear finite element analysis*. Comput Struct 1995;54(6):1183-1189.
9. Delfosse D, Poursartip A. *Energy-based approach to impact damage in CFRP laminates*. Compos Part A-Appl S 1997;28(7):647-655.
10. Caprino G, Crivelli Visconti I, Di Ilio A. *Composite materials response under low-velocity impact*. Compos Struct 1984;2(3):261-271.
11. Symons DD. *Characterisation of indentation damage in 0/90 lay-up T300/914 CFRP*. Compos Sci Technol 2000;60(3):391-401.
12. Elber W. *Failure mechanics in low-velocity impacts of thin composite plates*. NASA Technical Paper 2152, 1983.

13. Wu E, Shyu K. *Response of composite laminates to contact loads and relationship to low-velocity impact*. J Compos Mater 1993;27(15):1443-1464.
14. Kaczmarek H, Maison S. *Comparative ultrasonic analysis of damage in CFRP under static indentation and low-velocity impact*. Compos Sci Technol 1994;51(1):11-26.
15. Caprino G, Langella A, Lopresto V. *Indentation and penetration of carbon fibre reinforced plastic laminates*. Compos Part B-Eng 2003;34(4):319-325.
16. Lee J, Soutis C. *Prediction of impact-induced fibre damage in circular composite plates*. Appl Compos Mater 2005;12(2):109-131.
17. Caprino G, Langella A, Lopresto V. *Elastic behaviour of circular composite plates transversely loaded at the centre*. Compos Part A-Appl S 2002;33(9):1191-1197.
18. Caprino G, Langella A, Lopresto V. *Prediction of the first failure energy of circular carbon fibre reinforced plastic plates loaded at the centre*. Compos Part A-Appl S 2003;34(4):349-357.
19. Cesari F, Dal Re V, Minak G, Zucchelli A. *Damage and residual strength of laminated carbon-epoxy composite circular plates loaded at the centre*. Compos Part A-Appl S 2007; 38(4):1163-1173.
20. Breen C, Guild F, Pavier M. *Impact of thick CFRP laminates: the effect of impact velocity*. Compos Part A-Appl S 2005;36(2):205-211.
21. ASTM D 3763 – 06 *Standard test method for high speed puncture properties of plastics using load and displacement sensors*. Annual Book of ASTM Standards. West Conshohocken, PA: ASTM International, 2006.
22. Minak G, Ghelli D. *Design of a drop-weight machine for composite materials impact testing*. In: Proceedings of the ICCSM5 Congress, Matejiček F, editor. Trogir/Split (HR): Croatian Society of Mechanics, 2006.
23. ASTM D 7136/D 7136M – 05 *Standard test method for measuring the damage resistance of a fiber-reinforced polymer matrix composite to a drop-weight impact event*. Annual Book of ASTM Standards. West Conshohocken, PA: ASTM International, 2005.
24. Yang SH, Sun CT. *Indentation law for composite laminates*. NASA CR-165460, 1981.
25. Davies GAO, Zhang X. *Impact damage prediction in carbon composite structures*. Int J Impact Eng 1995;16(1):149-170.
26. Tsai SW, Wu EM. *A general theory of strength for anisotropic materials*. J Compos Mater 1971;5(1):58-80.

CHAPTER 3

Effect of different specimen diameter and boundary conditions on the impact behaviour of circular laminates*

3.1. Introduction

The damage caused by impact of external bodies has been recognized for many years as a primary concern regarding Carbon Fibre Reinforced Polymers (CFRP), and a great deal of experimental results have been obtained in a variety of test conditions. Although researchers have paid considerable attention to this topic, many aspects of phenomena taking place when a composite laminate is impacted are not yet fully understood [1-3].

Moreover, difficulties arise when information obtained in laboratory tests is to be used in the design of real components, because the test configuration hardly ever reproduces the actual component conditions, especially as regards constraints [4]. The final aim of this research field should be the ability to predict damage produced by special cases of impact on special structures without the need to undertake tailored tests for each case. Performing tests on components themselves appears wasteful, in particular when very large structures are dealt with; for this reason some researchers verify the validity of scaling rules that would allow the application of results obtained on small-scale models also to full-scale prototypes, as reviewed in [5]. Scaling rules developed by means of dimensional analysis techniques agree with experiments until laminates behave elastically; significant discrepancies exist, however, when the material is damaged. Since these discrepancies are introduced by the damage itself, they seem difficult to eliminate; in addition, their overall effect is a higher impact strength in a smaller specimen than in a larger one, so that applying information provided by the former to the latter can result in unsafe predictions [5, 6].

An alternative strategy to overcome these limits is based on a detailed study of the dynamic behaviour of laminates under impact; this is considered the first step towards a deeper understanding of damage mechanisms [3] that should permit an effective use of laboratory tests. Numerical calculation of the transient response of laminates is attempted by many authors, for instance [3, 4, 7-9]. This response is controlled, in general, by factors concerning the target structure, like geometrical and material properties, and by impact parameters, such as the

* This study was published as Minak G, Ghelli D. *Influence of diameter and boundary conditions on low velocity impact response of CFRP circular laminated plates*. Compos Part B-Eng 2008;39(6):962-972.

impactor mass and velocity. In particular, the dimensions and boundary conditions of the laminate are important, because they determine its flexural stiffness, for a given material whose thickness and stacking sequence are fixed. Some authors assess the effect of dimensions on impact response and damage experimentally [4, 10-13]. One of the most important findings is that the ratio between in-plane dimensions and thickness can affect the type of impact damage: in thicker laminates failures start from the impacted surface, due to high local contact stresses, while in thinner laminates failures initiate from the opposite surface, due to tensile bending stresses and shear [10]. On the other hand, only a few studies deal with the effect of boundary conditions [4, 14, 15].

This study examined the effect of the boundary conditions and in plane dimensions on the impact response of CFRP laminates. Impact events at various energy levels on circular plates with different diameters and constraints were reproduced by an instrumented drop-weight tower, and the experimental results were compared with numerical simulation of a finite element numerical model. Experiments showed that both diameter and boundary conditions influence the dynamic response of laminates to impact and, consequently, the failures induced in the material, because they determine the flexural stiffness of specimens. Stiffer plates undergo more extended delamination because they can store less elastic energy before failure. While the relationship between delamination area and impact energy differs according to the test configuration, the delamination area can be consistently related with absorbed energy or with maximum contact force, independently of dimensions and constraints in the range covered by the present test program. Numerical simulation gave reliable results in the earliest phase of contact, when the effect of damage on the mechanical behaviour of laminates is still negligible. Subsequently, disagreement between analysis and experiments, due to lack of a damage model in the former, was observed, especially in higher energy events. This indicated a strong reduction in stiffness of specimens, even if damage seemed not to be severe.

3.2. Experimental testing

Laminated plates made of T300 carbon fibre and epoxy resin matrix prepregs, with 16 plies arranged in a quasi-isotropic stacking sequence $[0_2/90_2/45/-45/45/-45]_S$, were considered in this study. The laminates were cured in an autoclave. The in-plane dimensions of the plates were 247 by 250 mm; total thickness was 2.7 ± 0.05 mm; the average density of the material was 1490 ± 10 kg/m^3. The elastic constants of the individual laminae were estimated by tensile and four-point bending tests on the laminates: the results are listed in table 1. For the in-plane Poisson ratio and in-plane strengths, the values indicated by the manufacturer were assumed to be valid.

Pure indentation tests were carried out on a laminate to determine the contact law between specimens and the stainless steel head of the load cell used in impact experiments (see below). In these tests the head was pressed against the laminate, which was placed on a thick steel plate,

by an Instron 8033 servo-hydraulic machine in load control. The test configuration prevented any bending of the composite specimen, allowing local contact deformation only. Applied force reached 5 kN (a greater value than those found in all impact tests); both force and relative displacement were measured directly by the machine. Interpolation of the obtained force-indentation curves according to the power law:

$$P = C\,\alpha^{n} \tag{1}$$

where P is the contact force and α is the indentation, gave the results reported in table 1 for C and n. Due to the approximation of the numerical model, which does not include the effects of material failures, the results obtained by using these values for C and n were accepted, instead of measuring the contact law with more rigorous and sophisticated methods like, for instance, the one employed in [16].

Table 1 – Material properties and parameters of the contact law

Elastic constants	
E_1	93 ± 2 GPa
E_2	10.5 ± 0.5 GPa
G_{12}	4.2 ± 0.5 GPa
ν_{12}	0.28
In-plane strengths	
X_t	1270 MPa
X_c	1130 MPa
Y_t	30 MPa
Y_c	141 MPa
S	63 MPa
Contact law parameters	
C	$1.9 \pm 0.1 \cdot 10^{10}$ N m^{-n}
n	1.9 ± 0.1

Low velocity impact tests were carried out in a drop-weight machine (shown in figure 1 of chapter 2) equipped with a laser device, for calculation of fall and rebound velocity of the impactor, and with a piezoelectric load cell attached to the impactor that measured contact force history. Both the load cell and the laser signals, as well as the signal of strain gauges (see below), were acquired at 100 kHz sampling frequency, without any filtering except the intrinsic one due to the measurement chain. The hemispherical head of the load cell (12.7 mm diameter) was the only part of the impactor hitting the laminates. Multiple collisions were avoided by means of an electromagnetic braking system. A detailed description of the machine can be found in [17].

The impactor mass was 1.22 ± 0.01 kg; three different drop heights of 0.5, 1 and 1.5 m were chosen, corresponding to a nominal potential energy of 6, 12 and 18 J respectively. The laminates were placed in a clamping fixture which consisted of two steel rings fastened to a cylindrical base, so that the geometry of a circular plate was reproduced; impact occurred exactly at its centre. Two pairs of rings of 200 and 76 mm internal diameter, respectively, were used to test the impact response of specimens of different sizes; the second diameter was chosen according to [18]. When a 200 mm diameter circular plate was simulated, 247 by 250 mm specimens were placed on the clamping fixture; after impact, four smaller square specimens of 100 mm per side were obtained by cutting the original laminates (excluding two perpendicular 50 mm wide strips, centred on the median axes, containing the damaged zone) and were employed with the smaller rings for impact tests on 76 mm diameter plates. As explained in the results section, the delaminated area created by impact had an elongated shape; its largest extent was approximately 80 by 20 mm. The width of the central strips was much larger than the

maximum delamination width, thus ensuring that the smaller specimens did not have any pre-existing damage before testing.

Two different boundary conditions were studied: full clamp and simple support. The first condition was accomplished by clamping the laminates between the two steel rings by four bolts; the second one was reproduced by simply placing the laminates on one ring (which was, obviously, fixed to the base) without using the second ring. It should be noted that the first arrangement was intended to prevent any motion of the plate boundary, both in-plane and out-of-plane; in the second condition in-plane motion of any point of the plate was free, upward and downward motion was allowed in the region bounded by the inner ring diameter, while only upward displacement was possible outside this region. Two (in the case of larger laminates) or three (in the case of smaller laminates) tests were performed for each combination of specimen diameter, constraint condition and drop height.

Some specimens were instrumented with a strain gauge on their back side, in order to compare numerically predicted strain with experimental values. A location far away from the path of the back-face splitting was chosen for the strain gauges, in order to prevent their failure during impact tests; for this reason they were placed along a diagonal of the rectangular specimens, at some distance from the impact point. The measuring grid was aligned with the diagonal in order to achieve the highest sensitivity, since flexural elastic waves caused by impact are approximately circular.

After impact, the specimens were first examined by visual inspection; for some of them the central zone was cut and incorporated in polyester resin, to allow subsequent cutting along two orthogonal directions through the impact point and observation of the laminate section by optical microscope.

According to [19], contact force versus time recorded by the load cell was divided by impactor mass and numerically integrated twice, using the impactor position (41 mm above the laminate upper surface) and velocity evaluated by the laser device as initial conditions, to obtain the impactor displacement as a function of time during contact. Knowing the force and position, the energy absorbed versus time was also determined by the procedure specified in [19].

3.3. Numerical modelling

Transient dynamic analysis of impact events was carried out by the finite element program described in chapter 1. Contact between laminate and impactor was modelled in a simplified way by applying contact force as an external load on a single node and introducing a nonlinear relationship linking contact force and indentation, following the generalized Hertzian law (1) experimentally determined in pure indentation tests. The same approach is accepted by many other investigators [3, 7, 8].

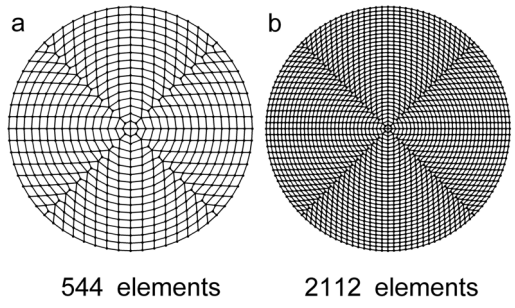

Figure 1 – Two examples of finite element discretizations used in numerical analysis.

Before numerical analysis, a convergence test was performed to decide what mesh refinement was necessary to achieve reliable results. All of the discretizations used consisted of four-node elements, and covered the entire laminate surface, to account for bending-twisting coupling due to ±45° layers. They were drawn in such a way that elements had a regular shape and similar dimensions, in order to keep the time integration step as large as possible. The convergence test indicated that results provided by a 544 element mesh (figure 1a) were satisfactory as regards displacements, but slightly less accurate for contact force; in order to achieve sufficient accuracy in strains and stresses, finer discretizations, up to 2112 elements (figure 1b), were required.

Due to the lack of experimental values, both the out-of-plane shear moduli G_{13} and G_{23} were assumed to be equal to G_{12} in all calculations, although this is not also true for transversally isotropic materials; the same simplifying assumption is adopted in [3, 7]. In order to verify the influence of the value of G_{23} (which is, in general, different from G_{12} and G_{13}) on the numerical results, some analyses were performed with G_{23} = 3.1 GPa instead of G_{23} = 4.2 GPa. Since the following relationship holds for transversally isotropic materials:

$$G_{23} = \frac{E_2}{2(1+\nu_{23})}$$

G_{23} = 3.1 GPa corresponds approximately to ν_{23} = 0.7; this was chosen as an extreme value in the sense that it is quite close to the upper limit of the range of ν_{23} in which the constitutive matrix of the material is positive definite. In the impact events where the numerically predicted contact force was the largest (thus it was expected that out of plane shear forces would be most significant) the change in G_{23} from 4.2 to 3.1 GPa produced changes within 5% in the values of membrane forces, bending moments and out of plane shear. This happened only in the central zone of the plate, very close to the concentrated contact force; elsewhere the influence of G_{23} was even lower. The predicted maximum contact force decreased by 1%; the increase in maximum deflection was 0.3%. Due to other limitations of the numerical analysis (most importantly, the absence of a damage model) the effects of the approximation $G_{23} = G_{12} = G_{13}$ were considered acceptable.

3.4. Results

After impact, all specimens showed back-face splitting starting from the impact point, together with delamination visible to the naked eye as a zone slightly protruding from the back surface of the laminate. Observation by optical microscope revealed that, in general, delamination took place at every interface between layers, even between plies with equal fibre orientation. In higher energy events fibre fracture also occurred, both in the 0° and in the 90° plies on the back side. The impacted surface of laminates was subjected to permanent indentation, without apparent failures, during the 0.5 m drop tests; higher drops caused matrix cracking and fibre fracture (both in tension, inside the dent, and in compression, just outside) associated with much deeper residual indentation. However, no test approached penetration of the laminate. The failure modes described above were qualitatively similar in specimens impacted in different test conditions. The only differences noticed regarded the extent and severity of damage: longer splitting, and more extended delamination and fibre fracture occurred in the 76 mm than in the 200 mm diameter coupons.

An overview of all impact tests performed is provided by figures 2, 3, 4 and 5. Actual impactor velocity ranged from 3.0 to 5.4 m/s. In figure 2 the absorbed energy at the end of each test is reported as a function of the initial kinetic energy of the impactor. Initial energy being the same, a larger amount of energy was absorbed by the clamped specimens than by the supported ones, and by the smaller laminates than by the larger ones.

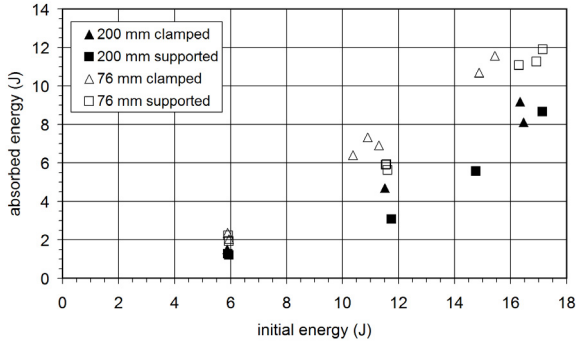

Figure 2 – Absorbed energy vs. initial energy.

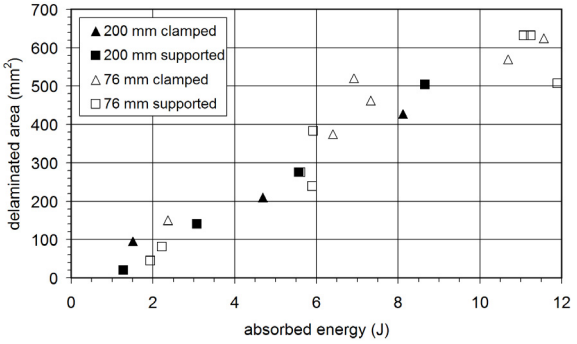

Figure 3 – Delaminated area vs. absorbed energy.

The relationship between absorbed energy and delamination area can be found in figure 3. The largest delamination, visible to the naked eye, always occurred at the lowermost interface between the 0° and 90° plies; its shape resembled that of a rhombus with the largest diagonal in the fibre direction of the 0° plies, thus its area was estimated as the area of a rhombus by measuring the length of diagonals. Observation of sectioned laminates by optical microscope confirmed the validity of this measure, which is the one reported in figure 3. Here the differences among points seem to be attributable to scatter; no definite dissimilar trends can be recognized between data which refer to different test conditions.

On the other hand, such a difference is evident in the relationship between the delaminated area and initial energy (see figure 4). A larger extent of delamination was found in the 76 mm laminates than in the 200 mm laminates; similar, but less pronounced, differences can be seen between clamped and supported specimens. If the maximum contact force is chosen as the independent variable, points referring to various test conditions are again superposed on each other, apart from experimental scatter (figure 5).

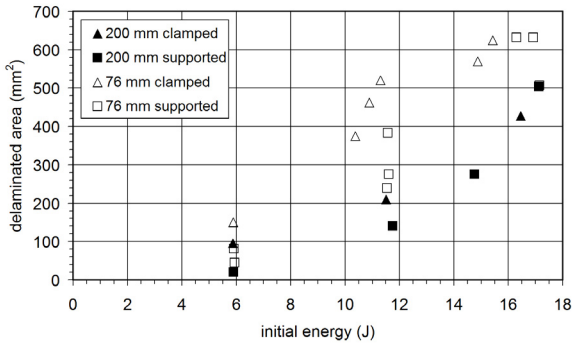

Figure 4 – Delaminated area vs. initial energy.

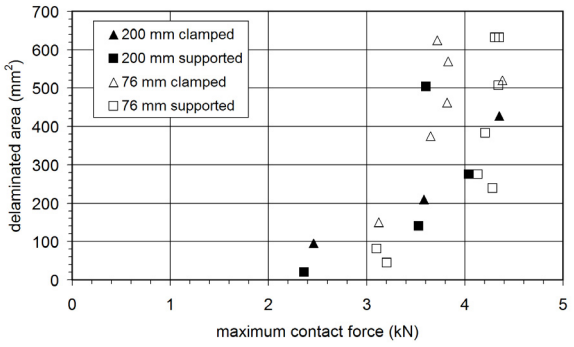

Figure 5 – Delaminated area vs. peak contact force.

Figure 6 presents an example of the effect of boundary conditions on impact response: two representative experimental load-displacement curves, obtained in two 200 mm laminates subjected to 1.5 m drop, are plotted. The actual impact velocity was 4.88 m/s in the case of the clamped coupon and 4.92 m/s in the case of the supported one. In the first case the maximum impactor displacement was smaller (8.0 mm vs. 9.3 mm), the absorbed energy was larger (6.75 J vs. 4.71 J) as was the delamination area (428 mm^2 vs. 275 mm^2), while maximum contact force was similar (4.04 kN for the supported specimen, 4.10 kN for the clamped one).

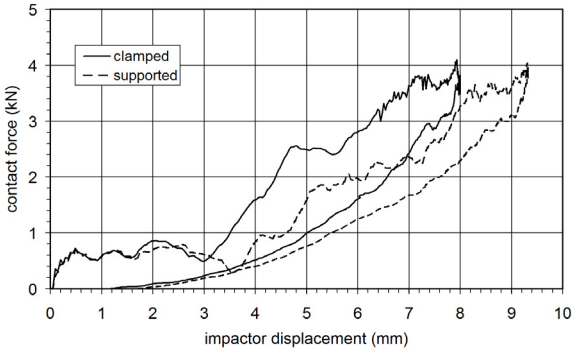

Figure 6 – Load-displacement curves for two impact tests with equal drop height (1.5 m) and specimen diameter (200 mm).

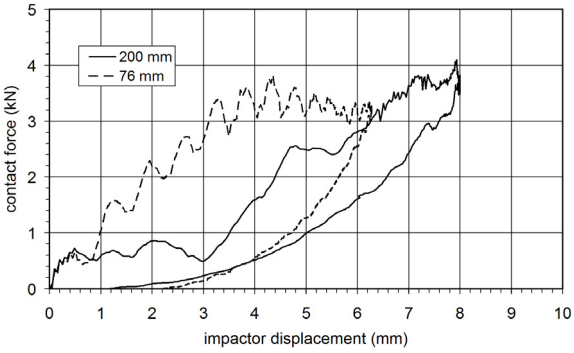

Figure 7 – Load-displacement curves for two impact tests with equal drop height (1.5 m) and specimen boundary conditions (clamped).

A similar, but much more evident, difference was observed between tests carried out in the same boundary conditions but on laminates of dissimilar diameter; figure 7 refers to two clamped plates that underwent a 1.5 m drop height impact. The energy absorbed by the 76 mm specimen (12.2 J) was significantly larger than the energy absorbed by the 200 mm specimen (6.75 J); the delamination areas were 570 and 428 mm^2, the maximum contact forces were 3.82

and 4.10 kN, the actual initial velocities were 5.17 and 4.88 m/s, the maximum deflections were 6.3 and 8.0 mm respectively.

Comparisons between experimental and numerical contact force histories are reported in figures 8 and 9. Numerical simulations were carried out on an 881 four node element discretization; the average dimension of the elements was approximately 5 mm and the time step was 0.5 μs.

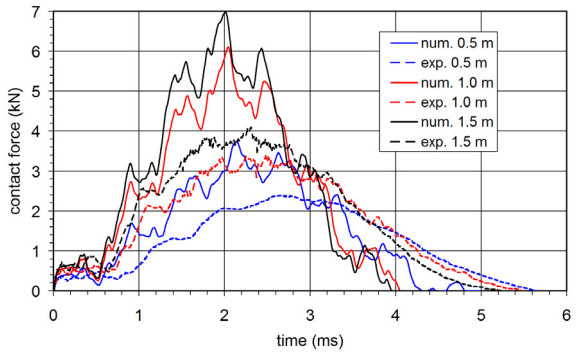

Figure 8 – Experimental and numerical contact force histories for clamped 200 mm diameter laminates subjected to different energy impacts.

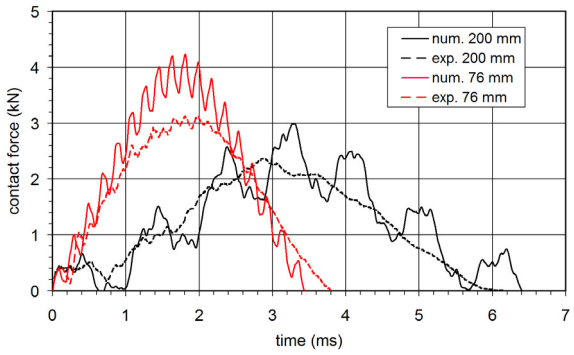

Figure 9 – Experimental and numerical contact force histories for simply supported specimens of different diameter subjected to a 0.5 m drop height impact.

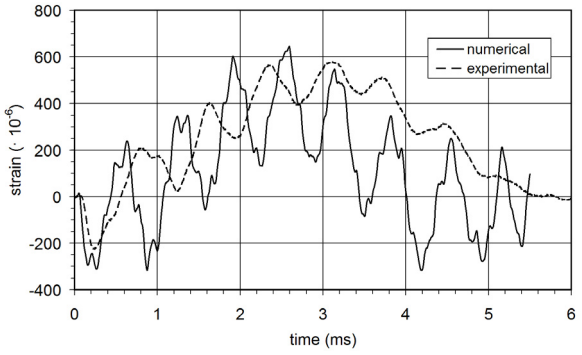

Figure 10 – Experimental and numerical strain in a clamped 200 mm diameter laminate subjected to a 0.3 m drop height impact.

Figure 8 refers to three impact tests (0.5 m, 1.0 m and 1.5 m drop height respectively) performed on clamped 200 mm specimens. Experimental impact velocity was 3.06, 4.40 and 4.88 m/s respectively. Figure 9 contains experimental and numerical contact force histories for two simply supported laminates of different dimensions; in both tests drop height was 0.5 m and impactor velocity was 3.1 m/s.

An example of comparison between numerical prediction and experimental measure of strain is presented in figure 10. This refers to an impact test in which a 0.3 m drop height was chosen, in order to ensure correct working of the strain gauge (however the strain measure proved reliable also in other tests with higher impact energy). The specimen was clamped in the 200 mm diameter fixture; the strain gauge was placed 45 mm from the impact point. Actual impactor velocity was 2.42 m/s. Numerical analysis was performed on a 2112 element discretization (the average dimension of the finite elements was approximately 3 mm) with a 0.4 μs time step.

3.5. Discussion

The relationship between initial and absorbed energy (figure 2) shows that a different energy balance holds for tests performed in dissimilar conditions. At the end of contact a part of the initial kinetic energy, which was transformed in elastic energy of the specimen, is recovered by the impactor; the remaining portion, which is the absorbed energy calculated according to [19], is partly converted into kinetic energy of the specimen and then dissipated, partly spent on creating failures. In low velocity impacts, like the ones reproduced in this study, the residual kinetic energy of the specimen is considered negligible [3] (see also chapter 2, section 2.6); in this case the absorbed energy can be regarded as a reliable estimate of the energy spent on damaging the material. It can thus be concluded that, as expected, in stiffer targets, with lower elastic energy storage capability, a greater part of the initial energy was spent on material damage.

In [12] it is demonstrated that the level at which absorbed energy becomes equal to impact energy (in other words, the impactor does not recover any kinetic energy after collision) corresponds to the threshold required for perforation of the laminate. Perforation was never observed in the present investigation (actually it was not the subject of the study), which covered only the range of low energies; this explains why the absorbed energy is always lower than the initial energy of the impactor in figure 2. The relationship in figure 2, however, is similar to the one reported in [12] as regards the corresponding energy interval.

The correlation linking absorbed energy to material damage is confirmed by figure 3 as regards delamination. It has been noted that this correlation does not depend on specimen diameter and boundary conditions, as clearly shown in the diagram; therefore absorbed energy appears to be a useful parameter to relate to the delamination area, especially when its value is low. Similar findings are described in [11]. Greater dispersion of experimental results is observed for higher energies; however in 76 mm laminates all of the 1.5 m drop height tests and also some of the 1 m tests caused delaminations that reached the boundary of the plates, thus propagation of damage was probably constrained in these cases. Another reason which could explain why the slope of the trend in figure 3 tends to decrease is that other failure modes, like fibre fracture, become important for high energies [3].

The relationship of the delaminated area with initial energy (see figure 4) is not as clear as the one with absorbed energy, because dimensions and boundary conditions of targets play an important role here, and experimental data are quite dispersed. A much better correlation can be found by plotting the delamination area vs. maximum contact force (figure 5): as in figure 3, different test configurations result in points clustered in a reasonably narrow band. This diagram is similar to the one reported in [4].

Quite dissimilar trends can be recognized in figures 3 and 5. The delamination area increases gradually as absorbed energy becomes greater, and extrapolation of data for low energy

indicates that the energy threshold required to initiate damage is very small. On the other hand, points in figure 5 show a quick increase of the delamination area when the maximum contact force exceeds a certain threshold that is quite high (probably close to 2 kN); this confirms that propagation of delamination is an unstable phenomenon, driven by fracture mechanics laws [4]. However a rigorous measurement of the delamination threshold, which would have required a larger number of tests (especially at low energy, to complete the data set with zero delamination area samples), was not the aim of the present investigation. Due to the scatter of data in figure 5, an experimental evaluation of the contact force threshold would be subjected to a significant error; this fact, together with the strong slope of the relationship between delamination area and contact force, leads to the conclusion that the maximum load is not a suitable parameter to predict the extent of delamination, while it could be used to find a delamination threshold [3, 20]. A numerical evaluation of the maximum contact force, even by means of linear simulations like those described here, may be efficiently used to predict whether the experimental threshold will be reached or not during a specific impact event. On the other hand, absorbed energy may allow a better estimate of the extent of delamination, due to the lower slope shown in figure 3. Of course absorbed energy is a measured parameter and thus can not be used to predict damage (a numerical simulation which should calculate the absorbed energy must include a damage model; it would therefore be able to predict the occurrence of damage itself), but only for comparison purposes when carrying out experimental tests.

It is worth noting that Cantwell [13] also finds a unique relationship between contact force and delamination for glass-polyester laminates, but with a gradually increasing trend like the one examined here for absorbed energy (figure 3). This difference may be attributed to material behaviour, since glass-polyester exhibits strain-rate sensitivity even at low impact velocity while graphite-epoxy does not [3], as proved also by the established analogy between impact and quasi-static indentation for the latter [21, 22] (which would not hold if the material was rate dependent). The observation that the delamination threshold does not depend on specimen diameter and constraints is usually explained by saying that out-of-plane shear forces (which do not depend on laminate dimensions and boundary conditions) rather than bending moments (which do depend on them) are responsible for initiation of delamination [3, 23]. The results of the present study confirm this interpretation.

Comparisons of specific impact events in figures 6 and 7 show the effects of diameter and constraints in detail. In figure 6, the supported plate exhibited a lower stiffness than the clamped one; this led to a greater displacement and a lower energy absorption (as can also be appreciated by the area enclosed by the curves on the diagram), which is associated with a lesser extent of damage. Due to large deflection with respect to the plate thickness, geometrical nonlinearity is important, particularly in the clamped specimen, as can be seen by the overall curvature of plots. The relationship between contact force and displacement shows increasing slope as displacement increases, which can only be attributed to membrane stiffening of the plate

(nonlinear material behaviour, in particular damage, may only lead to a decrease in slope since it tends to reduce the plate stiffness). It is also interesting to note that at the beginning of the loading phase of contact the boundary conditions have no influence on the dynamic response, as one can expect since elastic waves have not yet reached the boundary. The initial plateau which can be seen both in the load-displacement and in the load-time curves (see also figures 8 and 9) is most likely due to the dynamic effects of the first flexural wave produced by the impactor, which reveal themselves when the wave comes back to the impact point after being reflected by the boundary. It can be noted that this plateau is correctly predicted by numerical simulation (as shown in figures 8 and 9); thus it can not be attributed to effects which were not accounted for in the model, like material damage or any spurious phenomenon occurring in the experimental apparatus.

In the test configurations considered here, the effect of specimen diameter appears to be stronger than that of constraint because of the great difference between the diameters of the clamping fixtures (the difference between the plots in figure 7 is larger than the difference between the ones in figure 6). The smaller specimen had a stiffer behaviour and was subjected to more severe damage than the larger one. The difference in initial velocity of the impactor between the tests reported in figure 7 is not negligible; this, however, does not seem to have had a significant role in determining the huge difference in mechanical response, since similar differences were also shown by pairs of tests at equal initial velocity. Obviously maximum deflection was lower in the 76 mm laminate; therefore membrane stiffening was much less important, as shown by the linearity (apart from oscillations) of the force-displacement plot during the loading phase. It is important to recall that a significant part (more than 2 mm) of the impactor displacement (6.3 mm in this case) is due to local permanent indentation, thus it is not associated with overall deformation of the laminate.

Although each of the two pairs of tests presented in figures 6 and 7 exhibits different stiffness, the maximum contact force is similar in all cases (while one could expect higher force in stiffer conditions). An explanation of this result is suggested by figure 5, where the maximum load does not exceed a certain value (slightly larger than 4 kN), regardless of the initial energy and the test configuration. This value may be associated with an unstable propagation of delaminations. Should this be the case, this load level could not actually be exceeded in practice because, after it has been attained, further indentation of the laminate would result only in delamination enlargement, the material not being capable of withstanding a higher force. This is in agreement with experimental results presented in [12], where the impact energy range considered is much wider than in the present study, and also covers values which lead to perforation of the laminate.

As figures 8 and 9 show, numerically predicted contact force is substantially greater than the experimental results, and this difference is greater in higher energy events; numerical contact duration is smaller than the experimental values. A similar discrepancy is reported in [4], where

it is demonstrated that disagreement between numerical and experimental results is substantially reduced if a material damage model is employed. Thus the differences between numerical and experimental curves, both in figures 8 and 9, can be ascribed to material failures only, which do occur in experiments but are not accounted for in the present model. Therefore such a model can be reliable for impact events where the extent of failures is limited, or when the earliest phase of contact is considered. Indeed figures 8 and 9 show that contact force evaluation is correct for some tenths of milliseconds after the beginning of the collision. Higher frequency vibrations due to the propagation of flexural elastic waves, superposed on the fundamental mode, are visible in numerical calculation; they can also be recognized in experimental curves, particularly in the lowest velocity impact, but they have smaller amplitude and larger period.

This effect also is most likely due to damage, which reduces the stiffness of the laminate; it can be noted that dynamic behaviour of laminates is altered significantly even if failures do not seem severe. When initial energy of the impactor is higher, these oscillations are almost completely hidden; when the contact force is close to the maximum value, one or more sudden load drops can be seen that are usually interpreted as the effect of propagating delaminations [20]. However it is interesting to note that first damage cannot be recognized in contact force history as evident discontinuity or slope change, in agreement with the results described in chapter 2. The load levels at which sharp drops occur are quite larger than the threshold shown in figure 5, therefore they can be caused by propagation, not by initiation of delamination; when contact force is close to the maximum, they may also be attributed to fibre fracture. Matrix cracks, that usually trigger delamination and take place at even lower force values, are not distinguishable at all.

Comparing the curves obtained for the simply supported 200 mm plate (figure 9) with those plotted in figure 8 for the equal energy impact on the clamped specimens, a better agreement is observed for the supported laminate than for the clamped one. Once more, this is due to more severe failures in the second case. The different response of specimens of 200 and 76 mm diameter is well predicted in its essential features; the first higher frequency oscillations in the smaller plate are described accurately too.

It is useful to comment on the strain histories reported in figure 10. Agreement between numerical prediction and measurement is better than observed for contact force: the analysis underestimated the period of oscillations, but the values of peaks, especially in the first phase, are estimated correctly. These results, seemingly conflicting, can be explained by recalling that the contact force values are strongly influenced by failures taking place under the impactor head, which create a deep dent on the front side of laminates. This effect, which is not modelled, leads to much lower load and greater impactor displacement with respect to numerical prediction. Outside the contact zone, the plate deflection, together with strains, is smaller, thus closer to numerical values. The difference in period of oscillations is due to the reduced stiffness of the laminate.

As pointed out earlier, a numerical model which does not account for the degradation of the constitutive behaviour of the material caused by failures allows reliable prediction of contact force or impactor displacement only in the earliest phase of contact, unless the impact induced damage is very small. Nevertheless, such a model may be employed to predict whether delamination will or will not occur during an impact event, provided the delamination threshold value of contact force is known from experimental tests. The maximum value of contact force is always overestimated by the model; thus, if the delamination threshold is actually reached during an impact case, numerical analysis will surely predict this. Since the relationship between delamination area and maximum contact force is independent of the in-plane dimensions of the laminate and of its constraints, the experimental measure of the threshold obtained in particular conditions can be used for comparison with contact force evaluated numerically even in different conditions.

It has been noted that strains at a certain distance from the impact point are estimated with reasonable accuracy, considering the limitations of the present model. This result may also be useful, for example, to predict in what region of the laminate the strains (or stresses) exceed a given design allowable. It is expected that numerical values of strains are not reliable in the vicinity of the impact point, where damage is likely to occur; therefore it is not sure that the present model is able to evaluate the extent of the damaged zone. However the possibility of obtaining approximate prediction in this sense, for example by means of simple criteria like the ones cited in [3], may be further investigated.

3.6. Conclusions

Low velocity impact tests were performed on CFRP laminates, in order to assess the effect of dimensions and boundary conditions on dynamic response and material damage. Four different configurations, obtained by all combinations of two dimensions and two constraint conditions, were considered; experiments were carried out at three energy levels. Dynamic numerical analysis of impact events was also performed by means of a finite element model, and results were compared to experiments. The conclusions of this study can be summarized as follows.

Both diameter and boundary conditions have an evident influence on the impact behaviour of specimens, because they affect the target stiffness. Due to the different values of stiffness, the delamination area measured on laminates cannot be related to initial energy. More interesting relationships can be found with absorbed energy or with maximum contact force. In both cases the relationship is independent of the boundary conditions and the in-plane dimensions. While the delamination area gradually increases as absorbed energy rises, its relationship with contact force shows a sudden and rapid increase as force exceeds a certain threshold. The absorbed energy is a measured parameter; therefore it cannot be viewed as a prediction tool. On the other

hand, a numerical simulation can provide an estimate of the maximum contact force, which can be compared with an experimental measure of the delamination threshold. In this way a safe prediction, about whether a delamination is initiated or not, can be obtained even by means of simulations which do not account for material damage.

Failures caused by impact affect the dynamic response of laminates, as can be deduced from a comparison between numerical simulations (where no damage model is included) and tests. However, the essential features of the response are described correctly, and the numerical prediction is reliable in the earliest phase of contact, when material damage is still negligible. In particular, it has been shown that a satisfactory approximation is attained as regards strains and stresses at some distance from the impact point. Caution is necessary when considering the stresses near the impact point; however, the possibility of obtaining approximate predictions of the extent of damage may be further investigated.

References for chapter 3

1. Abrate S. *Impact on laminated composite materials*. Appl Mech Rev 1991;44(4):155-190.
2. Abrate S. *Impact on laminated composites: recent advances*. Appl Mech Rev 1994;47(11):517-544.
3. Abrate S. *Impact on composite structures*. Cambridge: Cambridge University Press, 1998.
4. Davies GAO, Zhang X. *Impact damage prediction in carbon composite structures*. Int J Impact Eng 1995;16(1):149-170.
5. Sutherland LS, Guedes Soares C. *Scaling of impact on low fibre-volume glass-polyester laminates*. Compos Part A-Appl S 2007;38(2):307-317.
6. Morton J. *Scaling of impact-loaded carbon-fiber composites*. AIAA J 1988;26(8):989-994.
7. Chen JK, Sun CT. *Dynamic large deflection response of composite laminates subjected to impact*. Compos Struct 1985;4(1):59-73.
8. Cairns DS, Lagace PA. 1989, *Transient response of graphite/epoxy and kevlar/epoxy laminates subjected to impact*. AIAA J 1989;27(11):1590-1596.
9. Collombet F, Lalbin X, Lataillade JL. *Impact behaviour of laminated composites: physical basis for finite element analysis*. Compos Sci Technol 1998;58(3):463-478.
10. Cantwell WJ, Morton J. *Geometrical effects in the low velocity impact response of CFRP*. Compos Struct 1989;12(1):39-59.
11. Robinson P, Davies GAO. *Impactor mass and specimen geometry effects in low velocity impact on laminated composites*. Int J Impact Eng 1992;12(2):189-207.
12. Liu D, Raju BB, Dang X. *Size effects on impact response of composite laminates*. Int J Impact Eng 1998;21(10):837-854.
13. Cantwell WJ. *Geometrical effects in the low velocity impact response of GFRP*. Compos Sci Technol 2007;67(9):1900-1908.

14. Khalili MR, Malekzadeh K, Mittal RK. *Effect of physical and geometrical parameters on transverse low-velocity impact response of sandwich panels with a transversely flexible core*. Compos Struct 2007;77(4):430-443.
15. Tiberkak R, Bachene M, Rechak S, Necib B. *Damage prediction in composite plates subjected to low velocity impact*. Compos Struct 2008;83(1):73-82.
16. Caprino G, Langella A, Lopresto V. *Elastic behaviour of circular composite plates transversely loaded at the centre*. Compos Part A-Appl S 2002;33(9):1191-1197.
17. Minak G, Ghelli D. *Design of a drop-weight machine for composite materials impact testing*. In: Proceedings of the ICCSM5 Congress, Matejiček F, editor. Trogir/Split (HR): Croatian Society of Mechanics, 2006.
18. D 3763 – 06 *Standard test method for high speed puncture properties of plastics using load and displacement sensors*. Annual Book of ASTM Standards. West Conshohocken, PA: ASTM International, 2006.
19. D 7136/D 7136M – 05 *Standard test method for measuring the damage resistance of a fiber-reinforced polymer matrix composite to a drop-weight impact event*. Annual Book of ASTM Standards. West Conshohocken, PA: ASTM International, 2005.
20. Schoeppner GA, Abrate S. *Delamination threshold loads for low velocity impact on composite laminates*. Compos Part A-Appl S 2000;31(9):903-915.
21. Sjöblom PO, Hartness JT, Cordell TM. *On low-velocity impact testing of composite materials*. J Compos Mater 1988;22(1):30-52.
22. Wu E, Shyu K. *Response of composite laminates to contact loads and relationship to low-velocity impact*. J Compos Mater 1993;27(15):1443-1464.
23. Caprino G, Langella A, Lopresto V. *Prediction of the first failure energy of circular carbon fibre reinforced plastic plates loaded at the centre*. Compos Part A-Appl S 2003;34(4):349-357.

CHAPTER 4

Impact and compression after impact testing according to two different ASTM standards

4.1. Introduction

In order to study the effects of low velocity impact of foreign bodies on Carbon Fibre Reinforced Polymers (CFRP), which still remain an important design issue involving phenomena that are not well understood [1], many researchers have examined results obtained in experimental tests performed on a wide variety of specimen geometries. Consequently, the effect of geometry on impact response of laminates and induced damage becomes a key factor when trying to compare results found in different conditions, and has already been discussed by several authors, for instance [2-5] (see also chapter 3).

The same also happens in the study of Compression After Impact (CAI) strength, which has been recognized for many years as the mechanical property suffering the largest reduction with respect to the typical values of the undamaged material [1]. In general, elastic instability is likely to occur during compression tests, especially in the case of thin laminates. Buckling phenomena are strongly dependent on the specimen geometry and size, thus the understanding of the effects of geometrical factors becomes even more important in this field. Many papers regarding the compressive residual strength of impacted laminates are available (for example [6-10]), in which a common concern is to avoid specimen buckling, by means of suitable support, in order to measure load values which do not depend on geometry, but only on the material itself.

It is however felt that, in addition to the work carried out up to now, conditions where buckling actually takes place should also be investigated, because this topic does not seem to have received sufficient attention so far. In slender components, where the compressive strength of the material can not be reached due to the danger of instability, the possible influence of impact damage on buckling behaviour and strength, together with its dependence on geometry, should be taken into account, as pointed out in [11].

In the present study low velocity impact tests were carried out on coupons of the same thickness but two different geometries, accomplished with support fixtures built according to two ASTM standards [12-13]. CAI tests were then done on specimens of both types, following the specifications of ASTM D7137 [14]; the only significant discrepancy between the specifications and the experiments was the laminate thickness, (2.75 mm in the present study,

instead of 5 mm), chosen in order to examine the behaviour of thin plates. The aim was to highlight the different impact and post-impact compression response of the two specimen types, trying to understand the interaction between damage propagation, buckling and residual strength.

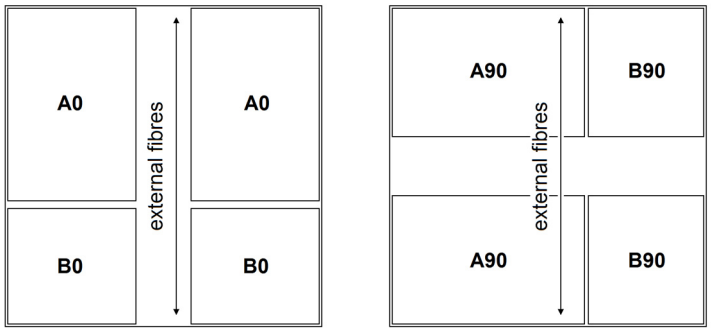

Figure 1 – Schematic of the four types of specimens tested.

4.2. Experimental method

4.2.1. *Material*

The material employed for the tests consisted in 16 ply T300 graphite fibre/epoxy matrix laminates, manufactured from unidirectional prepregs by curing in an autoclave, cut in rectangular specimens 100 mm wide and 150 mm (type A) or 90 mm (type B) long. The average thickness was 2.75 ± 0.05 mm. The values of the in-plane elastic constants of the single ply, supplied by the manufacturer, were as follows: E_1 = 100 GPa, E_2 = 11 GPa, G_{12} = 4.2 GPa, ν_{12} = 0.28.

The stacking sequence of the original laminates was quasi-isotropic $[0/0/90/90/45/-45/45/-45]_S$; two different lay-ups were obtained for the test plates, by cutting them in two orthogonal directions (see schematic in figure 1). In half of the specimens the fibres of the external layer were aligned lengthwise, or in the 0° direction (that is parallel to the 150 mm or 90 mm side for type A and B, respectively), thus maintaining the same arrangement of the original laminates. The remaining specimens had a $[90/90/0/0/-45/45/-45/45]_S$ lay-up, with

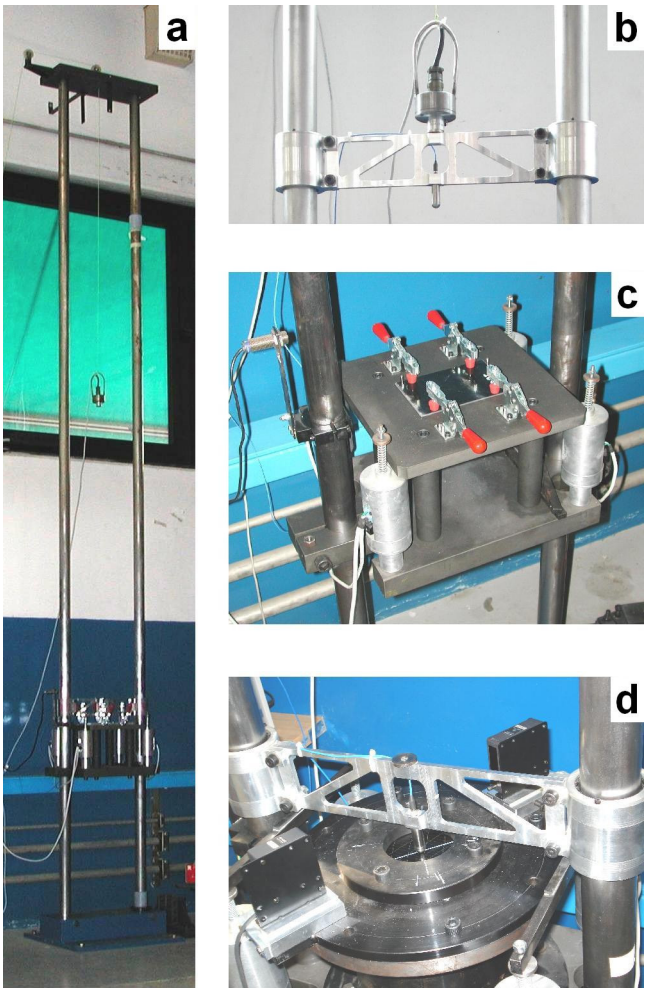

Figure 2 – Drop weight tester. a) Overall view of the machine. b) Impactor. c) Support fixture according to ASTM D7136. d) Support fixture according to ASTM D3763.

external fibres aligned widthwise (that is parallel to the 100 mm side). From here on, the four types of specimens resulting from all possible combinations of length and stacking sequence will be referred to as A0, A90, B0 and B90, as figure 1 shows. Nine coupons were available for each type, a total of 36 coupons being tested.

4.2.2. *Impact tests*

An instrumented drop-weight machine [15], shown in figure 2, was used to perform low velocity impact tests. A piezoelectric load cell attached to the impactor (whose 12.7 mm diameter hemispherical head is the only part indenting the target laminate), shown in figure 2b, allowed the measurement of the contact force history. The actual velocity of the impactor before and after collision was evaluated by a laser device located approximately 30 mm above the specimen surface. An electromagnetic braking system prevented repeated impacts. The signals of both load cell and laser were acquired at 100 kHz sampling frequency without any filtering. The velocity and the displacement of the impactor as a function of time, as well as the energy absorbed during impact, were calculated by numerical integration of the contact force history, as suggested in [12].

The overall impactor mass was 1.22 ± 0.01 kg; three different drop heights of 0.5, 1.0 and 1.5 m were chosen, corresponding to nominal impact energies of 6, 12 and 18 J respectively. At least two tests were performed at each drop height for every specimen type, and at least two specimens were kept undamaged. Impact-induced damage was examined by visual inspection. Subsequently, all specimens were tested in compression as described below.

Different support fixtures were used for type A and B specimens during drop-weight tests. The configuration used for type A laminates (see figure 2c) was compliant with the prescriptions in [12]: the coupon was placed on a rectangular steel base with a 125 by 75 mm rectangular opening, being correctly positioned thanks to three pins and held by four lever clamps with rubber tip. Type B laminates were clamped between two 76 mm internal diameter steel rings, according to [13] (see figure 2d). In both cases impact occurred exactly at the centre of the target.

4.2.3. *CAI tests*

All of the 36 specimens were subjected to compression tests in a servo-hydraulic machine (see figure 3). The laminates were supported in a fixture built according to [14], shown in figures 3b-d. Lateral support of the coupon was provided by two pairs of 8 mm thick plates, with flat edges in contact with the laminate faces, on the upper and lower ends, and by two pairs of plates with knife edges on the left and right sides, leaving a central rectangular 94 by 134 (type A specimens) or 94 by 74 (type B) mm unsupported zone. All of the supporting plates could be adjusted before testing so that the laminate fitted exactly in the facility without any

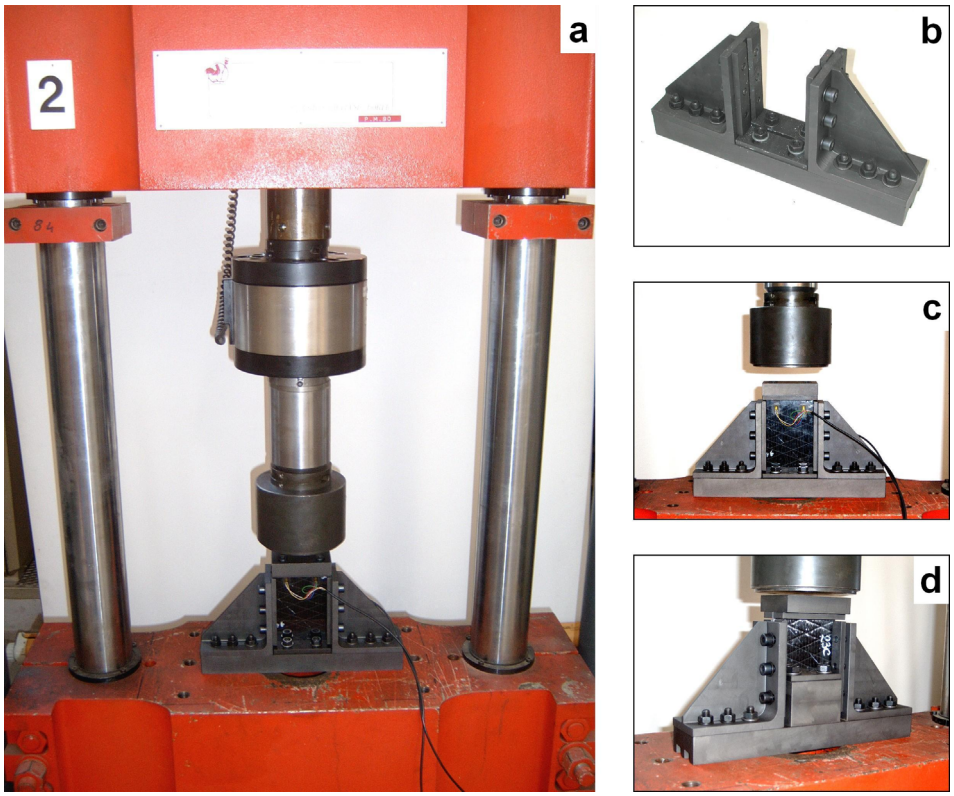

Figure 3 – Apparatus for CAI tests. a) Servo-hydraulic machine. b) Support fixture according to ASTM D7137 (without upper loading plate). c) Arrangement for type A specimens. d) Arrangement for type B specimens.

clearance between its faces and the surfaces supporting them. A 1 mm clearance was left, according to the standard, between the lateral sides of the specimen and the angles of the fixture holding the knife plates, in order not to prevent the lateral expansion of the specimen under compression. Since [14] prescribes 150 mm long specimens, the fixture, designed for this dimension, was also adapted to the 90 mm long type B laminates considered in the present study by inserting a 60 mm thick steel block between the base plate and the specimen (see figure 3d).

For both A and B laminates, the compressive load was applied in the lengthwise (vertical) direction, perpendicular to the 100 mm sides (that is in the direction of the 0° fibres). The tests were carried out in displacement control, at a crosshead velocity of 0.01 mm/s, until failure of the laminate, always accompanied by a dramatic load drop, was reached. In addition to the applied load and the crosshead displacement, measured by the control system of the machine, strains were recorded in most of the tests by means of strain gauges arranged in various patterns.

The most important difference between the recommendations in [14] and the present experiments was the laminate thickness, much smaller than the value of 5 mm suggested by the standard.

4.3. Numerical analysis

In order to highlight some results of the compression tests of the type A laminates, especially concerning the elastic instability of the specimens (which will be discussed on in the following section), a numerical analysis was performed to evaluate the critical buckling load and the mechanical response in postbuckling conditions, by means of the program described in chapter

1. For the aims of the present study, which required a static analysis, the dynamic relaxation algorithm was employed, which is known to be efficient and reliable when applied to strongly nonlinear phenomena such as elastic instability [16].

As explained in chapter 1, no material damage model was implemented: the constitutive equations were elastic linear, so the numerical solution did not consider the effect of failures on the mechanical behaviour of the laminates. It will be shown, however, that this simplifying assumption did not prevent from obtaining reliable results in good agreement with experimental data, which led to a better understanding of some aspects of compression tests.

The test apparatus, described in the previous section, is intended to prevent both the out-of-plane displacement and the rotation of the specimen along its upper and lower sides, while the knife edges of the supports along the vertical sides prevent only the displacement of the laminate, allowing a rotation about them. Therefore one may discretize only the 134 by 94 mm unsupported zone of the plate, model the upper and lower edges as built-in and leave the left and right sides free to rotate. Some preliminary calculations with such ideal boundary conditions, however, yielded improbably high values of the critical buckling loads. As a consequence, and given that a correct identification of the actual boundary conditions appeared not feasible, it was decided to model the whole 150 by 100 laminate and to constrain only the transverse displacement of the supported areas. In this way the out-of-plane motion of the 8 mm wide bands in contact with the supporting side plates, at the upper and lower ends, was prevented; at the same time the plate sections along the boundary of the central unsupported zone were free to undergo some rotation, but also had to maintain continuity with the adjacent part of laminate which could not move. This made it possible to achieve a satisfactory modelling of the actual boundary conditions. The discretization used had 1598 rectangular four-node elements, whose side length ranged from 2 to 4 mm.

4.4. Results and discussion

4.4.1. *Impact tests*

Figure 4 reports an overview of the data recorded in all impact tests. In all specimens, delamination was clearly visible to the naked eye on the back surface as a slightly protruding zone, which had roughly the shape of a rhombus whose diagonals were oriented in the directions of the fibres of the external 0° and 90° layers. The major diagonal of the rhombus was always parallel to the fibres of the outermost layer (0° in A0 and B0, 90° in A90 and B90 coupons); its position coincided approximately with the longest back-face splitting. Previous examination of polished sections of damaged laminates (identical to the ones employed for the present study, and impacted in similar conditions) by optical microscope showed that the extent of the largest delamination, always located at the lowermost interface (between the external 0° or 90° plies on

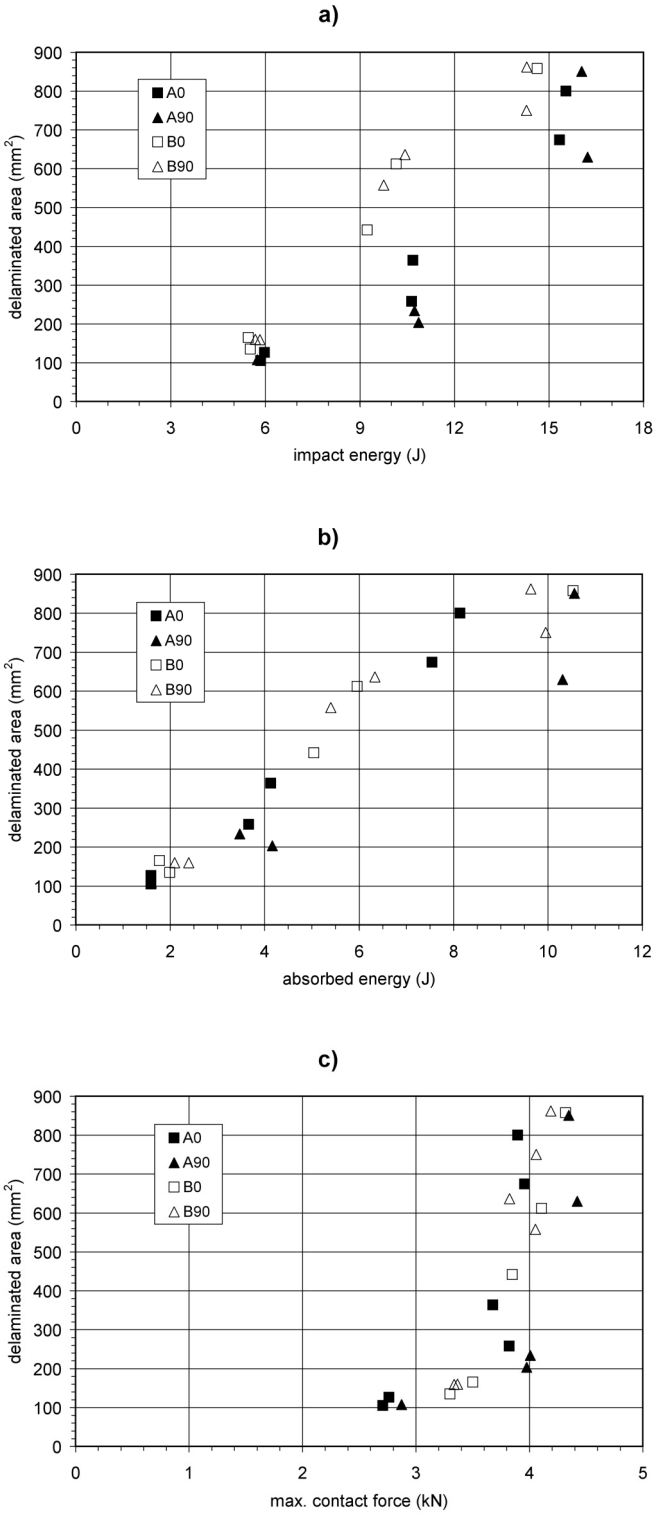

Figure 4 – Area of impact-induced delamination as a function of measured impact energy (a), energy absorbed after collision (b) and maximum contact force (c).

the back face and the 90° or 0° plies just above), corresponded to the dimensions of the protruding zone (see chapter 2, section 2.4). Therefore the area of a rhombus calculated by measuring the diagonals was used as an estimate of the area of the largest delamination in figure 4.

The length of the largest diagonal ranged from 20 ÷ 25 mm (after a 0.5 m impact on type A specimens) to 75 ÷ 80 mm (in A0, B0 and B90 specimens subjected to 1.5 m impact); in the latter case the delamination reached the clamping rings of the type B laminates. The boundary of the rectangular opening of the fixture employed for type A laminates was never reached by delamination: in the case of A0 coupons the greatest length of 80 mm was much smaller than the length of the opening (125 mm); in the A90 coupons the delamination, elongated widthwise, never approached the width of the opening (75 mm).

A90 specimens behaved differently as regards fibre fracture; they showed severe fibre damage of the external 90° plies (as well as in the 0° layer above) just below the impact point. In no other specimen type was damage of the external fibres on the back face observed; in A0, B0 and B90 some fibre damage was visible only after the 1.5 m impact in the layer above the external one, through the residual opening of the splittings of the external layer. On the other hand, the delamination was less elongated but slightly wider in A90 specimens than in A0, this being seen in similar areas.

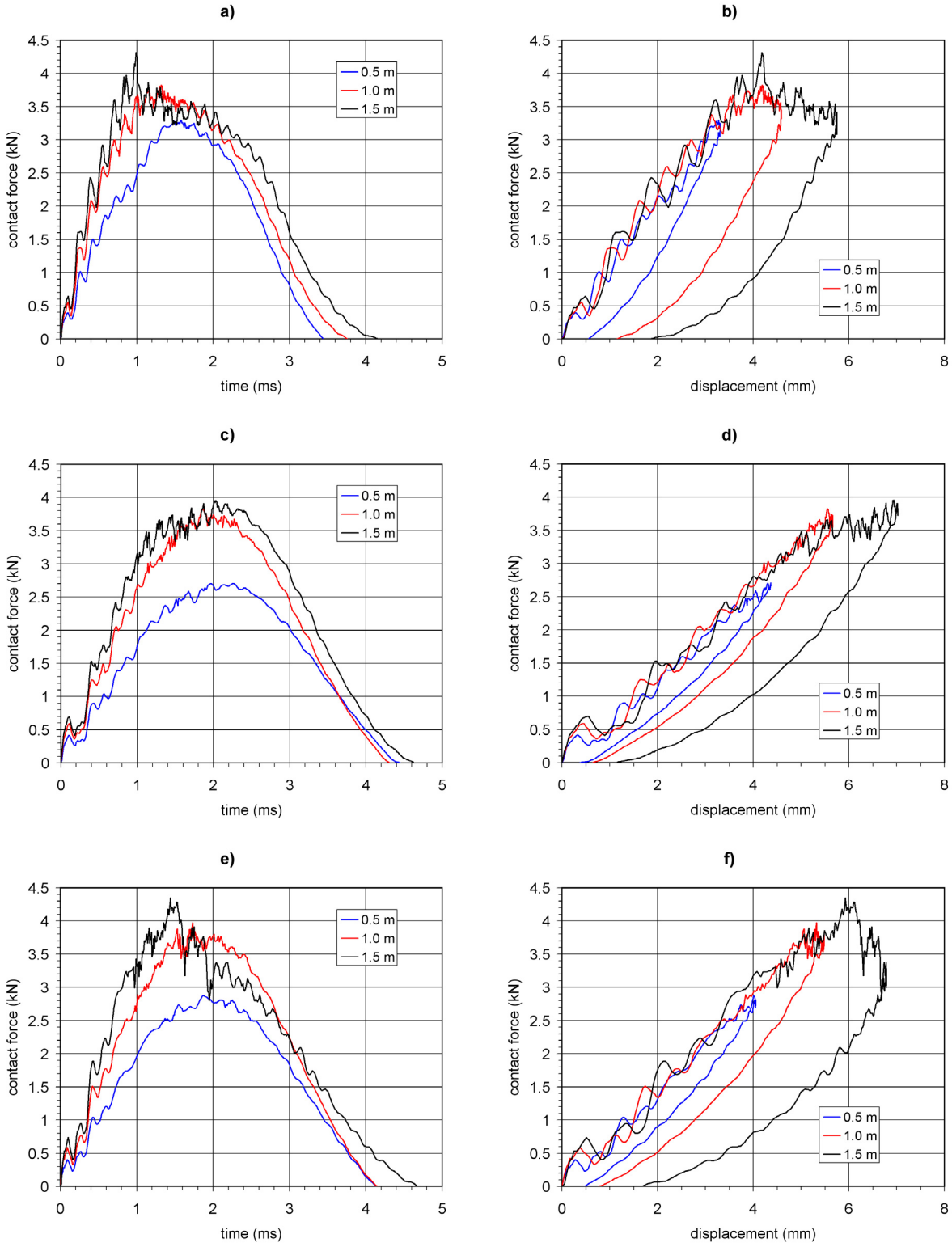

Figure 5 – Representative impact tests on B (a and b), A0 (c and d) and A90 (e and f) specimens. The legend in the diagrams indicates the drop height.

On the impacted face of the laminates the damage consisted in permanent indentation (visible at all energy levels), splitting and fibre fracture inside the dent (only in type A specimens which underwent a 1.5 m impact and in type B specimens after 1.0 m or 1.5 m

impact) and small microbuckling bands just outside the dent. The latter phenomenon appeared in most of the B coupons, had its largest extent in A90 specimens, but was absent in all A0 laminates except one. As regards the size of the permanent indentation, it was similar in A0 and A90 laminates (up to 7 mm diameter for the highest drop height), and slightly larger in B laminates for the same incident energy (up to 9 mm diameter).

While no difference in the impact response was noticed between B0 and B90 specimens (see the points in figure 4), as expected from the isotropy of the circular test rig, some differences were apparent when comparing A0 and A90, and can be explained by considering the contact force-time and contact force-impactor displacement curves displayed in figure 5.

A90 laminates showed slightly larger flexural stiffness than A0, because in the former the fibres of the external plies are parallel to the shorter side; this can be appreciated by the difference in slope of the load-displacement curves (figures 5d and 5f) during the loading phase of contact. The different stiffness is most likely the cause of the different impact response which can be observed both in the contact force history (figures 5c and 5e) and in the material damage (figure 4). Although impacted at the same initial energy, A90 laminates exhibited a higher contact force; the load-time curve was smoother in A0 than in A90 specimens, especially at greater energy when the contact force history of A90 presented repeated sharp load drops. Greater stiffness, thus higher stresses in the load-bearing 90° fibres, could explain the microbuckling phenomenon, which appeared in A90 but not in A0 specimens.

A significant difference in absorbed energy was also recorded after the 1.5 m drop height test: while the initial energy of the impactor was similar (see the four points at higher energy, approximately 16 J, in figure 4a), the energy absorbed during contact was much larger in laminates with 90° external fibres (the corresponding four points in figure 4b are quite distant). Since A90 coupons underwent more severe fibre fracture than A0 specimens, as noted before, the most probable explanation of this evidence is that in A90 more energy was spent in breaking the fibres, while the extent of delamination was similar in the two stacking sequences. Fibre fracture may also be the cause of the drops in contact force history. Another reason for the larger energy absorption of A90 specimens could be a different pattern of internal delamination, which can not be detected by visual inspection. The smaller length and larger width of the delamination visible on the back face of A90 laminates seem to support this hypothesis, the verification of which would need non-destructive techniques (not available for the present study).

As regards the comparison between the type A and B specimens, noticeable differences can be recognized. The smaller circular B samples had a much stiffer impact response (see the load-displacement diagrams in figures 5b and 5d); this resulted in shorter contact duration, more rapid load increase up to the maximum values and a longer phase in which the contact force was almost constant (apart from oscillations and drops), as can be seen in figure 5a. This phase is most likely associated with progressive indentation of the laminate (the impactor displacement

keeps increasing) and propagation of damage in the form of delamination and fibre fracture, according to the interpretation given in previous studies [17]. The stiffer behaviour of B specimens, and their consequent reduced ability to store elastic energy before failure, led to more extended delamination, initial energy being equal (see figure 4a); it is important to note that in 1.5 m drop height tests the propagation of delamination was probably constrained by the clamping rings.

Some general comments can also be made on the graphs in figure 4. As is well known, impact energy is not a useful parameter for establishing a relationship with the delamination area when different test configurations are dealt with, because a distinct relationship is found for each configuration [1]. It has been shown that when the delamination area is plotted against absorbed energy [3] or maximum contact force [4] an empirical relationship is obtained that is reasonably independent of test conditions (see also chapter 3). Results reported in figures 4b and 4c are in discrete agreement with this; some difference can be seen in figure 4c between A0 and A90 specimens (the latter requiring higher loads to produce the same delamination area). The fact that delamination area depends on maximum contact force only, regardless of the dimensions of the coupon, is usually interpreted by attributing the propagation of delaminations to out of plane shear instead of normal flexural stresses. Consequently, the difference indicated by figure 4c may suggest that in the present case bending moments also had a significant influence.

4.4.2. *CAI tests*

Global buckling occurred during the compression test of all specimens, both impacted and unimpacted. Lateral deflection of laminates was clearly visible before final collapse, and was accompanied by an evident loss of linearity in the load-displacement curve and in the strain measurements.

Some representative load-displacement plots are shown in figure 6. It can be seen that after an initial phase characterized by very small load, in which the clearances in the test fixture were eliminated, the applied force increased linearly with the displacement of the hydraulic cylinder. When a certain load level was reached, a bending in the load-displacement relationship was noticed which was consistently related with the first evidence of lateral deflection. Of course due to small imperfections in the specimen machining and in the test fixture the onset of buckling was never sudden, as would be in ideal conditions. In type A laminates instability became evident at load levels well below the maximum reached before failure, as can be seen in the examples reported in figures 6a-b where a loss of linearity is visible between 30 and 40 kN; in type B laminates buckling usually took place just before failure, so that bending of the load-displacement curve was barely visible or not visible at all (see examples in figures 6c-d).

In A0 and in all B samples the deformed shape of the buckled laminate had one half wave, both in the transversal and in the longitudinal direction (that is the direction of load application).

A90 specimens, undamaged or subjected to 0.5 m or 1.0 m impact, showed a buckling shape with one half wave in the transversal direction and two half waves in the vertical direction, not exactly antisymmetric with respect to the median horizontal axis, but anyway undoubtedly visible. When the drop height was increased up to 1.5 m, A90 specimens also exhibited a deformed shape with one half wave, as was the case of the other specimens.

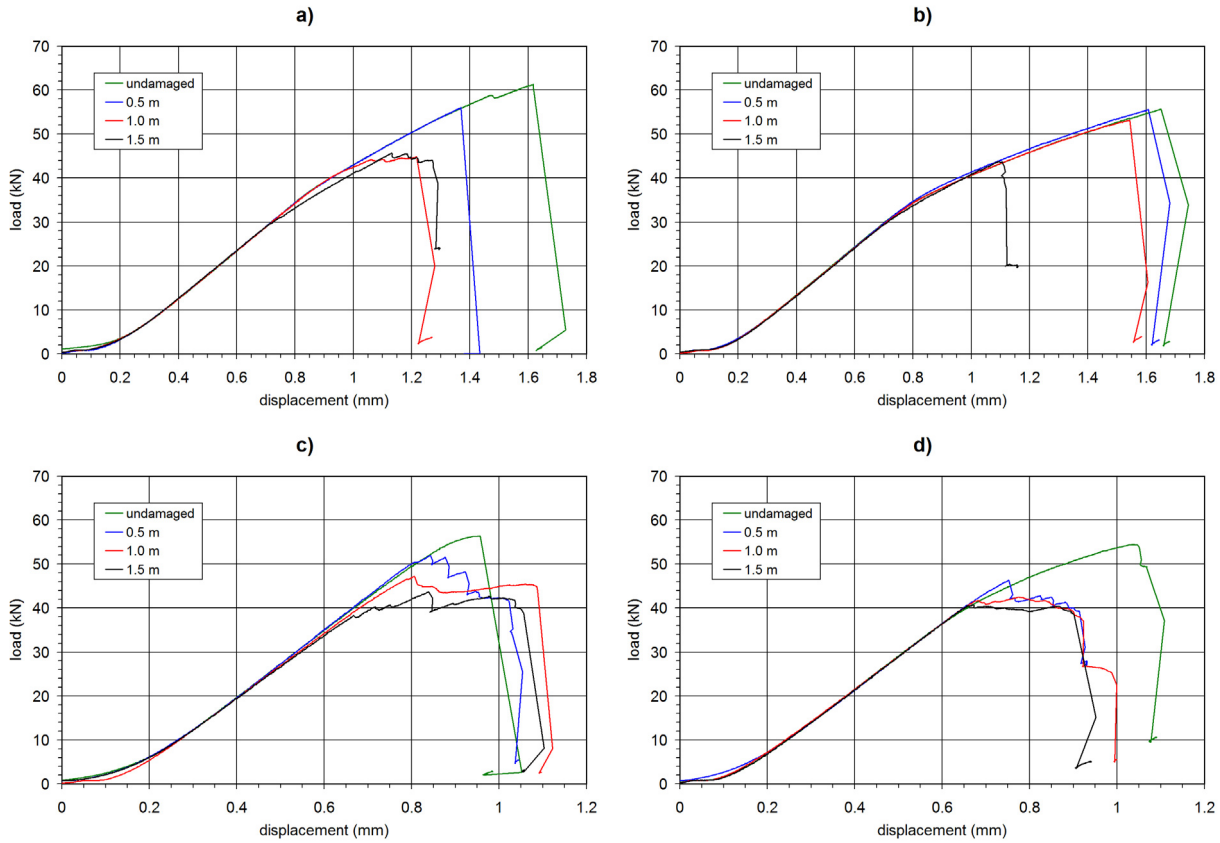

Figure 6 – Examples of axial force-axial displacement plots recorded during compression tests. a) A0 laminates. b) A90 laminates. c) B0 laminates. d) B90 laminates. The legend in the diagrams indicates the drop height of the corresponding impact tests.

The buckling shape of the laminates was confirmed by the strain gauge measurements and by comparison of them with the numerically predicted strains. Two examples of such a comparison are presented in figures 7 and 8, both of which refer to laminates subjected to a 0.5 m drop height impact. These cases were chosen for their small damage area in place of undamaged specimens because unfortunately the only strain-gauged unimpacted laminates did not give significant results during compression test. The instrumented A0 laminate exhibited an anomalous behaviour and failed due to end crushing, therefore could not be considered a reliable case study. The A90 specimen failed in an acceptable way but the strain gages, placed in the positions recommended by the standard [14], read very small strains as will be explained later.

According to the numerical analysis, the predicted critical load of the A0 laminates was 42.5 kN. At loads higher than this threshold, the only possible buckling mode was found to be that with one half-wave in both longitudinal and transversal direction (at least within the ultimate

strength of the undamaged laminates, approximately 61 kN), in agreement with the experimental observations.

Figure 7 shows the readings of the two pairs of strain gauges on an A0 specimen (the position of the sensors can be seen in the schematic in figure 7a) together with the corresponding numerical results. For each pair of strain gauges the membrane strain (that is the deformation of the middle plane of the laminate) was computed as the average of the two measures, while the bending strain was evaluated as half of the difference between them, as suggested in [14]; these data are plotted in figures 7c-d.

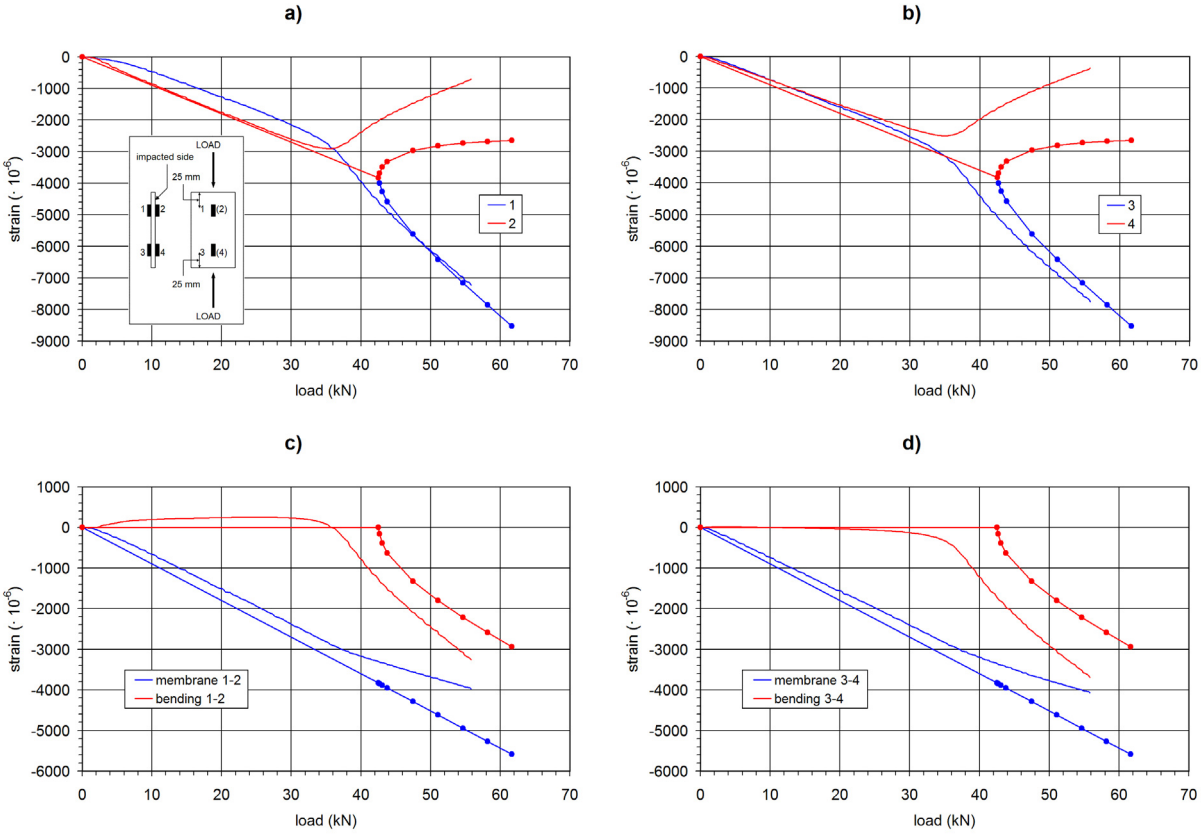

Figure 7 – Example of results of strain gauge measurements on A0 laminate. The lines without circles are experimental data, the lines with circles are numerical predictions.

Bearing in mind on the one hand the simplifying assumptions included in the model, and on the other hand the imperfections which cannot be completely eliminated from the test rig, the agreement with the experimental measures can be considered very good. The critical load was overestimated by the computation. It must be noted, however, that a precise estimate for the critical load could not be deduced from the experimental results, because the lateral deflection of the laminate developed gradually instead of starting suddenly. For this reason the drift of the bending strain from the ideal null value in figures 7c-d, observed at roughly 30 kN, most likely occurred at a smaller load than the critical threshold which would have been measured in an ideal situation. In addition it is well known that the buckling load is usually overestimated by

finite element calculations, also because the numerical boundary conditions never reproduce the actual ones exactly. Finally, part of the difference between the numerical and experimental plots in figure 7 can be justified by the reduction (which can be estimated at 2 kN from the tests) of the buckling load of the impact damaged laminate with respect to the undamaged one (to which the numerical results refer).

A comparison analogous to the one of figure 7 is presented in figure 8 for the compression test of an A90 specimen. In this case the numerical calculations predicted a first critical load at 40.5 kN (corresponding to the change in slope of the plots in figure 8), beyond which the laminate buckled with a shape identical to the one of A0 specimens. When a second critical load, estimated at 44 kN, was reached the buckling mode switched to a two-half-wave shape, analogous to the one recorded during the experiments both on the undamaged laminates and after a 0.5 m or 1.0 m drop height impact. The mode switching phenomenon is responsible for the discontinuity in the curves of figure 8.

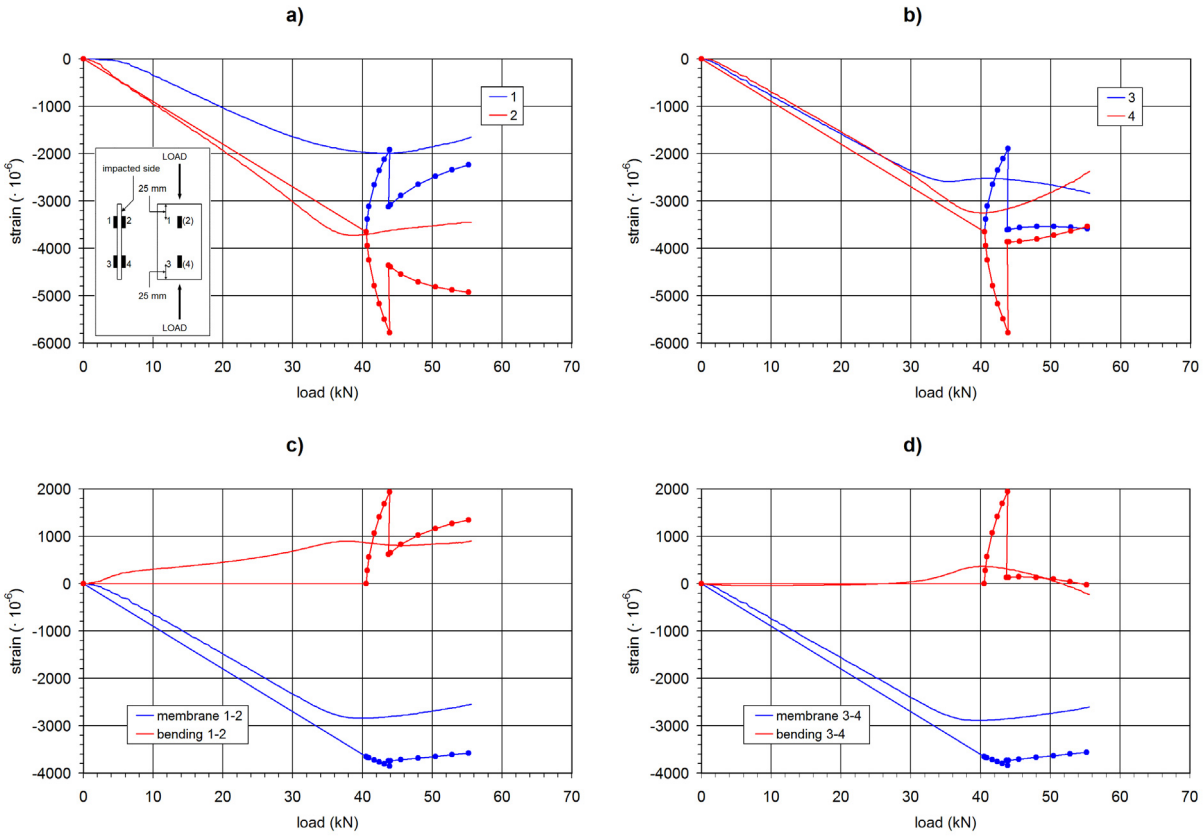

Figure 8 – Example of results of strain gauge measurements on A90 laminate. The lines without circles are experimental data, the lines with circles are numerical predictions.

As was the case of the A0 laminate, a reasonably good agreement can be seen between numerical and experimental results also for the A90 specimens. In this case the difference between predicted and observed first critical load must be attributed entirely to the imperfections in the test conditions and to the limitations of the model, because the experiments did not show

any decrease of the critical load in the A90 plates impacted from a 0.5 m height with respect to the undamaged specimens.

A distinct mode switch was not observed during the tests, where the only deformed shape clearly visible at the highest force levels had two half-waves in the loading direction. One possible explanation may be that the misalignments prevented the onset of the first mode and forced the plate to buckle directly in the second mode, which was consistently predicted by the finite element analysis for the whole load range from 44 kN up to the ultimate strength (56 kN). The data recorded by means of the strain gauges, however, show a temporary increase of the bending strain near 40 kN which faintly resembles the trend of its numerical counterpart. This suggests that a mode switching actually occurred during the tests just after the instability onset but was not discernible because the out-of-plane deflections were still small at that stage.

It is interesting to note that a peculiar feature of the two-half-wave shape was the decrease of the membrane strain with increasing load in the postbuckling phase, which was correctly predicted by the computations (see figures 8c-d). This can be contrasted to what happened in the case of A0 specimens (deformed shape with one half-wave), where the membrane strain continued to increase after buckling (see figures 7c-d). It was possible to highlight this difference only by placing the strain gauges along the median vertical axis (see figures 7a and 8a). In fact it was verified that if they were located in the positions specified by the standard [14], which requires both the pairs of strain gauges to be attached 25 mm far from the upper end of the specimen and 50 mm apart (thus closer to the left and right edges), the membrane strain would have been always increasing also in the A90 laminates. In addition, the bending component of strain was quite small in the case of A90 specimens because of their buckling shape, which had faint curvatures in those positions. Actually this was the motivation for moving the strain gauges towards the centre of the plate in the case of figure 8, and also in the case of figure 7 to facilitate direct comparison between them.

The damage created by impact had different effects on the compressive behaviour, depending on specimen geometry and stacking sequence. In all impacted A0 coupons compression failure occurred at the damaged zone. In one of the laminates subjected to 1.0 m impact and both of the ones subjected to 1.5 m impact a lateral expansion of the delamination was observed before failure. At a load level which could not be reliably evaluated, a progressive swelling of the external layers on the unimpacted face could be noted; this had the well-known peanut shape often reported in several studies [1] (with the major axis oriented in the direction of external 0° fibres), quite different from the rhombus described above. When the load approached the maximum value, the swelling enlarged more and more rapidly while the splitting left by impact was opening. The same phenomenon was recorded also in B0 specimens impacted at high energy.

Nothing similar occurred during testing of the A90 and B90 laminates. Moreover, while in all B90 specimens compression failure started from the impact damaged area (like in A0 and

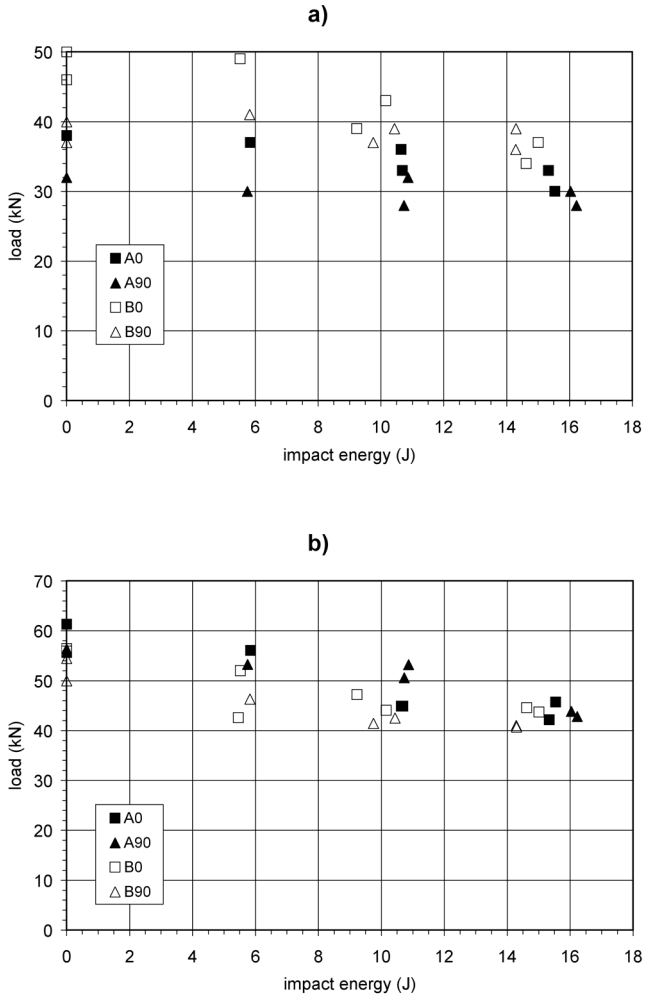

Figure 9 – Critical load (a) and maximum load (b-d) measured during CAI tests, as a function of significant parameters of impact.

B0), in A90 this happened only after 1.5 impact, associated with the one half wave buckling described above. All A90 laminates up to 1.0 m drop height underwent failure at the crest of one of the two half waves, approximately 20 mm away from the impact point, the delamination produced by impact showing negligible changes.

Common features of the compression failure in A0 and B0 samples were a very large delamination, extending mainly in the longitudinal direction, with longitudinal splitting and limited fibre fracture of the 0° layer, on the face which became convex due to buckling (usually the unimpacted one). The opposite face exhibited a kink band with severe fibre fracture in the superficial 0° layer, but less extended delamination and splitting. In A90 and B90 samples the delamination on the convex face was much smaller; when final fracture occurred at the impact damaged zone, the pre-existing delamination extended mainly in transversal direction (parallel to the external 90° fibres). On the concave face the kink band consisted in splitting and protrusion of the 90° plies and fracture of the 0° fibres below. The convex face (in the case of B90, which underwent instability with one half wave) was usually the unimpacted one; it is interesting to note the different behaviour of both A90 laminates subjected to 1.5 m impact, which buckled in the opposite sense.

All the data, regarding critical and maximum load, recorded during CAI experiments are collected in figure 9. In three tests the laminate failed close to the upper or lower end due to edge crushing; since this kind of rupture is considered not valid by the standard, the data obtained from those samples were excluded from analysis.

As was previously mentioned, it was not possible to assess unambiguous values for the critical load from the test results. Since a macroscopic effect of buckling was a deviation of the force-displacement curve from linearity, one may conventionally take the force value at which such drift occurred as the critical load. Where strain gauge measures were available, however, a

perhaps better criterion may be employed, defining the critical force as the one recorded when the bending strain, computed by a pair of strain gauges, departed from its initial value (close to zero). A comparison carried out on the strain-gauged specimens revealed that the two criteria yielded systematically different results, from 4 to 6 kN lower with the second method than with the first. Direct measurement of the out-of-plane displacements of the laminates (not used in the present study) would suffer from similar drawbacks. In view of these difficulties, the first criterion (based on the load-displacement curve) was accepted and used to build the diagram in figure 9a, because not all of the specimens were instrumented with strain gauges.

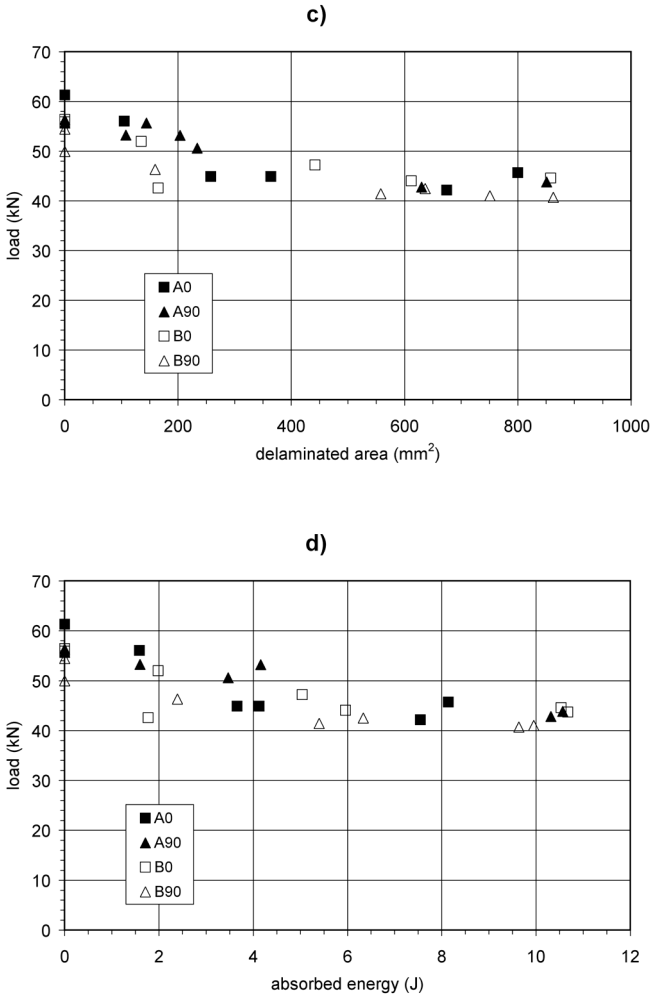

Figure 9 (continued) – Maximum load measured during CAI tests, as a function of delaminated area (c) and energy absorbed during impact test.

The different behaviour of A0 and A90 specimens during compression tests resulted in evident differences as regards the buckling load and the ultimate strength, as figures 9a-b illustrate. In A0 samples the major decrease in maximum load was recorded between 6 and 11 J impact tests (0.5 m and 1.0 m drop height), while the maximum load remained constant (approximately 25% lower than in undamaged specimens) when increasing the drop height from 1.0 m to 1.5 m (see figure 9b). A smaller decrease was noted between 0 and 6 J. This trend is likely to be determined by the influence that impact damage had on the progress of CAI tests: in A0 laminates the failure always initiated from the impact point, but evidently a significant strength reduction was produced only when local instability and extensive propagation of delamination (in the form of the swelling described above) took place before final collapse, that is after 1.0 m or 1.5 m impact. Figure 9a indicates that impact damage also caused a small decrease in critical load of the A0 laminates, suggesting an influence of pre-existing delamination on the global buckling behaviour.

Further information about the propagation of delamination under compression can be gained from the strain gauge measurements carried out on an A0 laminate which underwent a 1.5 m

drop height impact test (see figure 10). In this case a pair of strain gauges was placed near the upper edge of the specimen in central position, while a third sensor was attached to the unimpacted surface of the laminate, 15 mm aside with respect to the impact point, as shown in figure 10a. In this way the strain gauge was within the delaminated zone but was not damaged by the back face splitting caused by impact. The strain gauges 1 and 2 indicated the onset of the specimen bending, as in the examples of figures 7 and 8; however in the present case it can be seen that a deviation from linearity took place at a slightly lower load with respect to the A0 specimen of figure 7, as already mentioned commenting on figure 9a. On the other hand the force level at which the three strain gauges departed from the linear trend was similar (see figures 10a-b). This suggests that a mixed buckling phenomena occurred, in which the global instability of the specimen and the local instability of the delaminated zone took place simultaneously and interacted with each other. The propagation of delamination also was influenced by this phenomenon, as was clearly observed by visual inspection during the test and further confirmed by the huge drift of the strain gauge reading in figure 10b.

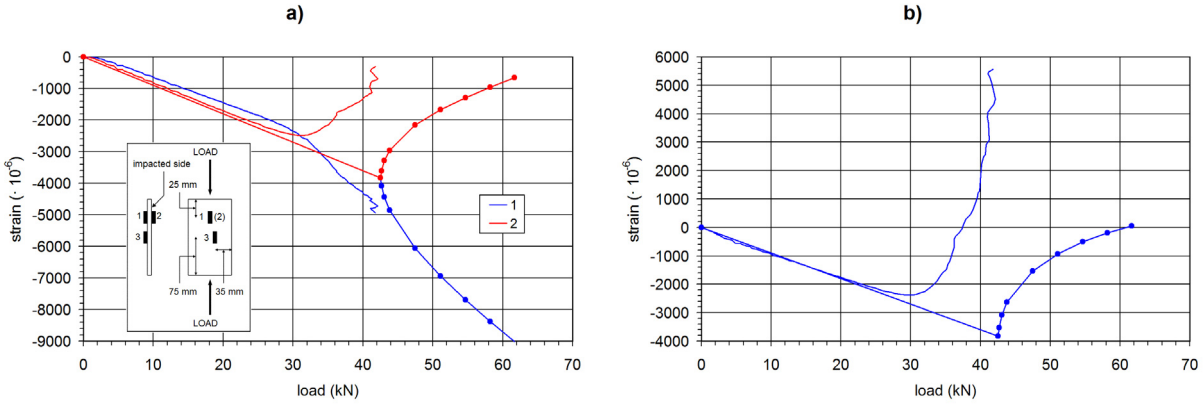

Figure 10 – Example of strain gauge measurements on A0 laminate showing mixed buckling and propagation of delamination. The lines without circles are experimental data, the lines with circles are numerical predictions valid for the undamaged laminate.

Unlike the A0, the A90 specimens exhibited almost constant maximum load (with loss of strength smaller than 5%), slightly lower than in A0, up to 1.0 m drop height (11 J impact energy), followed by a definite 15% decrease between 11 and 16 J. The changes in critical load were within experimental scatter. These results appear to be strictly related with the peculiar buckling behaviour of A90 coupons. Up to 11 J, the impact-induced damage did not affect the compressive strength, remaining unaltered after the test, and fracture on the crest of one half-wave was attributable to flexural stresses. Finite element analysis confirmed that the highest stresses during the postbuckling phase occurred in that region. More severe damage imparted by 1.5 m impact caused a change in buckling mode and triggered the failure under compression at the impact site. However, even in the latter case important differences were noticed with respect to A0 laminates: while in A0 specimens the compressive failure was preceded by propagation of delamination (accompanied by several load drops, visible in figure 6a for the specimens

subjected to the largest impact energies), in A90 specimens, even after 1.5 m impact, a sudden catastrophic fracture occurred, without significant damage propagation and load drops (see figure 6b). These facts, together with the appearance of the failed laminates, suggest that fracture in A90 specimens looks like a flexural one, which took place at the impact damaged zone only when this was sufficiently weakened (while after low energy impact it took place in a different part of the coupon).

Concerning type B laminates, the main difference with respect to type A was the influence of impact damage on compression failure, present in all cases, as indicated by the location of final fracture. The propagation of the pre-existing damage before collapse, always signalled by a long phase characterized by load oscillations (see figure 6), is probably the reason for the similar trend recorded for B0 and B90, with a strength loss of approximately 15% after 15 J impact in both cases. The critical load of B0 specimens appeared to be the most sensitive to impact energy, while it was almost independent for B90 specimens. The values of undamaged strength for type B laminates, lower than the ones found for type A, are quite surprising; since buckling was involved in both cases, one can expect greater critical loads (this did actually happen, as can be seen in figure 9a) and thus also greater strength in the case of smaller plates (which is the opposite situation to what is shown in figure 9b). It was not possible to find an acceptable explanation for this fact.

The compressive behaviour of all laminates was affected both by their dimensions and by the impact damage they underwent during drop-weight experiments. Since the impact damage was also different for types A and B, being influenced in turn by the test configuration, the question arises whether the differences in compressive strength (as a function of impact energy) are due to either the geometry itself or to the different impact response, or both.

To obtain further insight on this point, it may be useful to plot the maximum load versus the delamination area (figure 9c) or a parameter which proved consistently related to it, like the absorbed energy (figure 9d). In these diagrams the points obtained for A and B specimens appear clustered together, without appreciable distinction within the scatter of values, except in the field of small delaminated areas (or small absorbed energy); here the strength of type B remains lower than that of type A. This seems to suggest that specimens of both dimensions which undergo similar damage would have similar residual strength, thus the influence of geometry on the compressive behaviour is moderate. Of course this result can not be extrapolated to different conditions to those examined here, and in any case calls for further investigation.

Finally, some considerations can be made about the significance of the values obtained for residual strength. Since all specimens were subjected to instability, which strongly depends on the test conditions (dimensions and boundary), the present results can not be seen as a characterization of the material itself, but only of the specimens, intended as components, in the particular condition created by the support fixture. To avoid the problem of instability

maintaining the same laminate thickness, the critical load may be increased by using smaller specimens. But the extent of delamination can not exceed the dimension of the coupon (actually it should be quite smaller for this test method to work well [14]); thus in smaller specimens it may be impossible to impart damage sufficient to cause strength reduction of practical interest. Consequently, this test method does not appear to be suitable to perform the characterization of a material, when thin laminates are dealt with. On the other hand, the practical use of compressive strength values measured in conditions where buckling is prevented becomes questionable in slender components which are prone to instability, as complex phenomena involving local and global buckling as well as damage propagation can take place.

4.5. Conclusions

Low velocity impact and in-plane compression after impact tests were conducted on carbon/epoxy laminates of two different geometries according to two distinct ASTM standards, also considering two different stacking sequences. The analysis of data obtained from contact force and energy evaluation during impact events, from load, displacement and strain measurement during compression tests and from visual inspection of the specimens led to the following conclusions:

1) The difference in specimen dimensions and support fixture produced different impact response and damage, the smaller circular coupons being subjected to more extended delamination than the larger rectangular ones after impact at the same energy. The stacking sequence had no effect, as expected, on the behaviour of circular coupons. In the rectangular plates both the impact response and the failure modes showed differences depending on the lay-up, which were attributed to the difference in flexural stiffness due to orientation of the fibres in the external layers. The stiffer configuration, which had external fibres parallel to the shorter side of the specimen, showed a similar delamination area but underwent more severe fibre damage, which was thought to be the reason for much larger energy absorption during impact.

2) The empirical relationship of the delamination area with absorbed energy and with maximum contact force measured during impact appears to be independent of the test configuration and stacking sequence. A slight difference between the two lay-ups of the rectangular specimens, noticed in the relationship between delaminated area and contact force, suggested that not only shear, but also bending could be responsible for creation of delamination in these cases.

3) The relatively small thickness of the laminates studied led to the elastic instability of specimens during compression tests, regardless of dimensions and fibre orientation; this affected the measurement of compressive strength. In the smaller specimens, compressive failure occurred at the impact damaged zone; the residual strength was reduced by pre-existing delamination up to 15%, depending on the impact energy, stacking sequence having little

importance. In the larger specimens the two different orientations of external fibres resulted in significant differences in compressive behaviour, including a different deformed shape in buckling. A first finding was that impact-induced damage did not influence the compressive failure in every case; this depended on the extent of damage and on the buckling mode. The fact that delamination produced by impact could change the buckling mode and/or lower both the critical load and the ultimate strength (up to 25%), depending on the configuration, is particularly important.

4) Due to instability, a characterization of the compressive behaviour of the material itself is not possible, with the test rig employed, when thin laminates are to be tested. In any case, even if, hypothetically, values of compressive strength not affected by buckling were found, their use in practical conditions where buckling can take place would seem questionable. In the present study a number of findings are described indicating the occurrence of complex phenomena, involving global instability of laminates, local instability of sublaminates created by delamination and damage propagation, which deserve further investigation.

References for chapter 4

1. Abrate S. *Impact on composite structures*. Cambridge: Cambridge University Press, 1998.
2. Cantwell WJ, Morton J. *Geometrical effects in the low velocity impact response of CFRP*. Compos Struct 1989;12(1):39-59.
3. Robinson P, Davies GAO. *Impactor mass and specimen geometry effects in low velocity impact on laminated composites*. Int J Impact Eng 1992;12(2):189-207.
4. Davies GAO, Zhang X. *Impact damage prediction in carbon composite structures*. Int J Impact Eng 1995;16(1):149-170.
5. Cantwell WJ. *Geometrical effects in the low velocity impact response of GFRP*. Compos Sci Technol 2007;67(9):1900-1908.
6. Cantwell WJ, Curtis PT, Morton J. *An assessment of the impact performance of CFRP reinforced with high-strain carbon fibres*. Compos Sci Technol 1986;25(2):133-148.
7. Morton J, Godwin EW. *Impact response of tough carbon fibre composites*. Compos Struct 1989;13(1):1-19.
8. Hitchen SA, Kemp RMJ. *The effect of stacking sequence on impact damage in a carbon fibre/epoxy composite*. Composites 1995;26(3):207-214.
9. Reis L, de Freitas M. *Damage growth analysis of low velocity impacted composite panels*. Compos Struct 1997;38(1-4):509-515.
10. Sanchez-Saez S, Barbero E, Zaera R, Navarro C. *Compression after impact of thin composite laminates*. Compos Sci Technol 2005;65(13):1911-1919.

11. Asp LE, Nilsson S, Singh S. *An experimental investigation of the influence of delamination growth on the residual strength of impacted laminates*. Compos Part A-Appl S 2001;32(9):1229-1235.
12. D 7136/D 7136M – 05 *Standard test method for measuring the damage resistance of a fiber-reinforced polymer matrix composite to a drop-weight impact event*. Annual Book of ASTM Standards. West Conshohocken, PA: ASTM International, 2005.
13. D 3763 – 06 *Standard test method for high speed puncture properties of plastics using load and displacement sensors*. Annual Book of ASTM Standards. West Conshohocken, PA: ASTM International, 2006.
14. D 7137/D 7137M – 05 *Standard test method for compressive residual strength properties of damaged polymer matrix composite plates*. Annual Book of ASTM Standards. West Conshohocken, PA: ASTM International, 2005.
15. Minak G, Ghelli D. *Design of a drop-weight machine for composite materials impact testing*. In: Proceedings of the ICCSM5 Congress, Matejiček F, editor. Trogir/Split (HR): Croatian Society of Mechanics, 2006.
16. Underwood P. *Dynamic relaxation*. In: Computational methods for transient analysis, Belytschko T, Hughes TJR, editors, p. 245-265. Amsterdam: North-Holland, 1983.
17. Schoeppner GA, Abrate S. *Delamination threshold loads for low velocity impact on composite laminates*. Compos Part A-Appl S 2000;31(9):903-915.

CHAPTER 5

Influence of in-plane loading on the impact response of laminated plates

5.1. Introduction

Most of the research papers published to date, concerning the damage caused by low velocity impact of foreign objects on composite laminates, deal with the response of laminates which are free from pre-existing in-plane loads [1]. Although it is far more likely that components are impacted while they are subjected to some load during service, only a few contributions are available regarding the influence of such preload on the transient behaviour and on the failure mechanisms of laminates [2-15]. It should also be noted that some loading conditions are less investigated than others. For instance, [12, 13] are the only experimental studies on biaxial preload regarding continuous fibre composites; impact tests under compressive preload are reported only in [8, 9, 11], and [11] is the only experimental research focused on low velocity impact on laminates buckled in compression. The difficulties encountered in laboratory testing of that kind (machines able to apply very high forces to the specimens are needed [12]) are a probable justification for the apparent little interest in this topic.

According to the numerical calculations carried out by several authors, tensile prestress tends to induce a stiffer impact response, with smaller laminate displacement, shorter contact duration, larger vibration frequencies and higher contact force with respect to the unloaded case [2, 5, 6, 14, 15]. Compressive loads result in opposite effects, as long as they are lower than the critical buckling load [5, 6, 15]; in postbuckling conditions a stiffer behaviour is found again, because the buckled laminate acts as a shell and significant membrane forces are generated as a consequence of deflection [4]. The transient part of stresses (or strains) is decreased by tensile preloads, while compressive preloads increase it [2, 5, 6]; when the overall stresses are considered, an increment is observed both under compression and under tension [15]. However, the change in stress and contact force due to preload does not seem to have the same importance in different cases; no clear tendency is found regarding stresses for impact on buckled laminates [4].

Experimental tests partly confirm these trends, but the influence of in-plane load on material damage does not appear to follow definite rules. For example, both larger and smaller

delamination areas are described after impact under tensile preload, depending on the test condition [7, 9, 10]; a reduction of the threshold impact energy required to produce initial damage is reported in some cases [10], while in other instances it is not [9]. As regards compression prestresses, the most detrimental effects of preload seem to take place when the buckling load and the compressive strength of the laminate are close to each other, but only one reference is concerned with this point [11]. The possibility of catastrophic failure during impact, when a compressive load is applied, is also reported in [11].

It appears from the brief literature review above that the available information is far from providing a complete understanding of the subject, mainly because the validity of the results obtained in each single research may often be limited to the particular conditions examined in it. Besides, in many experimental studies some important pieces of information concerning the test configuration adopted (e. g. specimen dimensions and layup, material properties, impact parameters) are missing, thus making the interpretation of the results more difficult. Finally, dissimilar research approaches often focus on different test parameters, preventing a direct comparison between their conclusions. It is felt that there is a need for a more comprehensive investigation which should be able to assess some general guidelines, especially about how the effect of membrane preloads on the impact behaviour varies when the main test parameters are changed.

A study about the dependence of impact behaviour and damage of unloaded laminates on the specimen dimension (see chapter 3), together with several preliminary numerical analyses, suggested that the laminate span-to-thickness ratio could have a fundamental role in determining the influence of preload on the dynamic response of the laminate. Accordingly, a number of low velocity impact simulations were performed for composite laminated plates with different in-plane dimensions but equal thickness. Various preload conditions, including both tension and compression, both uniaxial and biaxial, were examined; regarding compression preloads, the case of impact on buckled plates was also considered. Particular attention was paid to the comparison of the maximum stresses obtained in each case.

The numerical model used for the analyses included geometrical nonlinearity, because the effect of large deflections proved crucial in explaining how the impact behaviour was affected by in-plane forces. On the other hand, no damage model of the material was implemented. By comparison of the present numerical results with the experimental findings described in the literature, this choice made it possible to distinguish between phenomena which can be justified without accounting for the material degradation and phenomena whose explanation does require a failure model.

The results of the present study showed that the in-plane dimensions of the impacted laminate compared to its thickness actually represent a critical parameter. A tensile preload can increase the maximum stresses and lower the impact energy threshold necessary to induce the first damage; however this effect is much stronger at small span-to-thickness ratio, and becomes

less and less important as the ratio increases. On the other hand, compressive in-plane loads exhibit beneficial effects at small span-to-thickness ratios, while they are not significant for very slender plates. Between these extreme conditions, at medium span-to-thickness ratio the most dangerous influence of preload was found. In this framework, some experimental results from the previous researches can be given a better interpretation and their significance can be clarified.

5.2. Main features of the numerical model

The transient analysis of the impact response of composite laminates was carried out by means of the finite element program described in chapter 1.

The impactor was treated as a rigid body. Contact between impactor and target was modelled in a simplified way, by applying the contact force as an external load on a single node of the discretized laminate. Following a generally accepted approach [1], a Hertz-type contact law was assumed to be valid:

$$P = k\,\alpha^{3/2} \tag{1}$$

where P is the contact force and α is the indentation of the impactor in the laminate surface.

Contact and large deflections were the only nonlinear phenomena accounted for in the numerical model. In particular, no post-failure degradation criterion of the material properties was implemented, so that the elastic constants did not change during the simulations even if failure was predicted. This simplifying assumption makes it possible to obtain reliable results as long as the actual material damage is limited, as shown in chapters 2 and 3; the parameters of the impact events studied herein were therefore suitably chosen in order to meet this condition.
The dynamic relaxation algorithm included in the program was used to evaluate the postbuckling configuration of the laminates subjected to in-plane compression, because this technique is known to be very simple and efficient in circumstances where strong nonlinear effects, like those related to elastic instability, are present [16].

5.2.1. *Choice of the case studies*

For the present study, a simple square laminated plate was chosen as the target structure subjected to impact. In order to highlight how the effect of preload on impact response varies depending on the test conditions, three different in-plane dimensions were considered: 25, 100 and 400 mm side. From here on, they will also be respectively referred to as “small”, “medium” and “large” laminates. The laminate thickness of 2.13 mm was kept constant in all cases, thus obtaining three different values of span-to-thickness ratio: 11.8, 47.0 and 188. The first one and

the third one were intended to represent two opposite limiting configurations (very thick and very slender plates); the second one was chosen to reproduce intermediate conditions.

The laminates considered consist of 16 carbon-epoxy unidirectional plies arranged in the symmetric quasi isotropic layup $[(45/0/-45/90)_S]_2$. For the elastic constants and the in-plane strengths of the single lamina (reported in table 1), as well as for the thickness and the stacking sequence of the laminate, the values in [10] were adopted. [10] was chosen among the cited references because it provides the most complete information about the mechanical properties of the specimens. However, for the present simulations the choice of their absolute values was not essential (of course they had to be realistic), the final aim being the study of the influence of other parameters, like preload and span-to-thickness ratio.

Table 1 – Mechanical properties of the single ply of the graphite/epoxy laminate used for the simulations

Elastic constants	
E_1	148 GPa
E_2	9.58 GPa
ν_{12}	0.287
G_{12}	5.61 GPa
G_{13}	5.61 GPa
G_{23}	3.0 GPa
In-plane strengths	
X_t	1630 MPa
X_c	1290 MPa
Y_t	45.6 MPa
Y_c	216 MPa
S	150 MPa

The mass density was assumed to be 1580 kg m^{-3}, a common value for carbon-epoxy. The contact stiffness k in (1) was determined with the formula used by Yang and Sun [17]:

$$k = \frac{4}{3}\frac{\sqrt{R_s}}{\frac{1-\nu_s^2}{E_s}+\frac{1}{E_2}}$$

where E_s and ν_s are the Young's modulus and the Poisson's coefficient of the impactor material and R_s is the radius of curvature of the impactor head. R_s was given the value of 6.35 mm, typical of many drop-weight experimental devices; considering the head as made of steel, E_s = 210 GPa and ν_s = 0.3. These assumptions yield $k = 9.78 \cdot 10^8$ N m$^{-3/2}$.

In all of the impact testers which are able to apply in-plane loads to the specimen, clamping devices are needed to grip its ends properly; rotation is thus prevented along the boundary of the unrestrained area. Even if the servo-hydraulic preloading apparatus is intended to accomplish a fixed displacement or fixed strain condition, as explicitly stated in some cases [12, 13], it is not possible to ascertain to what extent this ideal limit is approached during impact tests. The actual boundary condition is most likely neither a fixed load one nor a fixed displacement one; it is, however, probably much closer to the latter. In consideration of this, all the degrees of freedom along the plate boundary were constrained in the present numerical analyses, thus simulating a full clamp condition.

The initial impactor velocity was normal to the surface of the plate and contact occurred exactly at the plate centre. As a reference for the subsequent calculations including a membrane preload, one impact analysis was performed without preload for each of the three

aforementioned laminate dimensions. The initial energy of the impactor in these analyses was chosen so that the expected material damage was limited, in order to ensure that the present results, obtained without a damage model, were reliable. To verify this, the Tsai-Wu failure criterion [18] was applied to each lamina; the maximum values of the failure index attained during the transient response were computed and plotted (examples of these plots can be found in figures 2a, 4a and 6a). By trial and error, the impact energy was found which resulted in a small area where the index exceeded the threshold value 1 (corresponding to failure) in the lamina subjected to the highest stresses. By checking the stress components, it was concluded that this predicted failure should be a matrix cracking in tension. With the impactor mass of 6.8 kg (as in [10]), the initial velocities corresponding to this "small damage" condition were evaluated as 0.20, 0.45 and 1.8 m s^{-1} for the small, medium and large laminates, respectively. With such a low velocity the impact response is dominated by the first vibration mode; this allows the best understanding of the influence of preload, as will be shown later. The effect of changing the impact velocity will also be investigated separately.

5.3. Tension preload

5.3.1. *Case studies*

The impact events analysed for the study of tensile preload are summarized in table 2. The initial strain value of 2400 · 10^{-6}, the highest among the three tested in [10], was considered representative of common service conditions of composite laminates. In a first set of simulations, aimed at the evaluation of the influence of in-plane loads for specimens of different dimensions, the impactor mass of 6.8 kg was used in all cases; the initial velocity of the impactor was 0.20, 0.45 and 1.8 m s^{-1} for the 25 mm, 100 mm and 400 mm specimen respectively, as explained in the preceding section. A second group of simulations was performed in order to investigate how the previous results were affected by a change in impact velocity. These analyses concerned only the large laminates, for which the effect of velocity was found to be the most significant. In this second set the mass of the impactor was divided by 4 and by 16 as the velocity was increased to the new values of 3.6 and 7.2 m s^{-1}, so that the initial energy was the same in all cases. This ensured that the condition of small damage area was maintained with reasonable accuracy, as

Table 2 – Impact velocities and energies considered for the study of tensile preload

In-plane strain	25 mm (small)	100 mm (medium)	400 mm (large)
no preload	0.20 m s^{-1} (0.136 J)	0.45 m s^{-1} (0.689 J)	1.8 m s^{-1} 3.6 m s^{-1} 7.2 m s^{-1} (11.0 J)
2400 · 10^{-6} (uniaxial)	0.20 m s^{-1} (0.136 J)	0.45 m s^{-1} (0.689 J)	1.8 m s^{-1} 3.6 m s^{-1} 7.2 m s^{-1} (11.0 J)
2400 · 10^{-6} (biaxial)	0.20 m s^{-1} (0.136 J)	0.45 m s^{-1} (0.689 J)	1.8 m s^{-1} 3.6 m s^{-1} 7.2 m s^{-1} (11.0 J)

was confirmed by the numerical results obtained for the stress field. All of the three values considered fall in the range of low impact velocity according to the first criterion cited in chapter 2, section 2.1 [1], thus excluding phenomena which are typical of high velocity impacts.

The in-plane load was imposed to the laminates in the form of initial displacements of the nodes. It has to be noted that, even if the preload is expressed in terms of strain, "uniaxial" refers to the load, not to the strains. In other words the initial condition of the laminate under uniaxial preload was obtained by imposing the specified strain value in the load direction, while the material was free to shrink in the orthogonal direction due to Poisson effect, as would happen in a test machine when a uniaxial loading is required. In the case of biaxial prestrain, equal strains in two perpendicular directions were applied; this also leads to equal force resultants in any direction since the laminate is quasi isotropic.

The discretizations to be used were chosen after a convergence test for each of the three dimensions considered. The small specimen was discretized with a uniform mesh of 256 (16 by 16) square four node finite elements. The medium and large laminates required 1024 (32 by 32) elements for sufficiently accurate results. With the central difference algorithm the time integration step must be lower than the critical stability threshold, because the method is conditionally stable. In the present analyses the time step was 0.2 μs for the small, 0.4 μs for the medium and 0.7 μs for the large laminates.

5.3.2. *Results*

The results of the first set of analyses (with equal impactor mass) are presented in figures 1 to 6. The contact force history for the impacts on the 25 mm laminate subjected to different preloads is plotted in figure 1a. Figure 1b shows the curves of contact force as a function of the displacement of the node on which impact occurs. Analogous graphs can be found in figures 3 and 5 for the 100 mm and 400 mm specimens. The numerical values of maximum contact force, maximum displacement of the impactor and contact duration in all the conditions tested are collected in table 3.

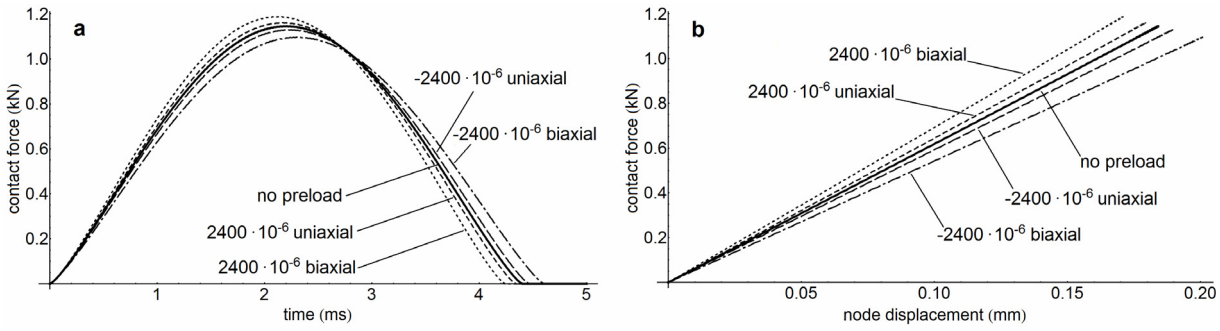

Figure 1 – Contact force as a function of time (a) or displacement (b) for the 25 mm laminate impacted under several preloads.

In figure 2 the plots of the Tsai-Wu failure index are compared for the three cases of impact without preload, under uniaxial and biaxial preload on the small specimens. The same type of

output is shown in figures 4 and 6 for the medium and large specimens respectively. In every case the highest values of the index were recorded in the lowermost ply, on the opposite side with respect to the impacted surface of the laminate. Therefore all the pictures refer to this ply and to the time when the overall stress state was the most severe during the transient response.

The results of the second set of simulations, regarding the influence of different impact velocities but with the same initial kinetic energy of the impactor, are presented in figures 7 and 8. Figure 7 shows contact force, displacement of the impactor and deflection of the impacted node as a function of time for the unloaded laminate and different velocities. Figure 8 displays the effect of membrane load on the contact force history for different impact velocities. The numerical values of the most important relevant parameters are reported in table 4.

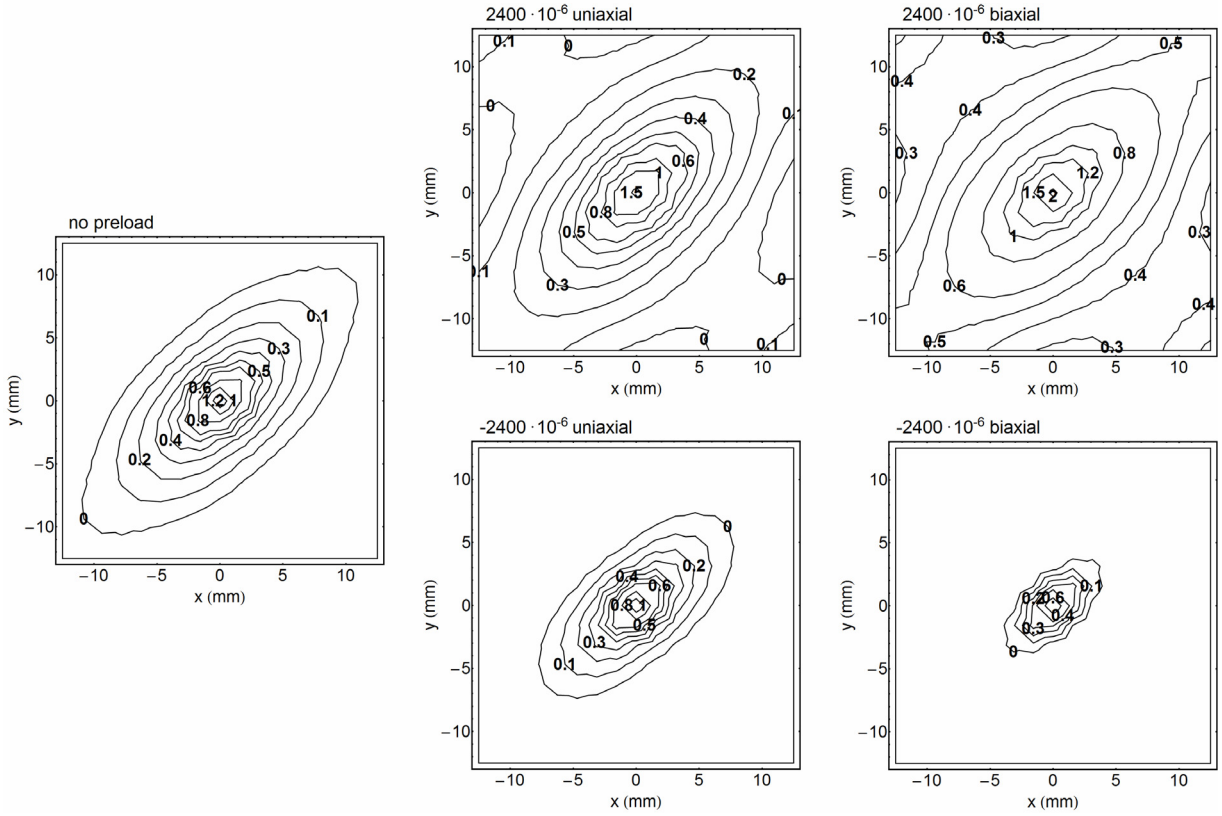

Figure 2 – Tsai-Wu failure index for the 25 mm laminate impacted under several preloads.

5.3.3. *Discussion*

In an attempt to comment on the results of the numerical simulations presented above, it is convenient to start from the impact events at the lowest velocity (figures from 1 to 6). In these cases the dynamic response of the laminate is dominated by the fundamental vibration mode: the contribution of higher modes is small (for the 100 mm and 400 mm specimens), as can be seen from the minor secondary oscillations in the contact force history in figures 3 and 5, or negligible (see figure 1). In this situation the transient behaviour of the target can be viewed as a

succession of quasi-static equilibrium states, thus the explanation of some features of the response is greatly simplified.

Table 3 – Main response parameters for laminates of different dimensions subjected to tensile preload and impact by the same mass (6.8 kg)

Laminate dimension		no preload	$2400 \cdot 10^{-6}$ (uniaxial)	$2400 \cdot 10^{-6}$ (biaxial)
small laminate	max. contact force (kN)	1.145	1.160	1.188
	max. impactor displacement (mm)	0.295	0.291	0.285
	contact duration (ms)	4.40	4.34	4.24
medium laminate	max. contact force (kN)	1.23	1.38	1.62
	max. impactor displacement (mm)	1.40	1.19	0.983
	contact duration (ms)	9.43	8.06	6.68
large laminate	max. contact force (kN)	4.32	4.09	4.90
	max. impactor displacement (mm)	9.85	7.20	5.01
	contact duration (ms)	14.1	11.7	8.62

In the 25 mm specimen the first failure is reached at very small transverse displacements due to the high plate stiffness. As a consequence, membrane stiffening due to the immovable edges has a negligible effect on the load-displacement curve, which does not show any deviation from linearity (see figure 1b). Since the influence of preload is strictly related to geometrical nonlinearity, it is expected that little differences exist between the unloaded and the loaded specimens. This is exactly what appears from the plots in figure 1, showing that the dynamic behaviour of the small laminate is almost unaffected by in-plane loads. On the other hand, the stresses in the preloaded laminates exhibit a definite increase with respect to the unloaded condition (see figure 2). This is easily explained, bearing in mind that in a quasi-static configuration the part of stresses due to bending depends on the deflection (in fact the peak stresses are attained approximately at the instant of maximum deflection), which is left unchanged by preload. Therefore the overall stress state is approximately a direct superposition of the pre-existing stresses on the bending stresses, the former representing a significant contribution.

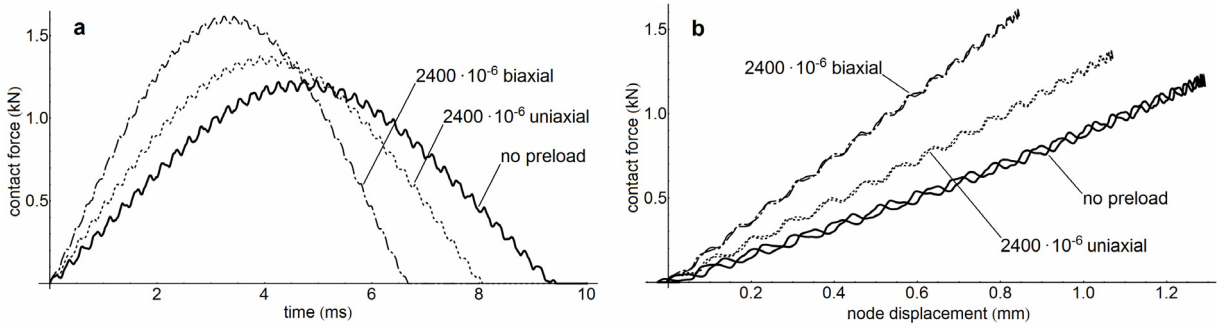

Figure 3 – Contact force as a function of time (a) or displacement (b) for the 100 mm laminate impacted under several tensile preloads.

Moving to the 100 mm and the 400 mm laminates, it can be noted that the influence of preload becomes more and more significant as regards the dynamic response: the contact

duration is shortened, the maximum force tends to grow, and the maximum displacement diminishes. On the contrary, the increase in stresses due to preload in the medium laminates is lower than in the small ones, and becomes almost invisible in the large plates.

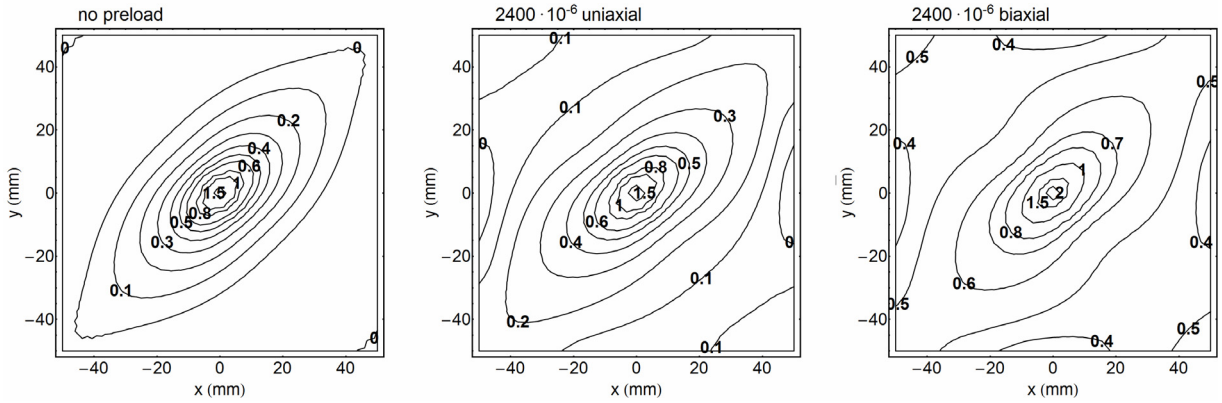

Figure 4 – Tsai-Wu failure index for the 100 mm laminate impacted under several tensile preloads.

The evident curvature of the force-displacement paths in figures 3b and 5b indicates that geometrical nonlinearity plays an important role in limiting the plate deflection; of course this phenomenon is more significant at higher span-to-thickness ratios. Therefore the overall stress state in the preloaded laminates is no longer the result of a superposition of the pre-stresses on the bending stresses of the unloaded specimen. The bending stresses are reduced due to smaller deflections (as found in previous studies [2, 5, 6, 15]) as the membrane forces are increased, and it is not possible to say a priori that either effect prevails. The present analyses show that, for low velocity impacts, the total stresses are larger when membrane preloads are applied; however, the difference with respect to the unloaded condition is strongly dependent on the span-to-thickness ratio of the target, and tends to disappear in very slender laminates, whose behaviour resembles that of a membrane.

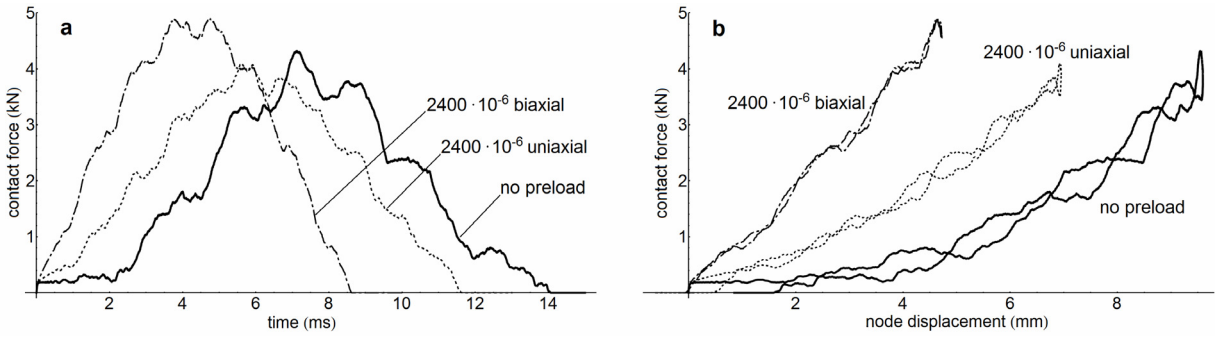

Figure 5 – Contact force as a function of time (a) or displacement (b) for the 400 mm laminate impacted under several tensile preloads (6.8 kg impactor mass, 1.8 m s^{-1} initial velocity).

Regarding the impact dynamics, the trends described above agree with the conclusions of other numerical analyses [2, 5, 6, 15]. The results of experimental tests partly confirm the theoretical predictions. When an influence of preload is recognized, it generally results in a

stiffer response of the target, with shorter contact duration and larger force [8-10, 12, 13]. However the effect of preload on the maximum contact force is often small, sometimes negligible. In view of the present results, this could be due to the span-to-thickness ratio. Unfortunately this parameter is hardly ever provided in the available reports of experimental studies. In [8] specimens with a span-to-thickness ratio of 36.8 are tested, so a difference even less pronounced than the one shown in figure 3 is expected; this is exactly what the contact force history plots in [8] display. In [12, 13] the ratio is larger (84.3 and 71.1 respectively) but the effect of prestrain on the contact force is hardly visible. However this seeming contradiction with the present study may be justified by the low level of prestrain (within $1500 \cdot 10^{-6}$). Other important factors which can obscure the influence of preload are experimental scatter (which alone could easily hide differences like those in figures 1 or 3) and material damage, which alters the contact force history, lowering the highest peaks predicted by a numerical simulation without damage model and extending the contact duration (see chapter 3). This is most likely true in [12] where significant damage was introduced, as far as perforation of the laminate.

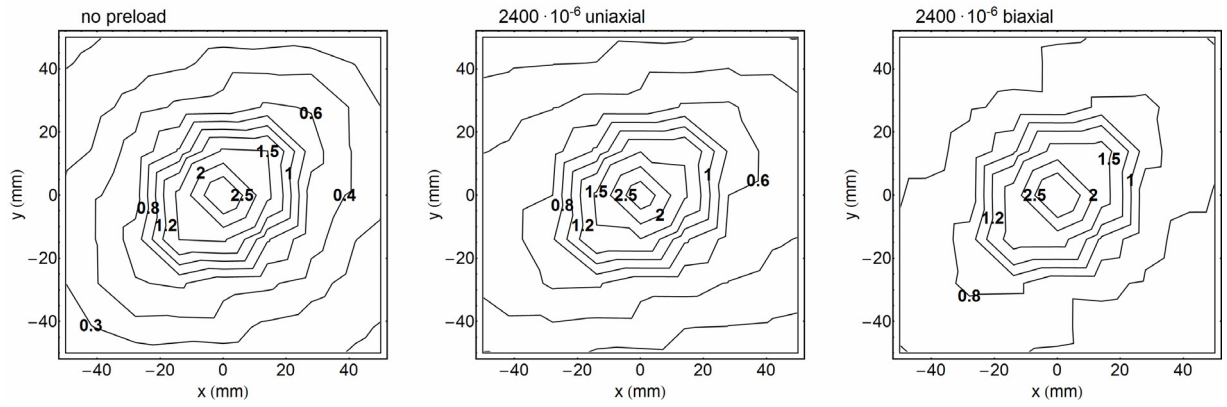

Figure 6 – Tsai-Wu failure index for the central zone of the 400 mm laminate impacted under several tensile preloads (6.8 kg impactor mass, 1.8 m s^{-1} initial velocity).

The extent of the damaged area, especially if very large, can not be reliably predicted by an analysis which does not take material degradation into account, as discussed in chapter 3. Consequently, it is not possible to deduce from the pictures of, for instance, figure 2 that a larger damaged zone is expected in the small preloaded laminates. These pictures are also relevant to the stress state within a lamina, thus they can not be intended as a prediction of delamination which is the form of damage usually detected after impact tests and referred to as "damaged area". As regards this parameter, conflicting results are reported in the literature. According to [8], in short fibre composites the damage area is left practically unchanged by a biaxial preload, while uniaxial tensile prestress can increase it. In [10] opposite effects are described for laminates of different thickness; a dependence on the impact energy is also highlighted. [9] finds larger delaminations with uniaxial in-plane loads, while in [13] no difference exists between unloaded and biaxially preloaded specimens, maybe because of the small initial strain. These findings, contrasting with the present simulations showing generally a more severe stress state

under preload, suggest that the implementation of a failure model is required to predict the extent of damage.

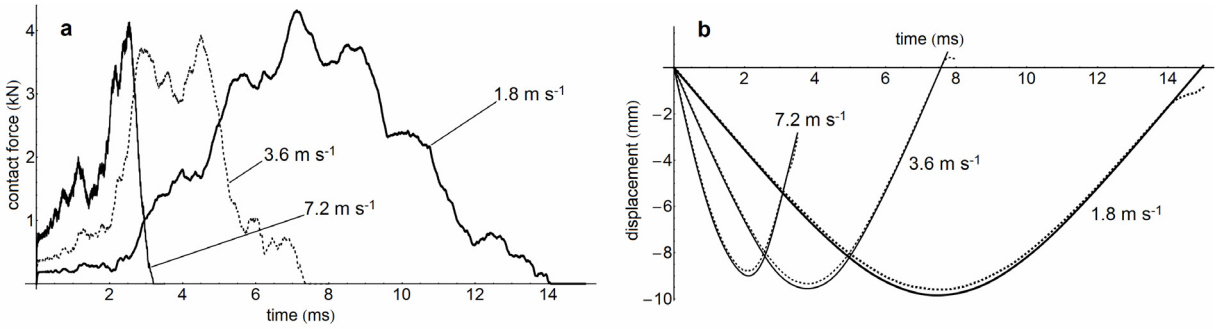

Figure 7 – 400 mm laminate impacted at different velocities in the absence of preload. a) Contact force history. b) Displacement of the impactor (solid lines) and of the target (dotted lines) as a function of time.

An important conclusion can instead be drawn concerning the impact energy threshold which initiates damage. The graphs in figures 2, 4 and 6 show that, impact energy being the same, the stresses are higher under initial membrane load. Therefore it is expected that a lower impact energy is required to induce the first damage under preload; the difference with respect to the laminate free from prestress will be larger for thicker plates. Only three papers present results concerning the impact energy threshold, probably because the evaluation of this parameter is quite expensive (many tests at several energy levels are needed); unfortunately the span-to-thickness ratio of the coupons is never indicated. In [7] the preload is found to decrease the energy threshold, but for beam-like specimens impacted at medium velocity (10-40 m s^{-1}). In [9] the threshold does not seem to be sensitive to the preload, whereas in [10] it diminishes in every test condition. In any case, the present results suggest that possible future studies should investigate the relationship between energy threshold and span-to-thickness ratio experimentally.

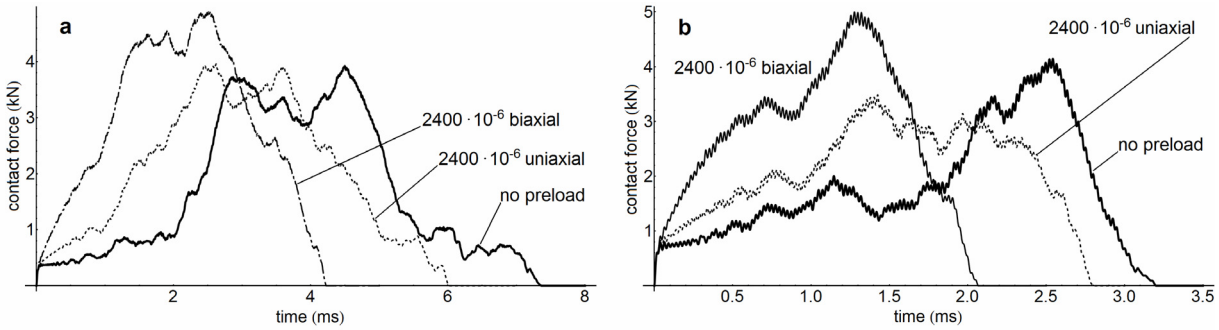

Figure 8 – Contact force history for 400 mm laminates impacted at 3.6 m s^{-1} (a) and 7.2 m s^{-1} (b) with the same initial energy, under several tensile preloads.

Figures 7 and 8 indicate how the guidelines discussed so far are affected by higher impact velocities. Keeping the energy constant results in maximum force and maximum deflection approximately equal to the lowest velocity event. The peak stresses (not shown here) also remain similar to what is displayed in figure 6. Figure 7 shows that the contact force history

becomes more and more irregular, because the contribution of higher vibration modes is no longer negligible. The dynamic response can not be considered a succession of quasi static equilibrium states, since it is governed by wave propagation phenomena, clearly distinguishable in the plate deformed shape plotted in figure 9. These effects are more evident in a larger laminate, where it takes longer for the waves to reach the boundary and be reflected back; for this reason the 400 mm specimen was chosen here to highlight them.

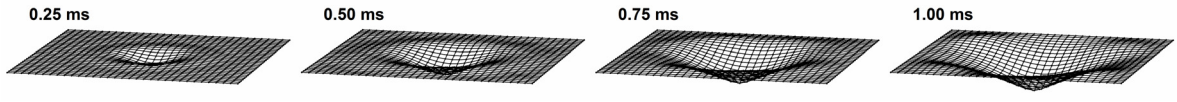

Figure 9 – Deformed shape of the 400 mm laminate after a 7.2 m s^{-1} impact in the absence of preload.

A general rule concerning biaxial preload emerges from the results. In every test configuration a biaxial initial load has much stronger influence than a uniaxial one, both on the impact response and on the stresses. To a certain extent, this also holds when the velocity is not so low (see figure 8).

However, figure 8 suggests that the trends found for low velocity impacts tend to lose their validity when the velocity is increased; for instance, the maximum force under uniaxial prestrain can be lower than in the unloaded case (see figure 8b). Localised peaks of contact force may induce the maximum stresses and have major importance. In the conditions simulated here for the large laminate the effect on stresses is likely limited, as mentioned above; this agrees with the results obtained in [14] for an infinite plate. Nevertheless, for even higher velocities a wave dominated response can be obtained also in smaller plates, where the influence of preload proved more significant. In such circumstances the danger created by preload can not be quantified a priori, and a suitable calculation is necessary for the specific case to be examined.

Table 4 – Main impact response parameters for 400 mm laminates subjected to different impact velocities under tensile preload

Impact velocity		no preload	$2400 \cdot 10^{-6}$ (uniaxial)	$2400 \cdot 10^{-6}$ (biaxial)
1.8 m s^{-1}	max. contact force (kN)	4.32	4.09	4.90
	max. impactor displacement (mm)	9.85	7.20	5.01
	contact duration (ms)	14.1	11.7	8.62
3.6 m s^{-1}	max. contact force (kN)	3.92	3.96	4.89
	max. impactor displacement (mm)	9.55	7.06	4.92
	contact duration (ms)	7.42	6.03	4.23
7.2 m s^{-1}	max. contact force (kN)	4.14	3.48	5.00
	max. impactor displacement (mm)	9.00	6.78	4.80
	contact duration (ms)	3.20	2.80	2.07

5.4. Compression preload

5.4.1. *Case studies*

Table 5 contains the data of all the impact tests simulated for the study of compressive preload. The initial velocity of the impactor was the same as in the first set of analyses performed under tensile prestrain; the impactor mass was kept constant to 6.8 kg in every case, thus the corresponding kinetic energy assumed the values in table 2. The discretizations and time steps used were identical to the ones chosen for the previous simulations.

Table 5 – Initial in-plane load or strain values considered for the study of compressive preload

	25 mm (small) 0.20 m s^{-1}	100 mm (medium) 0.45 m s^{-1}	400 mm (large) 1.8 m s^{-1}
uniaxial preload	prestrain $-2400 \cdot 10^{-6}$	0.50 N_{cr} 0.90 N_{cr}	0.50 N_{cr} 0.90 N_{cr} 1.07 N_{cr} (1.10 ε_{cr}) 1.35 N_{cr} (1.50 ε_{cr}) 1.67 N_{cr} (2.00 ε_{cr}) 1.99 N_{cr} (3.00 ε_{cr})
biaxial preload	prestrain $-2400 \cdot 10^{-6}$	0.50 N_{cr} 0.90 N_{cr} 1.05 N_{cr} (1.10 ε_{cr}) 1.24 N_{cr} (1.50 ε_{cr})	0.50 N_{cr} 0.90 N_{cr} 1.05 N_{cr} (1.10 ε_{cr}) 1.25 N_{cr} (1.50 ε_{cr}) 1.48 N_{cr} (2.00 ε_{cr}) 1.93 N_{cr} (3.00 ε_{cr})

In the small specimen no instability phenomenon was predicted by the dynamic relaxation analysis, even at very high prestrain levels which would most likely cause failure of the laminate in practice; of course this is due to the low span-to-thickness ratio. For this reason the critical load was not evaluated and preload was expressed in terms of strain and given the same absolute value already used for tensile preload. This specimen dimension was intended to reproduce the limiting condition in which damage is not influenced by global elastic instability.

In the medium and large laminates, buckling was predicted by numerical calculations to occur at lower strain values (within $4000 \cdot 10^{-6}$); these cases can therefore represent a more common circumstance in practical applications, where the allowable stresses are dictated by instability because the true compressive strength of the material (measured with testing devices which prevent buckling) can not be reached. For these laminates the first critical loads, both uniaxial and biaxial, were evaluated numerically together with the corresponding strains, and the values of initial in-plane load to be tested were expressed as fractions of the critical load N_{cr}.

As for the analysis of tensile membrane forces, the compressive preload was applied through displacements imposed to the nodes of the finite element model, and "uniaxial" means uniaxial load (not strain) wherever used. In the determination of the postbuckling shape of the laminates, their boundary was constrained to maintain its rectangular shape, in order to reproduce the usual experimental configuration where the specimen sides are clamped. This means that equal displacements were imposed to all the nodes of each side in the direction perpendicular to the boundary. Obviously the resulting in-plane forces are not constant along the boundary; therefore the fractions of N_{cr} were calculated as average values on the whole side length. When larger than

1, the fractions of the critical strain ε_{cr} refer to the ideal planar configuration of the plate (loaded beyond the critical level), used as the initial condition of the dynamic relaxation analysis which served to find the postbuckling shape. In impact simulations the postbuckling displacements represented the initial condition of the target, with the same boundary constraints as in the previous dynamic relaxation analysis. For the sake of brevity, only impacts on the concave face of the buckled laminates were considered.

5.4.2. *Results*

The force-time and force-displacement diagrams for the 25 mm laminate under compression can be found in figure 1; figures 2d and 2e present the plots of the Tsai-Wu failure index. The relevant main parameters are listed in table 6.

Table 6 – Main impact response parameters for 25 mm laminates impacted under compressive preload (impact velocity 0.20 m s^{-1})

prestrain		maximum contact force (kN)	maximum impactor displacement (mm)	contact duration (ms)
0		1.145	0.295	4.40
$-2400 \cdot 10^{-6}$	uniaxial	1.129	0.299	4.47
	biaxial	1.096	0.309	4.60

The critical strains of the 100 mm laminate were $3950 \cdot 10^{-6}$ and $1450 \cdot 10^{-6}$ under uniaxial and biaxial load, respectively; the corresponding force resultants were 480 and 253 kN/m. In the postbuckling configuration under uniaxial compression the stresses on the convex surface of the laminate exceeded the first failure level: for this reason no impact test was carried out in this condition. The same happened with biaxial compression, but only beyond 1.50 ε_{cr}.

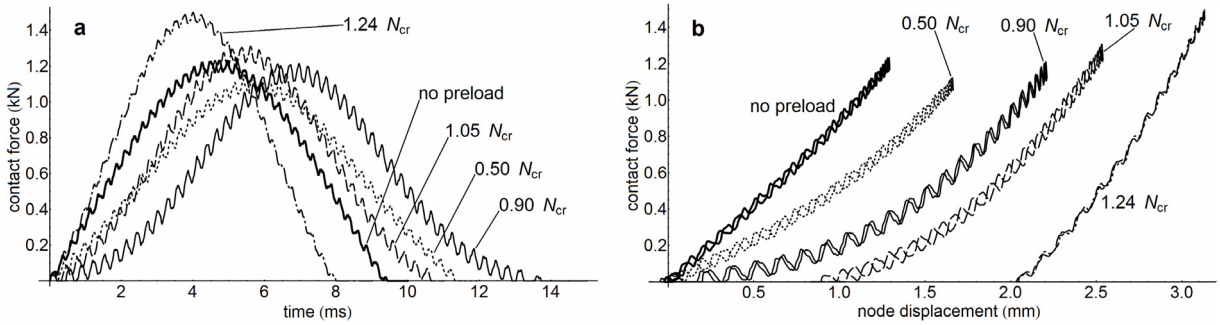

Figure 10 – Contact force as a function of time (a) or displacement (b) for the 100 mm laminate impacted under several biaxial compressive preloads.

Figure 10 shows the contact force history and the force-displacement curves for all the tested values of biaxial preload. As can be seen from the numerical values in table 7, in the cases of 0.50 N_{cr} and 0.90 N_{cr} uniaxial and biaxial prestrain gave practically identical results as regards the impact response, thus only the curves regarding the latter case have been plotted. The diagrams of the Tsai-Wu failure index are presented in figure 11 (for preloads below the critical values) and figure 12 (for the buckled laminate under biaxial preload).

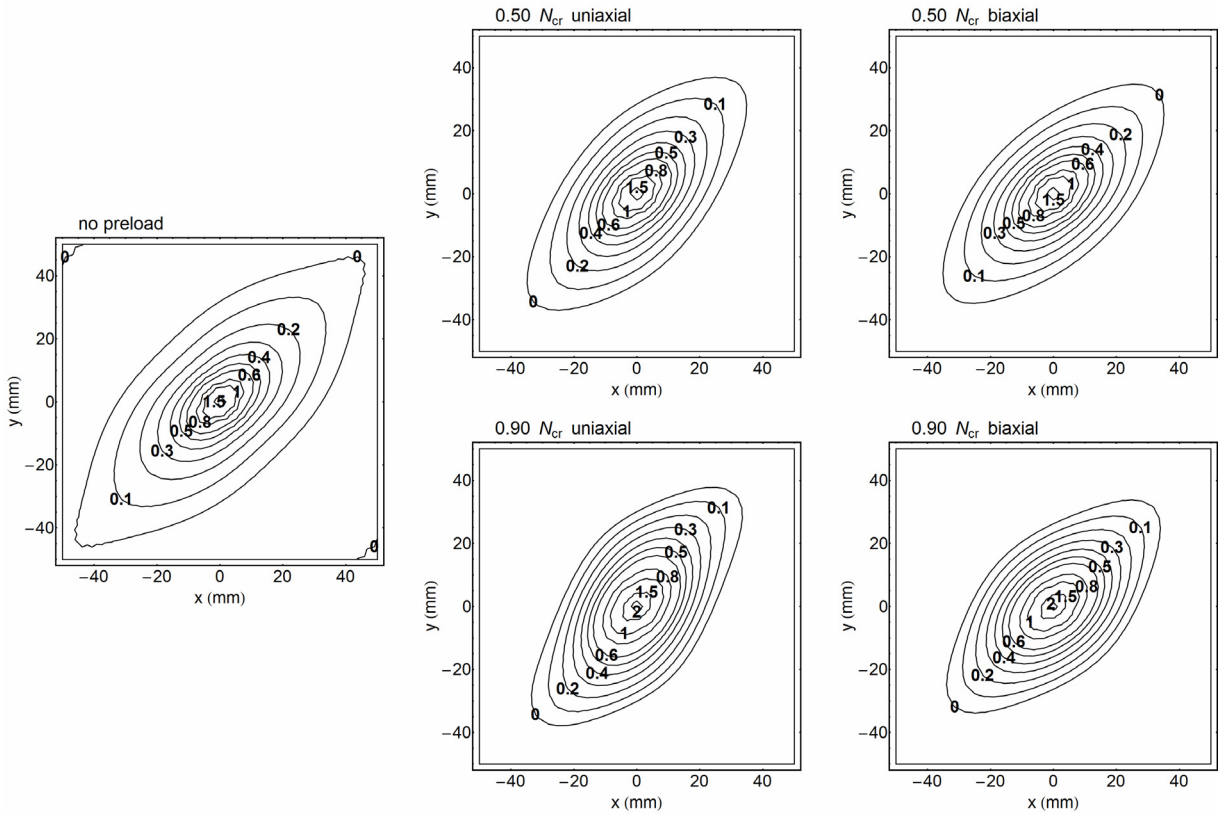

Figure 11 – Tsai-Wu failure index for the 100 mm laminate impacted under several compressive preloads smaller than the critical values.

The critical strains of the 400 mm laminate were $258 \cdot 10^{-6}$ (uniaxial) and $94 \cdot 10^{-6}$ (biaxial); the corresponding in-plane forces were 31.3 and 16.4 kN/m. In all the postbuckling configurations examined, the stresses were far below the in-plane strengths of the material. In figure 13 the contact force is plotted as a function of time or deflection for the biaxial preloads lower than the critical load; as in the case of figure 10, the curves obtained for uniaxial initial strain are not displayed because they are hardly distinguishable from the others. The relevant Tsai-Wu plots are collected in figure 14. The contact force histories for all the case studies regarding buckled laminates are presented in figure 15. The numerical values of maximum contact force, maximum deflection and contact duration can be found in table 8.

Table 7 – Main impact response parameters for 100 mm laminates impacted under compressive preload (impact velocity 0.45 m s^{-1})

preload		max. contact force (kN)	max. impactor displacement (mm)	contact duration (ms)
0		1.23	1.40	9.43
0.50 N_{cr}	uniaxial	1.13	1.75	11.3
	biaxial	1.13	1.77	11.3
0.90 N_{cr}	uniaxial	1.22	2.31	13.7
	biaxial	1.21	2.32	13.7
1.05 N_{cr}	biaxial	1.31	1.76	10.7
1.24 N_{cr}	biaxial	1.50	1.22	8.00

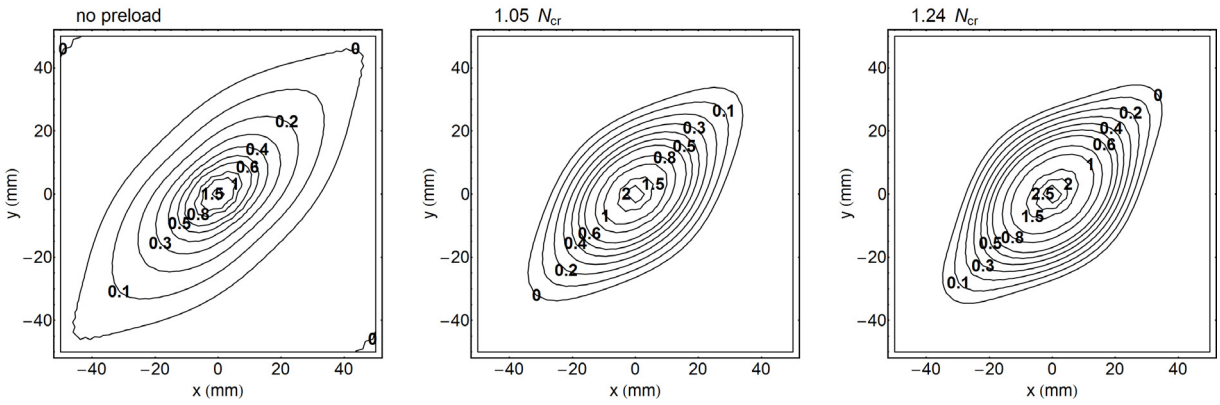

Figure 12 – Tsai-Wu failure index for the 100 mm laminate impacted under several biaxial compressive preloads larger than the critical values.

5.4.3. *Discussion*

In the small laminate, which is not prone to buckling, the influence of compressive preloads is exactly the opposite with respect to tensile preloads, as can be seen by comparing the curves in figure 1 and the Tsai-Wu diagrams in figure 2. The change in impact response (contact force, laminate deflection) is small due to the low span-to-thickness ratio. On the other hand, the stresses appear to be quite sensitive to the initial strain in this condition. The superposition of a compressive load to the bending stresses related to deflection leads to a much less severe stress state. As a consequence, the impact energy threshold associated with the first material damage will be significantly increased by the in-plane load.

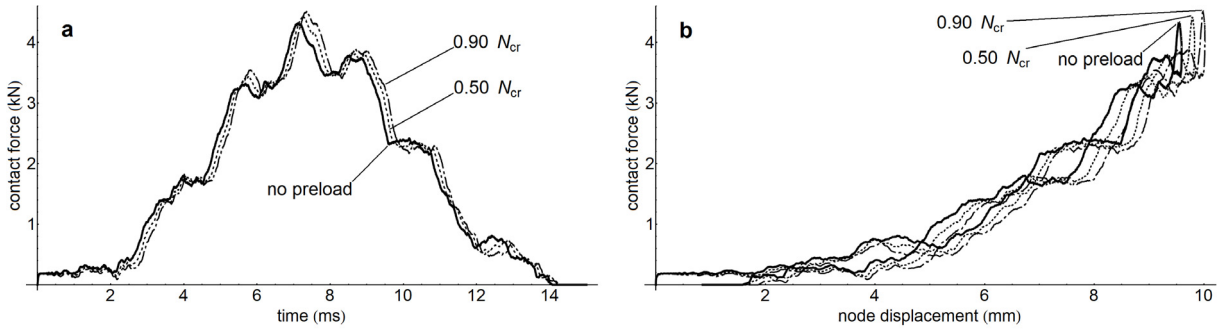

Figure 13 – Contact force as a function of time (a) or displacement (b) for the 400 mm laminate impacted under several biaxial compressive preloads smaller than the critical values.

It is important to point out that the Tsai-Wu failure index of figures 2d and 2e, as in all the other images, refers to the lowermost ply, which is subjected to tension; therefore it has to be considered as a prediction of possible failure in tension. With the level of preload considered, the stress state on the impacted side is far from causing failure in compression. Of course if the membrane load was increased the compressive stresses on the uppermost ply would eventually become the most severe and induce the first damage. However this situation was not considered in the present study.

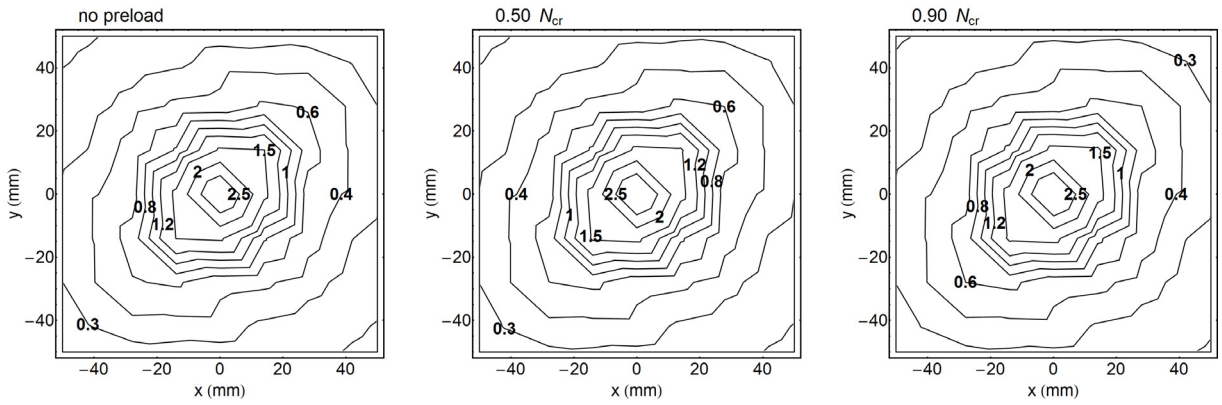

Figure 14 – Tsai-Wu failure index for the central zone of the 400 mm laminate impacted under several compressive biaxial preloads smaller than the critical values.

The large specimen is subjected to instability at very low in-plane loads. This justifies the negligible effect of preloads below the critical values, as regards both impact dynamics (figure 13) and stresses (figure 14). Even if a tensile initial strain considerably affects the transient response (see figure 5), in figure 13 the effect of a compressive preload appears much smaller due to the low absolute values of the applied stress. The Tsai-Wu index for uniaxial preload (not shown) is practically identical to the one calculated under biaxial preload.

While in the previous cases the contact duration has a tendency to rise because of preload, if the in-plane forces overtake the critical load their influence on the impact behaviour is the opposite (see figure 15). These trends agree with the results of previous studies, both concerning specimens preloaded within the critical level [5, 6, 15] and buckled specimens [4, 11]. In any case the differences observed here, especially as regards the maximum contact force, are again very small. The same happens for the maximum stresses (no diagram is presented for these cases because it would be a repetition of the ones in figure 14): it can thus be concluded that the impact energy threshold should also be substantially unaffected by in-plane loads.

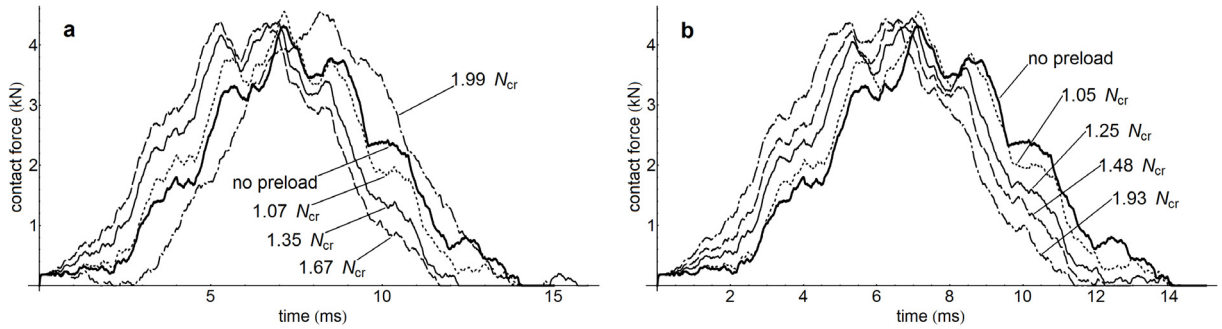

Figure 15 – Contact force history for 400 mm laminates impacted under several uniaxial (a) and biaxial (b) compressive preloads larger than the critical values.

Among the force-time curves in figure 15a, it is worth noting the one obtained for the highest preload, showing a different shape and associated with a much larger displacement than in every other case (see table 8). The reason for these peculiarities lies in a mode switching phenomenon occurring under uniaxial compression between 1.67 N_{cr} and 1.99 N_{cr}. In the latter

case the buckling mode presents two half-waves in the loading direction, whereas in the former (as in every other case, including all the examples of biaxial preload) the deformed shape of the buckled specimen has one half-wave in both directions. The response of the laminate buckled into a two-half-wave shape to an impact in its centre (where the initial transverse displacement is zero) is illustrated by the images in figure 16. The impactor forces the plate to turn to the first buckling mode; after its rebound the original second mode is restored, with the two half-waves oscillating back and forth thereafter.

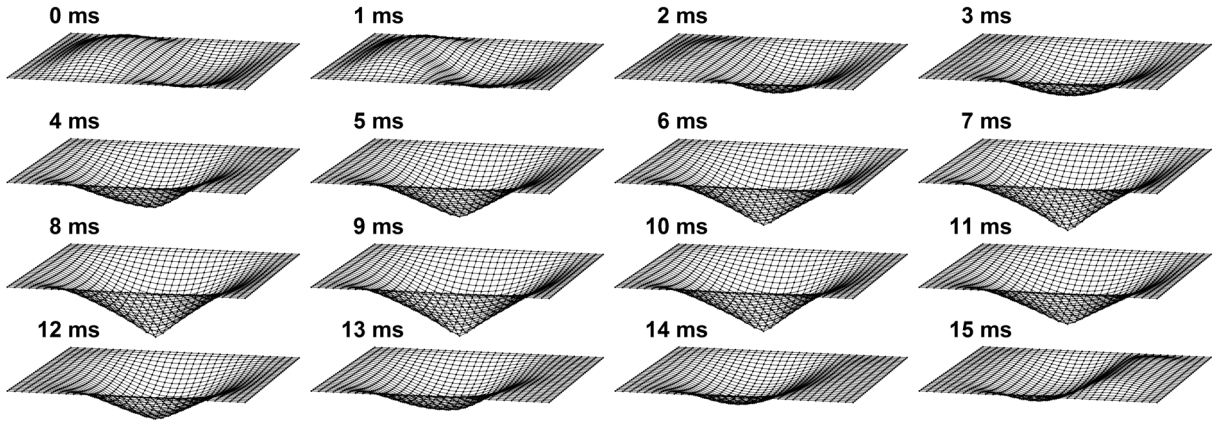

Figure 16 – Deformed shape of the 400 mm laminate impacted after second mode buckling under uniaxial compression preload.

The most interesting situation, with the largest reduction of the impact energy threshold, takes place in the medium laminate. The impact behaviour is definitely affected by preload (see figure 10); below the critical load a less stiff response is induced (but the maximum force increases at 0.90 N_{cr} with respect to 0.50 N_{cr}), while above it the overall stiffness of the specimen grows quickly, as shown by the slope of the force-displacement curves in figure 10b. The stresses exhibit a strong increment when the initial strain, either uniaxial or biaxial, approaches the critical value (figure 11), and increase further in buckled laminates (figure 12). Evidently the higher bending stresses due to larger deflections (with respect to the impact without preload) are only partially compensated by the superposition of the initial compressive stresses. In addition, in buckled plates a strong membrane stiffening takes place which adds a tension contribution.

This particular combination of conditions can occur only in medium size laminates. In small laminates the critical load can not be reached and the change in deflection due to preload is negligible. On the other hand, in large specimens the deflection might theoretically be strongly affected by preload (as happens under tension), but actually it is not because the critical load is very low. In fact the critical load must be low enough to be attainable before first failure is induced, but at the same time must be high enough for the corresponding preload to have significant influence on the dynamic response. Therefore it can be concluded that the most dangerous situation may take place in laminates of intermediate span-to-thickness ratio impacted

under compression. This danger should be considered with great care by designers, because in the condition just described compressive strength and instability limit are unfortunately close to each other, which would be desirable for the mechanical properties of the material to be fully exploited.

Table 8 – Main impact response parameters for 400 mm laminates impacted under compressive preload (impact velocity 1.8 m s^{-1})

preload		max. contact force (kN)	max. impactor displacement (mm)	contact duration (ms)
0		4.32	9.85	14.1
0.50 N_{cr}	uniaxial	4.43	10.08	14.3
	biaxial	4.43	10.09	14.4
0.90 N_{cr}	uniaxial	4.48	10.27	14.8
	biaxial	4.51	10.28	14.3
1.07 N_{cr}	uniaxial	4.56	9.27	14.3
1.05 N_{cr}	biaxial	4.55	9.44	14.0
1.35 N_{cr}	uniaxial	4.39	8.16	15.7
1.25 N_{cr}	biaxial	4.45	8.50	14.3
1.67 N_{cr}	uniaxial	4.39	7.49	11.7
1.48 N_{cr}	biaxial	4.42	7.89	12.2
1.99 N_{cr}	uniaxial	4.55	11.5	13.9
1.93 N_{cr}	biaxial	4.43	7.18	11.4

It is interesting to compare these findings with the experimental results described in [11]. The authors tested laminates of two different span-to-thickness ratios: 100 and 50. In the first case the observed influence of preload is small, as regards both the impact response parameters (maximum force, contact duration) and material damage. Even the impact test on the laminate buckled into a two-half-wave shape shows no significant difference with respect to the others. In the second case, where the compressive strength of the undamaged specimen is not much larger than the first critical load, the effect of in-plane loads becomes important. The highest preload level (1.2 N_{cr}) leads to a strong increase in the delaminated area. The authors conclude that the most detrimental effect of membrane stresses takes place when the critical load is close to the compressive strength and at the same time the applied preload is comparable with those two parameters.

The present study provides a satisfactory explanation of these conclusions, showing that the influence of preload is strongly dependent on the span-to-thickness ratio and that this dependence can be justified by considerations regarding the dynamic behaviour of the target, without the need for a damage model. Obviously the extent of damage, as well as some complex phenomena reported in [11] (like the instantaneous collapse of the preloaded laminate during impact, observed in one test) do need some modelling of damage, because they probably involve both global buckling and local instability of sublaminates created by delamination, which in turn can affect the propagation of delamination.

5.5. Conclusions

A number of finite element analyses were performed in order to evaluate the effect of membrane initial stresses on the low velocity impact behaviour of composite laminates, and to study how this effect changes for different span-to-thickness ratios of the target. The results, showing that this ratio actually has a major importance in determining the influence of membrane stresses, can be summarized as follows.

1) A tensile preload can increase the peak stresses induced by a low velocity impact, thus lowering the impact energy threshold required to initiate damage. These effects are larger for biaxial than for uniaxial preloads, and become weaker and weaker as the span-to-thickness ratio increases. However a higher initial velocity of the impactor leads to a wave dominated transient behaviour in which those trends are less definite.

2) A compressive preload can have beneficial effects on the peak stresses and increase the impact energy threshold at the lowest span-to-thickness ratios. On the contrary, very slender laminates are practically insensitive to such a preload, even if it is larger than the buckling load. The most detrimental influence of initial stresses was found at medium span-to-thickness ratios, when the compressive strength of the laminate and its buckling load are close to each other, for preloads comparable to the critical load.

A comparison with the experimental investigations carried out by other authors indicated that some phenomena and also seeming contradictions among them can be explained by the present results with considerations regarding the dynamic response of the specimen, without taking into account the material degradation due to damage. Especially the effect of preload and different span-to-thickness ratios on the impact energy threshold and on the contact force history can be justified, as well as the danger represented by compression preloads in particular conditions. On the other hand, a reliable prediction of the extent of damage, together with a complete understanding of some complex phenomena described in the literature, can be achieved only with a proper modelling of material failures.

References for chapter 5

1. Abrate S. *Impact on composite structures*. Cambridge: Cambridge University Press, 1998.
2. Sun CT, Chattopadhyay S. *Dynamic response of anisotropic laminated plates under initial stress to impact of a mass*. J Appl Mech-T ASME 1975;42(3):693-698.
3. Butcher BR, Fernback PJ. *Impact resistance of unidirectional CFRP under tensile stress: further experimental variables*. Fibre Sci Technol 1981;14(1):41-58.
4. Chen JK, Sun CT. *Analysis of impact response of buckled composite laminates*. Compos Struct 1985;3(2):97-118.

5. Sun CT, Chen JK. *On the impact of initially stressed composite laminates*. J Compos Mater 1985;19(6):490-504.
6. Chen JK, Sun CT. *Dynamic large deflection response of composite laminates subjected to impact*. Compos Struct 1985;4(1):59-73.
7. Sankar BV, Sun CT. *Low-velocity impact damage in graphite-epoxy laminates subjected to tensile initial stresses*. AIAA J 1986;24(3):470-471.
8. Robb MD, Arnold WS, Marshall IH. *The damage tolerance of GRP laminates under biaxial prestress*. Compos Struct 1995;32(1-4):141-149.
9. Chiu ST, Liou YY, Chang YC, Ong CI. *Low velocity impact behavior of prestressed composite laminates*. Mater Chem Phys 1997;47(2-3):268-272.
10. Kelkar AD, Sankar J, Rajeev K, Aschenbrenner RJ, Schoeppner G. *Analysis of tensile preloaded composites subjected to low-velocity impact loads*. In: 39th AIAA/ASME/ASCE/AHS/ASC Structures, Structural Dynamics and Materials Conference, Part 3, p. 1978-1987. Long Beach (CA, USA), 1998.
11. Zhang X, Davies GAO, Hitchings D. *Impact damage with compressive preload and post-impact compression of carbon composite plates*. Int J Impact Eng 1999;22(5):485-509.
12. Whittingham B, Marshall IH, Mitrevski T, Jones R. *The response of composite structures with pre-stress subject to low velocity impact damage*. Compos Struct 2004;66(1-4):685-698.
13. Mitrevski T, Marshall IH, Thomson RS, Jones R. *Low-velocity impacts on preloaded GFRP specimens with various impactor shapes*. Compos Struct 2006;76(3):209-217.
14. Khalili SMR, Mittal RK, Panah NM. *Analysis of fiber reinforced composite plates subjected to transverse impact in the presence of initial stresses*. Compos Struct 2007;77(2):263-268.
15. Choi IH. *Low-velocity impact analysis of composite laminates under initial in-plane load*. Compos Struct 2008;86(1-3):251-257.
16. Underwood P. *Dynamic relaxation*. In: Belytschko T, Hughes TJR, editors. Computational methods for transient analysis. Amsterdam: North-Holland, 1983. p. 245-265.
17. Yang SH, Sun CT. *Indentation law for composite laminates*. NASA CR-165460, 1981.
18. Tsai SW, Wu EM. *A general theory of strength for anisotropic materials*. J Compos Mater 1971;5(1):58-80.

Conclusions

Some specific aspects of the impact behaviour of composite laminates have been studied. In view of the complexity of the issues considered, the results presented herein are not intended to be conclusive. As pointed out in the concluding remarks of each chapter, however, they can provide an advancement on the understanding of some points, and suggest other points which deserve further interest. It is felt that future research on each of the topics discussed in the previous chapters could be considered necessary and welcome by the scientific community. In particular the influence of pre-existing in-plane loads on the impact response of a laminate, treated in chapter 5, appears to be a subject that still needs significant contributions, as regards both experimental testing and numerical modelling.

In addition, some general comments can be made about the numerical model employed here. Nowadays many material degradation models are being studied and implemented in commercial finite element codes. Therefore a numerical analysis like the present one, which does not take into account the effect of failures, may seem not to be useful for research purposes at first sight. It is felt, however, that the results which have been obtained with this type of analysis give evidence to the contrary. Not only can a simple model provide important information, but its results have also the advantage of being easier to control and verify, as well as useful to serve as a reference for other results yielded by more complex models. Moreover, a simulation without a damage model can help in distinguishing between phenomena that can be explained with this type of analysis (and are thus independent of material failures) and phenomena which can not (thus depend on damage).

Nevertheless, it is obvious that the absence of a degradation criterion of the mechanical properties of the material constitutes a limitation, as evidenced throughout this study. In addition to the improvement which would be achieved by removing it, other modifications should be accomplished. Whatever the damage model one decides to employ, its proper working requires the stress field to be computed with sufficient accuracy; as a consequence, the implementation of different finite element formulations, such as higher order interpolations, should be considered. Curved shell, in place of flat shell elements, may be included in the program, in order to overcome the drawbacks of the latter in the discretization of curved laminates. A more detailed contact model should replace the one adopted so far, whose main deficiency is the stress singularity created by the concentrated contact force. All of these modifications may make

it possible for a two-dimensional element type to achieve a significant improvement. Further advances can be accomplished only by means of three-dimensional models, mainly for two reasons. Firstly, a triaxial stress state is usually responsible for the failures caused by impact, especially under the contact area between impactor and target: this calls for the normal stress through the thickness, as well as the out-of-plane shear stresses, to be evaluated with a better approximation than what can be reached by means of plate or shell theories. Secondly, since delamination is considered the most important failure mode of laminated composites, proper modelling of this phenomenon is necessary, for which a discretization consisting of three-dimensional finite elements seems to be more appropriate.